ANNALES
UNIVERSITATIS SCIENTIARUM BUDAPESTINENSIS DE ROLANDO EÖTVÖS NOMINATAE

SECTIO GEOLOGICA

TOMUS XII.
1968

REDIGUNT
B. GÉCZY
J. KISS
L. STEGENA

BUDAPEST
1969

ANNALES
UNIVERSITATIS SCIENTIARUM BUDAPESTINENSIS DE ROLANDO EÖTVÖS NOMINATAE

SECTIO BIOLOGICA
incepit anno MCMLVII

SECTIO CHIMICA
incepit anno MCMLIX

SECTIO GEOLOGICA
incepit anno MCMLVII

SECTIO GEOGRAPHICA
incepit anno MCMLXV

SECTIO HISTORICA
incepit anno MCMLVII

SECTIO IURIDICA
incepit anno MCMLIX

SECTIO MATHEMATICA
incepit anno MCMLVIII

SECTIO PHILOLOGICA
incepit anno MCMLVII

SECTIO PHILOSOPHICA ET SOCIOLOGICA
incepit anno MCMLXII

FABRIC AND JOINTING IN PYROXENE ANDESITES, CSERHÁT HILLS, NORTHEAST HUNGARY

by
P. ÁRKAI
(Geochemical Research Laboratory of the Hungarian Academy of Sciences)
(Received: 21st September 1968)

РЕЗЮМЕ

В статье рассматриваются литоклазные системы пироксеноандезитовых горных пород центрального и юго-западного участков горы Черхат, а также направленность их текстуры. Для изучения текстуры отчасти проводились измерения методом Федорова, а отчасти применялся простой статистический метод. Исследования показали, что система столбчатого расщепления характерна в основном для лавы, уже не движушейся на позднем этапе остывания, на этапе отверждения (текстура без направленности), в то время, как расщепление уступами (хотя оно может происходить также только на воздействие сжатия при остывании), чаще всего наблюдается в лавах, выполняюших значительное ламинарное движение на позднем этапе остывания (различная в параллельном и перпендикулярном направлениях ступенчатости но значительная направленность). Плоскости среза, образуюшиеся в пластичном веществе соответствуют плоскостям ступенчатости. Первичные литоклазные системы вулканических горных пород определяются совместным эффектом условий остывания, зависящих от размеров, формы, температуры массива горных пород, от температуры и теплопроводимости окружающей среды, а также движения лав, связанного с углом наклона, вязкостью и степенью пополнения вещества. По изменениям направленности литоклазных систем можно делать тектонические выводы, в то время, как территориальное распределение типов литоклаза позволяет судить о палеогеографических условиях.

Review of relevant literature

Jointing in igneous rocks, especially columnar jointing, has attracted the attention of researchers at an early stage. Columns were first ascribed to contraction on cooling by Raspe (1776). His ideas were further developed by Thomson (1863) and Iddings (1886). A mathematical-physical theory of columnar jointing was given by Mallett (1863) and Becker (1893). The form types of columnar jointing were classified by Tomkieff (1940) who distinguished autonomic (regular) columns and heteronomic ones (pseudocolumns). In the former, each joint is a common face of precisely two columns, whereas in the latter there are transcurrent joints belonging to more than two

columns. Klüpfel (1952) in this "Basaltgeologie" gave just a morphological classification of forms of jointing. Szádeczky-Kardoss (1958) stated columnar jointing to be typical of relatively thin and extensive sheets of basic, low-viscosity magmas; the more isometric masses of neutral higher-viscosity magmas tend to present bedding joints or lamination due to cooling in just one direction. In acid lavas flow striation is often observed.

The assumption that the forms of jointing and the movement of the cooling melt are related is not very recent, either. Benard (1900) observed the formation of hexagonal cells of convection in cooling melts. His finding was used by Dauzère (1908) to explain the formation of columnar jointing in basalt. His following included Glangeaud (1913), Longchambon (1913); his opponents suspected the relation between the two phenomena to be a purely formal one [Sosman (1916), Smedes, Lang (1955)]. The connexion between lava movement and forms of jointing was studied in much detail by Brinkmann (1957). He stated regular hexagonal jointing to form in lava at rest; in flowing lava, where tensions will arise, forms distorted in the flow direction will come to exist. The long axis of the tectonic sum polygon includes an acute angle with the flow direction, as in glaciers. Heteronomic columns are due to intense distension, i.e. to relatively rapid flow. Brinkmann recognized also some fabric regularities (plagioclase laths arranged parallel to the dyke wall or to the lava surface); still, in his concluding remarks he denied any connexion between fabric orientation and jointing.

The morphological features connected with recent flowing lava were first observed by volcanologists [Bergt (1914), Lacroix (1919) etc.]. The fact that laminar flow results in an oriented fabric* was proved in a plaster-of-Paris experiment by Philipp (1921). In the clarification of the relationship between movement and form, the correct interpretation of glass-industry melts played an important role [Eitel (1934)]. The connexions between movement and texture in volcanics of various chemical composition were analyzed in detail by Philipp (1936).

The striation of obsidian from Lipari and Milos is due to crystallization in laminar-flow surfaces. Basaltic rocks with similar features are called venites = = laminites. Accumulation of volatiles in shear planes (distension = pressure decrease) results in an autopneumatolytic mineral assemblage. Bedded and laminated rocks are formed like the laminites out of lavas in violent motion in the last stages of solidification, but whereas in laminites some chemical differentiation takes place, in laminated "stratified" rock the movement results in a purely mechanical ordering and in shear. Columnar jointing develops in lavas at rest.

Bernauer (1936–38) distinguished three forms of lava movement in the order of decreasing temperature: (1) turbulent flow, (2) laminar flow, (3) block displacements, planar slip, faulting. He emphasized the identity of forms due to cooling and flow in laminated "stratified" volcanics. With advancing lamination, sigmoidal joints (Tildenspalten) turn into plane glide surfaces, which subsequently meet the conditions also of contraction. Bernauer gave

* By orientation we shall mean preferred orientation throughout, except where randomness is expressly stated.

on the basis of his observations on Mt Vesuvius and the Burfjell in Iceland the following basic profile for lava flows (from the top downwards):

thickness	rock
0 – 2 m:	top layer of scoria
1 – 2 m:	vacuolar lava, often bedded, laminate
1 – 4 m:	lava with minute vacuoles; short sigmoidal joints
2 – 25 m:	massive lava with extensive shear jointing (Scherfungen),
0 – 1 m:	bottom layer of scoria.

Sander (1948) in his comprehensive treatise on structure denied the laminar flow theory of lavas. Provided the lava has sufficient mobility, turbulent flow arises, with a statistically regular orientation of whorl axes (structural *b* axis). Laminar movement (lamination) arises in the last stage of lava movement (the stage of solidification) and results in a deformation. According to Rittmann (1960), flow in the interior of a lava sheet is laminar. The forms of cooling and solidification of the outpouring lava depend on viscosity, gas content, slope angle and cooling rate. It is these factors that determine the surface features of the lava sheet or volcanic shield, including also its petrofabric orientation. According to Einarsson (1961), the velocity of lava flow according to observations on the volcano Hecla on Iceland is:

$$v = \frac{g\varrho h^2 \sin \alpha}{2\eta},$$

where g is the acceleration of gravity, ϱ is the density of the melt, h is the thickness of the lava sheet, α is slope angle and η is viscosity. Flow velocity on the surface is twice the velocity of advance of the lava flow, which is due to a mechanism of movement similar to that of a caterpillar tread. A similar phenomenon was observed by Vörös (1967) on basalts of the Balaton Highland.

The advance direction of the magma (lava) can be derived from petrofabric orientation. H. & E. Cloos (1927 – 28) derived the mechanism of intrusion of subvolcanic domes of trachyte and andesite from the orientation of sanidine and amphibole phenocrysts, respectively. They concluded that the connexion between parallel-orientation fabrics and laminar jointing is an indirect one. Petrofabric studies were lately performed also by Water (1960) and Szőke (1966). According to the latter, the general flow direction of the lava can be derived from a statistic analysis of the (010) faces of plagioclase in andesites. In oriented fabrics, these faces tend to concentrate into a girdle, the axis of which (c) indicates the direction of flow. The highest-density pole (a) of the girdle of plagioclase plates coincides with the pole of projection of laminar parting, or in the case of columnar jointing with the pole of the joints perpendicular to the columns. The plagioclase laths in the matrix have a similar orientation, except that the poles are evenly distributed all over the girdle. Buda (1966) emphasized some differences between fabric orientation in volcanic and subvolcanic rocks. Schminke (1967) derived flow directions from the shapes and arrangements of vacuoles in vacuolar lava sheets.

Petrofabric analysis of Cserhát Hills pyroxene andesites

The aim of the petrofabric work in point was on the one hand to look for possible connexions between structure and jointing in the Middle and Southwest Cserhát volcanics, and on the other to collect some evidence concerning the existence and nature of oriented fabrics which should serve as a basis for a palaeovolcanological and palaeogeographical evaluation. It was during the actual performance of petrofabric measurements that the perspective of a possible clarification of the genetic relationship suggested earlier by P h i l i p p (1936) between petrofabric orientation (lava flow) on the one hand and parting types on the other opened up.

For a summary description of the Cserhát Hills volcanism the reader is referred to Á r k a i (1968). We call "amafic" those andesites which contain very few pyroxene phenocrysts or none at all (the earlier term for them was andesite with microlites of augite). It may be stated in summary that (1) the volcanics of the Cserhát forming the subject of this paper correspond to the middle andesite group of the Mátra, more precisely to a marginal facies of the same, (2) the andesite dykes and lava flows are contemporaneous and can readily be parallelized, (3) the substantial similarity of features between Mátra Mountains and Cserhát Hills volcanism suggests a similarity of origin as regards geological conditions and time of eruption, although there is a difference in the location of the centres of eruption, and in the volumes and intensities of the eruptions.

Joint analysis

At each sampling locality (quarry) we have measured 90 to 200 joints and plotted the results on a lower-hemisphere Schmidt net. Each stereogram represents the plot of a single locality. Figs. 1 to 8. represent the typical joint systems of bronzitic augite andesite and amafic andesite. The types of joint systems and the statistical parameters of the orientation are summarized for pyroxene andesite rocks in Table I.

The dykes of the area are characterized by three mutually orthogonal sets of joints (parallel and perpendicular, respectively, to the dyke wall and parallel or perpendicular to the ground surface at the time of origin). The only exception is the bronzitic augite andesite dyke of Bercel-Bér where columnar jointing perpendicular to the wall of the dyke reflects according to P h i l i p p (1936) the solidification of a melt at rest.

The situation is less simple in the case of lava sheets and flows: there are quite substantial differences between the various types of volcanic masses on the one hand, and between various portions of one and the same lava mass, on the other. The sheets of bronzitic augite andesite (Ecskend Plateau, Nagy Hill at Bér) exhibit columnar jointing (irregular five- or six-faced columns, locally twisted: transitions between autonomic and heteronomic columnarity). The rock is massive on Nagy Hill, vacuolar on the Ecskend Plateau; the flattening perpendicular to the column axes of the vacuoles suggests a slow laminar movement (deformation) in a late stage of solidification. The bronzitic augite ande-

Fig. 1 to 4. Stereograms of the columnar joint systems of a bronzitic augite andesite shield. Ecskend Plateau, SW Cserhát Hills. Projection on the lower hemisphere. One percent contours

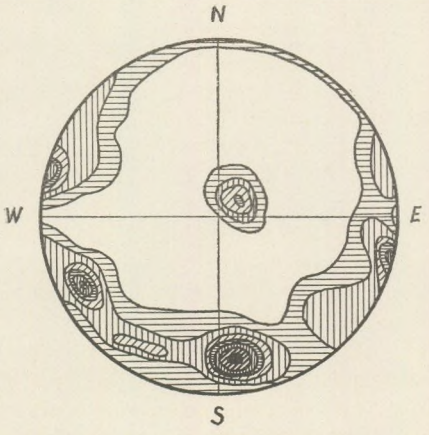

Fig. 1. Püspökhatvan, sampling locality I/A/1–4

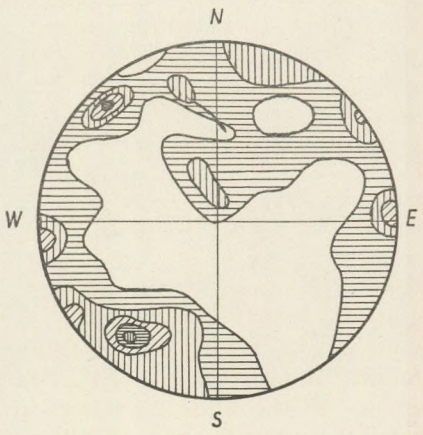

Fig. 2. Ibidem, sampling locality I/C/6

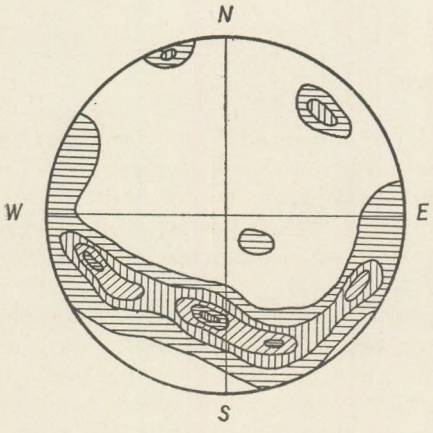

Fig. 3. Galgagyörk, sampling locality IC/1 (Hegyes Hill)

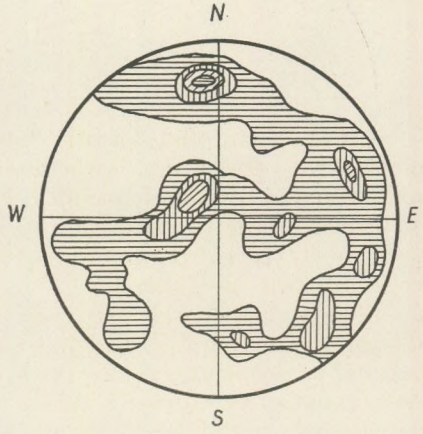

Fig. 4. Ibidem, sampling locality IC/2

site bodies of the northeastern part of the Western Cserhát are characterized by laminar jointing.

In the amafic andesites, a considerable variety of forms of parting is observed. The small-size amafic andesite lava flows of the Ecskend Plateau exhibit a blocky (columnar-blocky) jointing, whereas in the Middle Cserhát the shield fragments of the monogene fissure volcanoes of Bercel and the Szanda are columnar (regular five- of six-faced, seldom heteronomic or twisted). In

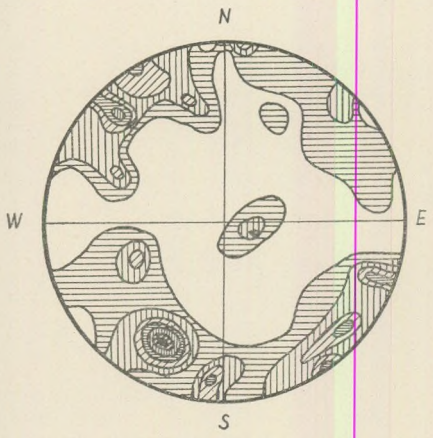

Fig. 5. Stereogram of the columnar joint system of a bronzitic augite andesite shield. Eskend Plateau. Galgagyörk, sampling locality IC/3

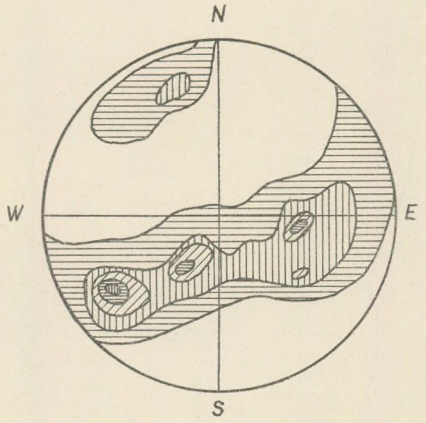

Fig. 6. Ibidem, sampling locality IC/4

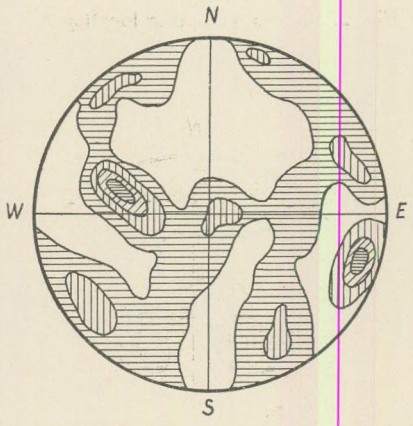

Fig. 7. Stereogram of joint system of amafitic andesite lava flow, Eskend Plateau, SW Cserhát Hills, sampling locality III/2–3 (Rózsakút)

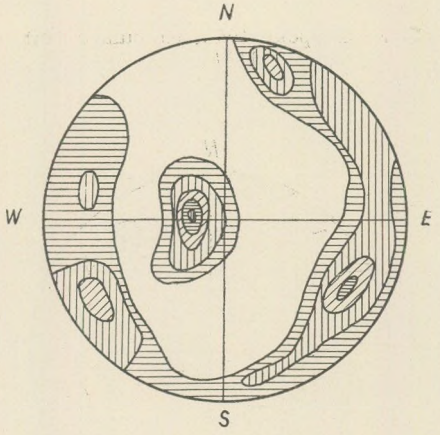

Fig. 8. Stereogram of amafic andesite flow of laminar jointing, Buják quarry

the eastern part of the Middle Cserhát an extensive but relatively thin body of amafic andesite composed of several lava flows exhibits laminar jointing, the individual flows agree with the profile given by Bernauer (1936–38).

Vacuolar andesite is locally laminar, most often blocky; block size may exceed 2 m. The orientation of elongation of the vacuoles varies from one block to the next, which may be due to the disruption between blocks; the phenomenon itself reminds of the gas-saturated viscous block lava of Rittmann (1960).

The massive microandesites exhibit bedded and laminar types of jointing. The beds seem to hug the underlying palaeorelief. In the microandesite flows

Table 1.

pheno = **phenocrysts**, mat = **matrix**

Rock	Region	Formation	columnar	laminate	blocky	Orientation/scatter/ $\sigma_{\parallel}$ pheno	$\sigma_{\parallel}$ matr	$\sigma\perp$ pheno	$\sigma\perp$ matr	$\sigma_{\parallel}/\sigma\perp$ pheno	$\sigma_{\parallel}/\sigma\perp$ matr	σ matr/σ pheno //	σ matr/σ pheno $\perp$
			type of joints										
Micro-andesite	Middle Cserhát	Buják – Bér lava flows		x		–	26.0 – – 45.0	–	22.0 – – 40.0	–	1.29	–	–
		Bér, Virágos psz, dyke			x	–		–		–		–	–
	SW Cserhát	Ecskend Pl. lava flow		x		–	25.0 – – 40.0	–	23.0 – – 30.0	–	1.31	–	–
Vacuol. andes.	SW Cserhát	Ecskend Pl. lava flow			x	29.0	30.0	24.0	25.0	1.21	1.20	1.03	1.04
Amafic andesite	Middle Cserhát	Buják – Bér lava flows		x		43.7 – – 50.5	45.5 – – 50.5	29.5 – – 49.5	38.0 – – 50.0	1.30	1.28	1.00	1.09
		Szanda shield	x			43.0 – – 50.7	46.0 – – 52.0	39.0 – – 50.0	42.0 – – 52.0	1.05	1.03	1.10	1.10
		Peres Hill dyke			x	45.3	47.9	40.3	45.0	1.13	1.07	1.06	1.11
		Bercel shield	x			48.5 – – 52.0	51.0 – – 52.0	44.6 – – 50.7	52.0	1.03	1.02	1.06	1.05
		Mulató Hill dyke			x	50.2	51.8	49.3	49.6	1.02	1.04	1.03	1.01
	South-west Cserhát	Ecskend Pl. lava flow			x	30.2	36.3	26.4	29.3	1.16	1.24	1.20	1.11
		South dyke Csörög			x								
Bronzitic augite andesite	Middle Cserhát	Filagoria Hill lava flow		x									
		Nagy Hill shield	x			51.8	52.0	50.8	52.0	1.02	1.00	1.01	1.04
		Bercel – Bér dyke	x			42.5 – – 50.5	46.0 – – 52.0	42.2 – – 51.0	45.0 – – 52.0	1.02	1.03	1.08	1.05
	South-west Cserhát	Ecskend Pl. shield	x			49.2 – – 52.0	49.5 – – 52.0	46.0 – – 52.0	1.01	1.02	1.05	1.05	1.04
		Cseke Hill north dyke			x	49.7	50.3	49.8	50.5	1.00	1.01	1.01	1.00

σ = scatter parameter, $_{\parallel}$ = sample perpendicular to column axis or parallel to lamination, $\perp$ = sample parallel to column axis or perpendicular to lamination

of the Ecskend Plateau, there are portions combining laminar and columnar forms, with S-shaped columns at the middle of the lava body, indicating that the central part of the flow was the last to come to rest. The origin of the upper scoriaceous level in the microandesite sheets is due to a degassing prosess near the top of the ancient lava body. It corresponds to Rittman's medium-viscosity "Brockenlava" type.

Orientation of fabrics

The manifold forms of jointing observed in the pyroxene andesites of the Cserhát volcanic complex tend to confirm the opinion of V a d á s z (1967) that the jointing of volcanic rocks cannot in its often staggering variety be satisfactorily ascribed to the cooling process alone, and that a detailed analysis of causes and effects is still lacking. This is why I set myself the task of studying the connexions between lava movement and jointing. To establish the direction of movement, I had to rely on petrofabric examinations. Similar work carried out so far [S z ő k e (1966), B u d a (1966)] revealed a parallel orientation of crystals in the latest stage of flow just preceding the final consolidation, as well as slip along planes parallel to the laminar jointing and perpendicular to the column axes. Whorls indicating turbulent flow at higher temperatures are restricted to the proximity of the centres of eruption [K u b o v i c s (1966)].

Petrofabric investigation methods as applied to the study of lava flow include the following.

(1) The method of S z ő k e (1966) and B u d a (1966) is based on the universal-stage determination of the orientation of the (010) faces of plagioclases. My stereograms of the petrofabric orientation of a few characteristic rock types are shown as Figs. 9. and 10.

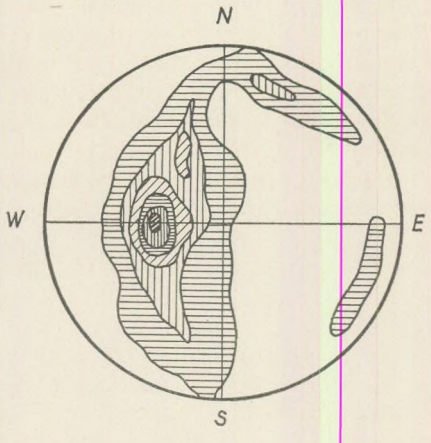

Fig. 9. Stereogram of orientation of (010) faces of plagioclase phenocrysts in amafic andesite with bedding joints (Filagoria Hill) One percent contours

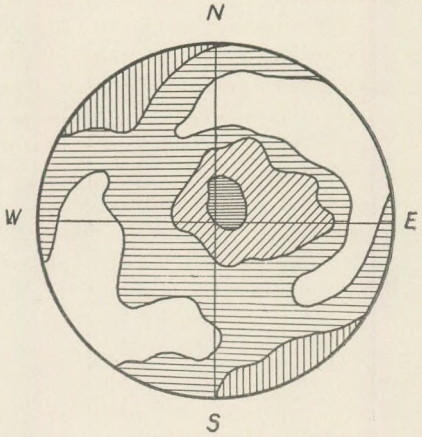

Fig. 10. Stereogram of orientation of (010) faces of plagioclase phenocrysts in bronzitic augite andesite of columnar jointing (Ecskend Plateau) One percent contours

The poles of 250 to 350 grains measured in three mutually perpendicular oriented sections have been plotted on a lower-hemisphere Schmidt net. The results agree with those of Szőke. In a rock of laminar jointing the plagioclase phenocrysts are arranged parallel to the joints (maximum perpendicular to the joint plane); the girdle axis is parallel to the flow direction, the distribution of poles over the girdle is uniform. Orientation is less pronounced in rocks of columnar jointing. In a sample from a 25 m thick volcanic shield of the Ecskend Plateau, orientation is rather weak and perpendicular to the column axes, whereas in the remnants of the thicker (100 to 200 m) andesite shields of the Szanda and Bercel, in the bottom portions close to the contact with the floor, the plagioclase phenocrysts are parallel to the column axes. This may be due to a gravity-induced slow sinking of the phenocrysts in a melt slowly cooling while at rest.

Owing to the complications of three-dimensional orientation statistics and to the large number of necessary measurements this method is little suited to the determination of quantitative parameters of orientation and to a quantitative comparison of a large number of samples on the basis of the parameters thus obtained.

(2) A rapid method introduced somewhat earlier [Árkai, (1967), Dienes (1967)] possesses the advantage that measurements of orientation performed under a simple revolving-stage microscope on suitably selected equivalent planes yield data accessible to a fairly simple mathematical treatment: also, the required number of measurements is less (200 to 250) and the results are suitable for comparison. As far as lava (magma) movement is concerned, planes that can be considered as equivalent are those parallel to the ancient surface or contact in the case of lava sheets or flows, parallel to the dyke walls in the case of dykes, and perpendicular to the column axes (planes of lamination). Sections perpendicular to these planes and oriented in the direction of the girdle maxima (i.e. perpendicular to the banking and parallel to the column axes) form another equivalent set. It is in these two sets of planes that I have measured the orientation of the long axes of plagioclase phenocrysts on the one hand and of plagioclase laths in the matrix on the other. The results are plotted in frequency histograms of 10° unit division. The parameters of orientation computed from these data were the mean square deviation from the mode of the distribution and the deviation from the arithmetic mean. The distribution of orientation for these mineral grains is nearly normal; skewness varies in the range $\pm 0{,}5$ and scatter is practically equal to the mean square deviation from the mode.*

The orientation parameters of the fabrics and jointings of the main types of volcanics of the Cserhát region are shown in Table I. The results seem to justify the following general conclusions.

(1) The deviation between the orientation parameters of rocks with laminar and columnar paring as measured parallel to the lamination (in the first case) and perpendicular to the column axes (in the second) is relatively slight ($\delta_{\text{columnar}}/\delta_{\text{banked}} = 1{,}20$).

* In the case of a fabric of wholly random orientation (having the same number of data in each division) scatter is $\delta = 52.0$; if all measurements fall within the same division, scatter is $\delta = 0$.

(2) The deviation in orientation is highly significant between sections perpendicular to the lamination and parallel to the column axes, respectively. Whereas in samples of laminar jointing $\delta_{\parallel}/\delta_{\perp} = 1.30$, this same ratio is 1.00 to 1.06 in the case of columnar jointing; greater values are due to the vertical orientation of plagioclases (due to gravity-induced sinking in a melt at rest).

(3) The orientation of plagioclase laths in the matrix exhibits similar relationships.

(4) A comparison of the orientation parameters of the phenocrysts and the matrix shows that the phenocrysts are more markedly oriented. The difference is presumably due on the one hand to the slowing down of lava movement at the time when the crystals were forming in the matrix, and, on the other, to causes to be expounded in point (5) below.

(5) As regards orientation in the various types of rock, the pronounced orientation of the matrixes of microandesites, by far exceeding those of the andesites containing phenocrysts, is most remarkable. This may be due partly to the fact, that microandesites being the last products of the volcanic cycle, slope angles were at this late stage of evolution of volcanic structures greater on the average than earlier. On the other hand, a relatively complete ordering by lamination could in the late stages of solidification develop more easily in a melt not containing phenocrysts than in normal andesite melts where the phenocrysts, forming a framework, could to a certain extent inhibit the ordering by lamination of the matrix.

In profiles across subvolcanic or volcanic bodies of rock, variation in orientation will shed some light on certain details of lava movement.

Fig. 11. shows this variation in a profile perpendicular to the wall of the bronzitic augite andesite dyke of Bercel-Bér. The difference in orientation between the sections perpendicular and parallel to the column axes is minimal. Orientation is most pronounced near the dyke wall, where besides the columnar jointing there are also joints parallel to the wall. Orientation distribution in the amafic shield remnant of the Szanda is shown in Fig. 12. Pronounced orientation is restricted to the central portion of the rock body, where the columns are irregularly twisted, bent and laminated. The bottom part of the ancient lava body and its actual top part exhibit five- and six-faced regular columns whose fabric is practically unoriented. In the bottom portion one observes a vertical orientation of plagioclase plates (gravity settling effect). In the amafic andesite flows of the eastern part of the Middle Cserhát, profiles similar to the one described as typical on p. 5 of Bernauer's paper (1936—38) could be observed (Figs. 13., 14.).

In bedded lava flows, slides parallel to the bedding rather widely differ in orientation from slides perpendicular to it. It is in the lava flow of Filagoria Hill that the upper scoriaceous, degassed layer is most pronouncedly oriented. The profile of the Buják quarry presents a more complicated picture. Under the degassed scoriaceous lava crust, looking like an agglomerate, there is a blocky lava with vacuoles distended in a vertical direction, reflecting the degassing process. Underneath this latter there is a thin layer of laminate andesite underlain in turn by a thick-bedded horizont with sigmoidal joints Further downwards one encounters an alternation of thin- and thick-bedded andesites. The best oriented part of the lava sheet is the horizont with short

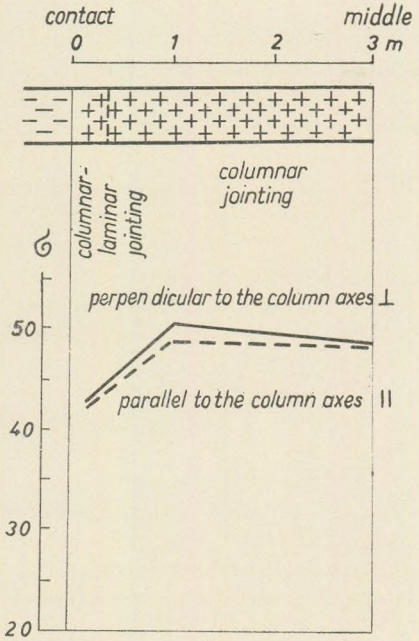

Fig. 11. Change of orientation in a transverse profile of the bronzitic augite andesite dyke of Bercel – Bér

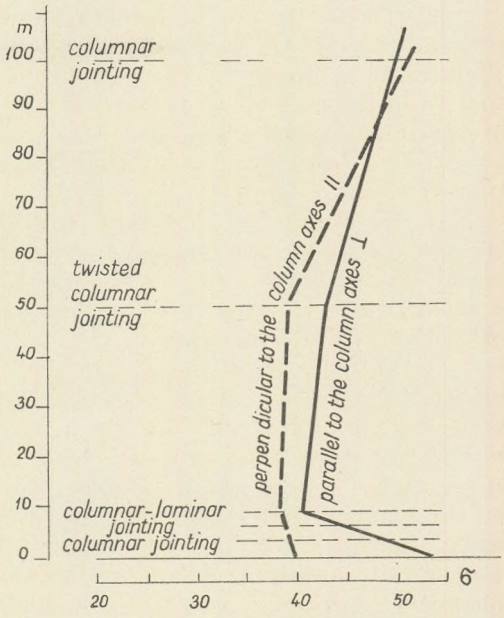

Fig. 12. Change of orientation in a vertical profile of the amafic andesite shield of the Szanda

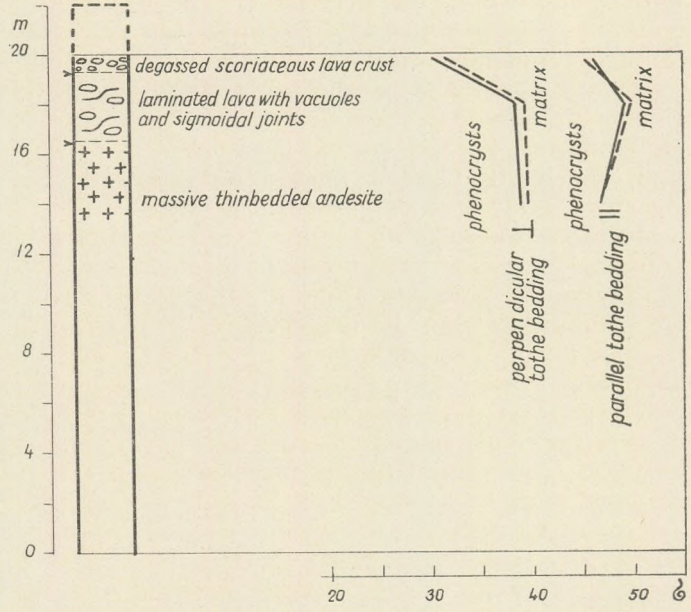

Fig. 13. Change of orientation in a vertical profile of the amafic andesite flow of Filagoria Hill

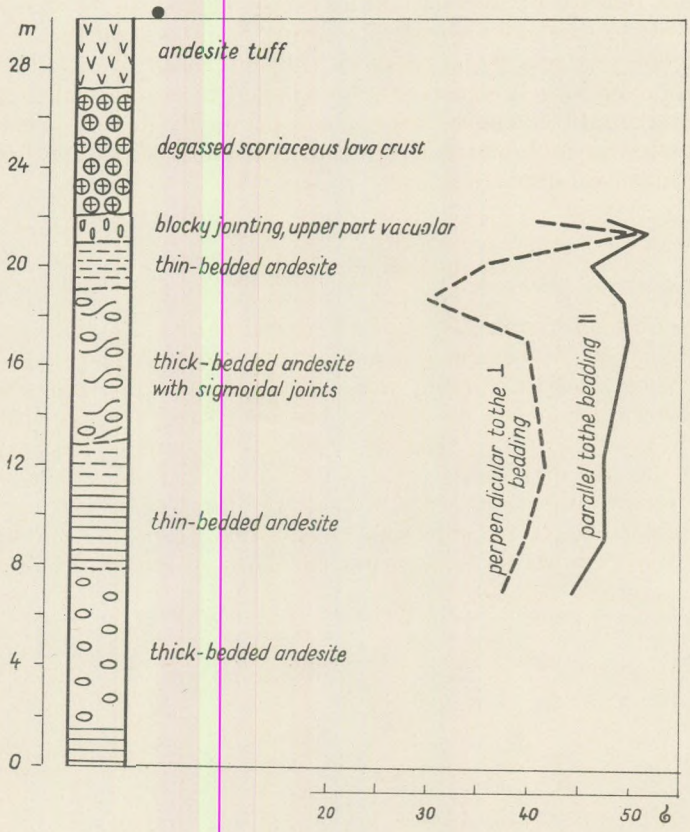

Fig. 14. Change of orientation in a vertical profile of the amafic andesite flows of Bujak

shear joints and the lower thick-bedded andesite. In the uppermost scoriaceous-vacuolar portion, orientation is almost identical in slides parallel and perpendicular to the bedding.

In summary we may state that primary jointing in a volcanic rock is due to the joint influence of a set of factors including the size, shape and temperature of the magmatite body, its rate of cooling (depending on the temperature and heat conductivity of the host rock), and the nature of its displacement (as determined by slope angles, viscosity, gas content and material supply). Columnar jointing is a result of contraction purely by cooling, whereas laminar jointing appears as a result of a combination of displacement (shear) and contraction (cooling) in a lava still in motion in the late stages of cooling (although it might form as a result of pure cooling, too). Of course, there are any number of transitions between these two types. Even columnar structures may show some lamination (as proved by the shapes and distribution of vacuoles) Twisted, bent and otherwise distorted columns and columns with cross-sections elongated in a certain direction also reflect some movement. More intense deformation by lamination produces short sigmoidal joints from which a bedded structure

due to shear can readily be derived. Blocky parting can be of various origin. In dykes it comes to exist as a result of cooling from several directions and a simultaneous tectonic stress (compression) (the slightness of orientation shows this to have happened largely at a late stage of solidification in a hardly moving melt). Blocky parting in volcanic rocks occurs primarily in lava sheets of small size, but orientation in such blocks is intense, as a result of cooling from several directions and intense lamination.

Geological conclusions

(1) The orientation in space of the surfaces of parting depends on the position of the original lava surface and contact surface (on the position of the dyke wall in dykes) and, of course, also on subsequent displacement. Hence, from the primary jointing the position of these surfaces can be inferred even in poor enough exposures. The first to draw conclusions concerning volcano structure from the dip of bedding was Szádeczky-Kardoss (1958). In rock of columnar jointing it is the planes parallel to the column axes that play the role equivalent to the surfaces of bedding. In dykes, the orientation of the joint system permits to reconstruct the dip and strike of the dyke wall.

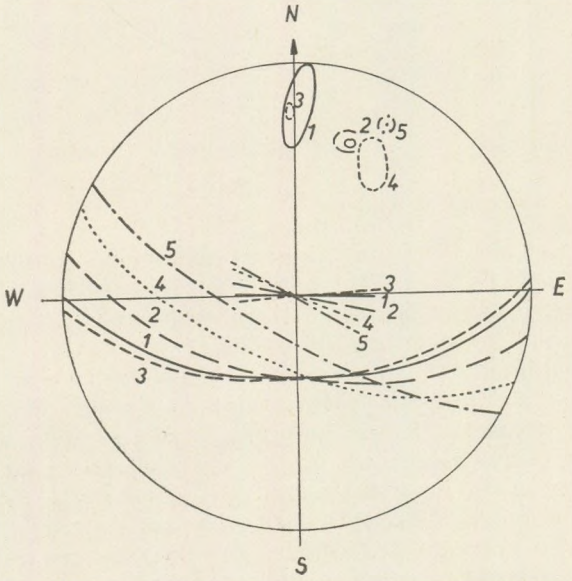

Fig. 15. Change of orientation of a columnar joint system in a horizontal profile of the bronzitic augite andesite dyke of Bercel – Bér

Fig. 15. shows systems of columnar joints perpendicular to the dyke walls in various parts of the bronzitic augite andesite dyke of Bercel-Bér. The deviations of the girdles of the joints parallel and perpendicular to the column axes agree with the deviations in the strike of the dyke (the dip is nearly constant). Fig. 16.

represents joint systems measured in a blocky amafic andesite dyke of Szanda-Pereshegy. One plane of the blocky jointing is parallel to the dyke wall; the other two are perpendicular to it. The system as a whole permits the determination of the dip of the dyke wall even where it is not exposed.

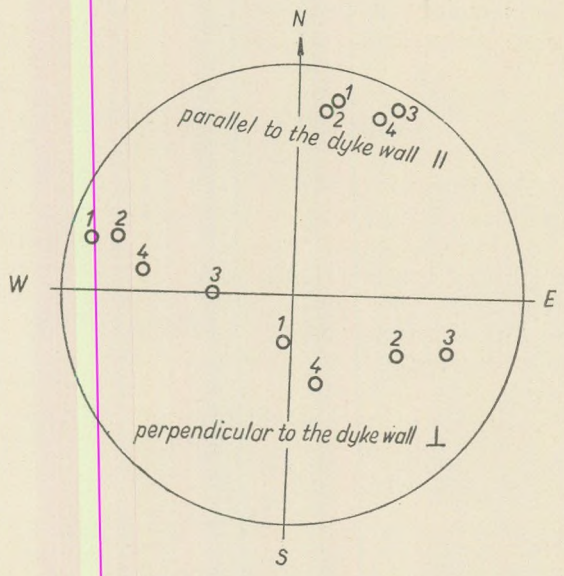

Fig. 16. Changes of orientation of the blocky joint system in a horizontal profile of the amafic andesite dyke of Peres Hill

(2) The regional distribution of the various forms of jointing permits some palaeogeographic and palaeovolcanologic conclusions to be drawn. The joint patterns of superimposed sequences of lava rocks show that the lavas of the first eruptions tended to form shield-like bodies over a relatively plane substratum, whereas the subsequent eruptions produced lava sheets and flows of smaller horizontal extent and deformed by lamination, as a result of the gradual build-up of the volcanic superstructure. The bronzitic augite andesite shield forming the volcanic base of the Ecskend plateau and the monogene fissure-volcano shields of the Nagy Hill, the Szanda and Bercel of the Middle Cserhát were lavas that had flowed into a smooth and horizontal or possibly concave relief. The lava sheets and flows with an exclusively laminar parting in the eastern part of the Middle Cserhát reflect a rather sloping terrain (stratovolcanic type). In the northeastern part of the Middle Cserhát the bedded and laminate structure of the bronzitic augite andesite indicates an earlier volcanism (this is substantiated also by chemical considerations), whereas on the Ecskend Plateau, the bronzitic augite andesite was the first eruption. All in all, the western part of the Middle Cserhát is characterized by shields that issued from monogenic fissure volcanoes; its eastern part has a stratovolcanic structure, whereas the eastern part of the Southwestern Cserhát (Ecskend Plateau) has a rudi-

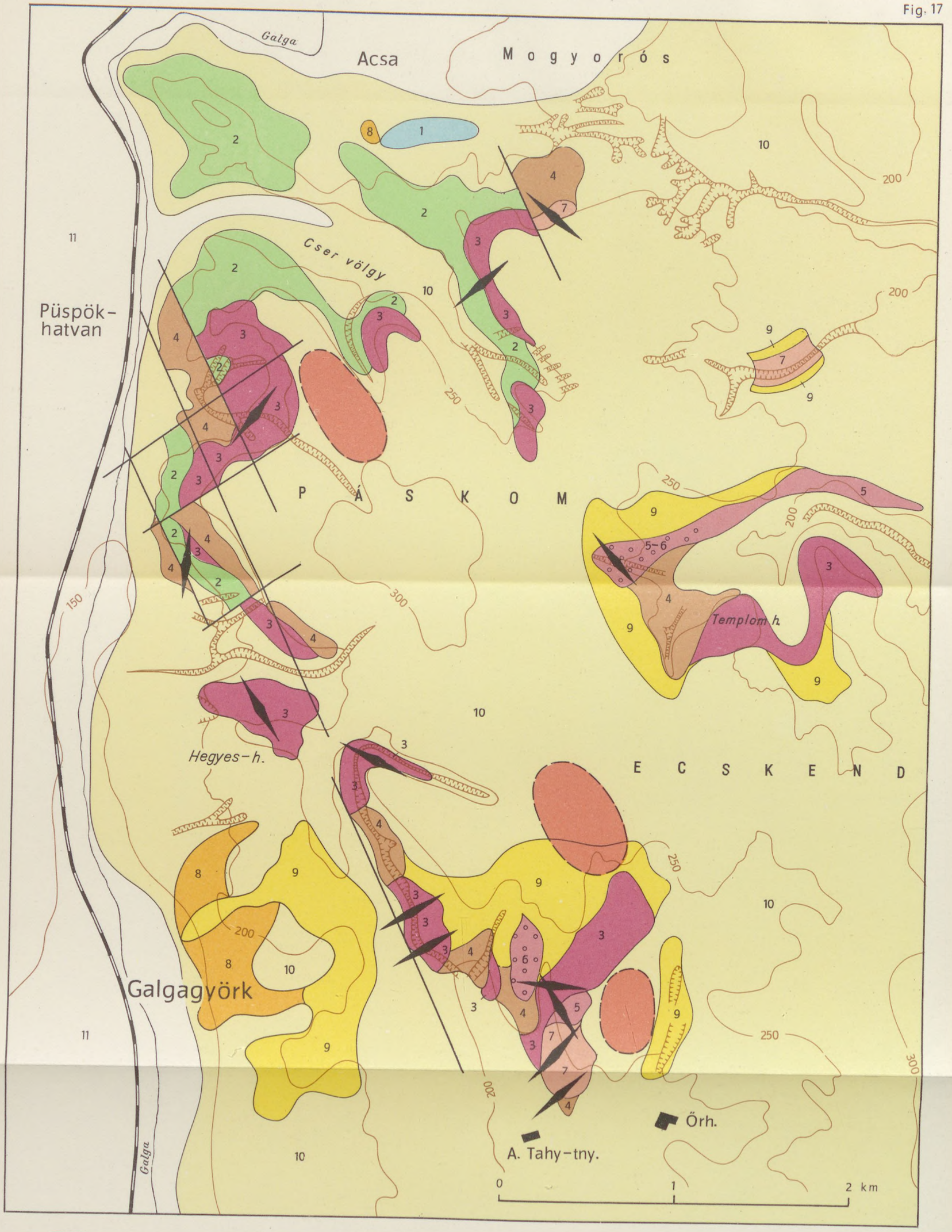

11 Recent floodplain deposites

10 Pleistocene loess

9 Pannonian sans clays

8 Sarmatian limestone

7 Microandesite

6 Vacuolar andesite

5 Amafic andesite

4 Andesite tuff and agglomerate

Suggested volcanic centres

3 Bronzitic augite andesite

2 Helvetian Schlier and sandy limestone

1 Upper oligocene sandy clay

Lava flow directions

Fault

mentary stratovolcanic structure overlying a basal shield of bronzitic augite andesite.

(3) The rapid petrofabric analysis of slides parallel to the ancient surface permits to determine the flow direction of the lava and to point out centres of volcanism. Fig. 17. shows the results of measurements on marginal outcrops of the Pannonian- and Pleistocene-covered Ecskend Plateau. The results suggest three centres of eruption.

REFERENCES

Árkai, P. (1967): A DNY-Cserhát földtani és kőzettani vizsgálata. (Geology and petrography of the Southwest Cserhát Hills.) D. Sc. Thesis.

Árkai, P. (1967): Correlation of quantitative petrographic characteristics of pyroxene andesites in the volcanic complex of the Southwestern Cserhát Hills. Ann. Univ. Sci. Budapestinensis Sectio Geol. XI.

Becker, G. F. (1893): Finite homogeneous strain, flow and rupture of rocks. Bull. Geol. Soc. Amer. 4. 13.

Benard, H. (1900): Les tourbillons cellulaires dans une nappe liquide. Rev. Gen. Sc. 11. 1261.

Bergt, W. (1914): Der Vulkan Quilotoa in Ecuador und seine schiefrige Laven. Veröffentl. d. Städt. Mus. f. Länderkunde in Leipzig H. 13.

Bernauer, F. (1936–39): Bewegungs- und Schwundformen von Laven. Zeitschr. für Vulkanologie 17.

Bernauer, F. (1937): Geschichtete Lava an isländischen Vulkanen. Zeitschr. d. Deutschen Geol. Ges. 89. 88.

Billings, N. (1952): Structural geology. New York.

Brinkmann, R. (1957): Kluft- und Korngefügeregelung in Vulkaniten. Geol. Rundschau. 46. 526.

Brothers, R. N. (1964): Petrofabric analysis of Rhum and Skaergaard layered rocks. J. Petrology 5.

Buda Gy. (1965): Statistische Verteilung und qualitative Kennzeichnung der Feldspate im Andesit-Lakkolit des Csódi-Berges. Annales Univ. Sci. Budapest. Sect. Geol. 9. 123.

Clark, R. H. (1952): The significance of flow structure in the microporphyritic ophitic basalt of Arthur's Seat. Trans. Geol. Soc. Edinburgh. 15. 69.

Cloos, H. – Cloos, E. (1927): Die Quellkuppe des Drachenfels am Rhein. Ihre Tektonik und Bildungsweise. Zeitschrift f. Vulkanologie 11. 33.

Cloos, H. – Cloos, E. (1927–28): Das Strömungbild der Wolkenburg im Siebengebirge. Zeitschr. f. Vulkanologie 11. 93.

Dauzère, C. (1908): Solidification cellulaire. J. Phys. 7. 930.

Dienes I. (1967): A nógrádi Medvés bazalttakarójának földtani vizsgálata. (Geology of the Medvés basalt sheet in Nógrád County, Hungary.) B. Sc. Thesis.

Eitel, W. (1932): Studien über die Strömungs-Vorgänge bei der vollautomatischen Glasverarbeitung im Owens-Prozess. Glastechn. Berichte 10.

Ferguson, D. K. (1936): The structure of the Queen's Canon rhyolite, Glen Coe, Argyllshire. Scot. J. Geol. 2. 153.

Glangeaud, P. (1913): Sur la prismation des roches volcaniques. C. R. Soc. Geol. France 12.

Hewes, L. J. (1948): A theory of surface cracks in mud and lava and resulting geometrical relations. Am. J. Sci. 248. 138.

Iddings, J. P. (1886): The columnar structure in the igneous rocks on Orange Mountain, New Jersey, A. J. Sci. 131. 321.

James, A. V. G. (1920): Factors producing columnar structure in lavas. J. Geol. 28. 458.

Klüpfel, W. (1952–53): Basaltgeologie. Zeitschr. d. Deutschen Geol. Ges. 104.

Lacroix, A. (1919): Dacites et dacitoïdes à propos des lavas de la Martinique. C. R. Ac. Sc. Paris 168. 207.

Lafeber, D. (1956): Columnar jointing and intercolumnar differentiation in basaltic rocks. Verh. Geol. Mijnb. Gen. 16. 245.

Longchambon, M. (1913): Considerations sur la formation des colonnes prismatiques dans les coulées de roches eruptives. Bull. Geol. Soc. France. 4. 13.
Mallet, R. (1875): On the origin and mechanism of production of the prismatic structure of basalt. Phil. Mag. 4. 122.
Philipp, H. (1921): Beitrag zur Kenntnis der Bewegungsvorgänge in hochviskosen geologischen Flüssigkeiten. Centralb. f. Miner. 679.
Philipp, H. (1936): Bewegung und Textur in magmatischen Schmelzflüssen. Geol. Rundschau 27.
Rudich, K. N.; Timerbajeva, K. M. (1965): Über gebänderte Laven des Vulkans Bolshaya Simina. Chetvert. Vulkanism Nekotorykh Rayonov SSSR 3–13.
Schmincke, H. U. (1967): Flow directions in Columbia river basalt flows and paleocurrents of interbedded sedimentary rocks, South-Central Washington. Geol. Rundschau, 56. 992.
Smedes, H. W.; Lang, A. J. (1955): Basalt column rinds caused by deuteric alteration. A. J. Sci. 253. 173.
Sosman, R. B. (1916): Types of prismatic structure in igneous rocks. Journ. Geol. 24. 215.
Spry, A. (1953): Flow structure and laminar flow in bostonite dykes at Armindale, New South Wales. Geol. Mag. 90. 248.
Spry, A. (1962): The origin of columnar jointing, particularly in basalt flows. Geol. Soc. Australia J. 8. 191.
Thomson, J. (1863): On the origin of the jointed structure in basalts and other igneous rocks. Trans. Brit. Ass. Adv. Sci. 33d meeting, Newcastle, 89.
Tomkieff, S. I. (1940): Bull. Volcanologique 6.
Trommsdorf, W. E.)1934): Fahrströmungen in Eruptivmagmen. Naturwiss. 22. 21.
Rittmann, A. (1960): Vulkane und ihre Tätigkeit. Stuttgart.
Szádeczky Kardoss E. (1958): A vulkáni hegységek kutatásának néhány alapkérdéséről. (On some fundamental problems of research in volcanic mountains.) Földt. Közl. 88.
Szőke A. (1966): Petrofabric analysis of magmatic rocks in the area of the Carpathian Tertiary volcanism. Acta Geol. 10.
Sander, B. (1948): Einführung in die Gefügekunde der geologischen Körper, Wien.
Waters, A. C. (1960): Determinig direction of flow in basalts. Am. J. Sci. 258-A. 350.

ON THE OLIGOCENE AND MIOCENE STAGES OF THE CENTRAL PARATETHYS AND ON THE FORMATIONS OF THE EGERIAN IN HUNGARY

by
T. BÁLDI
(Institute of Geology, Eötvös University)
(Received the 25th November 1968.)

SUMMARY

The author discusses by way of introduction the stage concept and some general problems of chronostratigraphy. Starting from his conclusions, he exposes the motives for the new terminology and subdivision lately proposed by Czechoslovak, Austrian and Hungarian authors for the Neogene of the Central Paratethys. The author outlines the field conditions, lithology, palaeontological content, faciology and extent of the formations distinguished so far within the Egerian stage in Hungary, namely those of the formations of Eger, Mór, Mány, Törökbálint and Kováčov. He finally proposes the introduction of a new stage, to be termed Kiscellian, and presumably easy to distinguish all over the Alpine-Carpathian region.

In 1968, a proposal coordinated by the Paratethys Working Team of the CMNS was made concerning a new subdivision of the Neogene into stages in the Central Paratethys area and suggesting a nomenclature for these stages. The new proposal and many of its aspects were discussed in papers by Papp (1968), Cicha et Seneš (1968) and Báldi (1968). In the present paper, the author wishes to raise some further questions and to make a few complementary remarks.

Necessity of introducing the new stages

The stage is a chronostratigraphic unit: "body of rock strata which is unified by representing the rocks formed during a specific interval of geologic time" (XXI. Intern.Geol.Congr., Copenhagen 1960, Att.-1, Sec.III, circ.11, p.7.) Going into details would be superfluous, as there is an excellent summary given by Reiss (1966) on the fundamental principles of stratigraphy in the spirit of the Copenhagen congress. Reiss writes. "It is a major goal of stratigraphic research to establish worldwide (or regional, as the case may be) agreement on the rank, scope, boundaries, geochronological position, and names of the exist-

ing chronostratigraphic units of particular value, in order to achieve – if possible – a single and uniform standard sequence of consecutive, but mutually exclusive, units to which geological events and geochronology could be related" (p. 16).

The establishment of chronostratigraphic subdivisions for restricted, regional usage, such as the one proposed for the Central Paratethys, is apparently at cross purposes with the aim stated above of setting up a standard sequence of stages covering the entire Earth. One is, however, forced to admit that no standard stratigraphic subdivision of such an all-embracing, global extent is possible as yet either on a world-wide scale or just in respect of the Paratethys. The reason for the difficulty of doing so is also clear: the stage boundaries (which should be isochronous surfaces in principle) are defined by means of lithostratigraphic or – more often and more efficiently – biostratigraphic interfaces. The restricted extent of lithostratigraphic units in space, the heterochronous nature of their conformable or unconformable boundaries are matters of common knowledge. The biostratigraphic boundaries (datum surfaces) can be traced over much more extensive areas and – considering the fast spread of new taxa, instantaneous on a geological time scale – can be considered isochronous (the approximation is particularly good in the case of acrozones or range zones based on evolutionary series). Even zonal boundaries based on pelagic organisms can often be recognized only in one or another area of the Earth, depending on the location of climatic or other barriers. Hence, *the recognition of stages is geographically limited in practice*, an idea that has found expression also at the Copenhagen congress: "Many stages are still primarily regional in usage and it should be recognized that useful stages may exist provisionally in one region which may not necessarily carry the same name or coincide in time scope with those of another region." (circ.14, p.9). A similar conclusion was stated also by the fourth, Bologna congress of the CMNS in 1967: "Also the succession of stages as proposed during the sessions in Vienna and Berne proves to be difficult to apply beyond certain regional limits."

In respect of the Paratethys, difficulties are multiplied by the more or less complete isolation of this sea basin, indeed, sometimes by its dissection into sub-basins: this is the justification for the restriction of the new stages to the Central Paratethys.

So far, no regional stratigraphic system with an idependent terminology has been set up for the Central Paratethys. The Neogene formations of this region were, on grounds of geographical proximity, identified partly with the Southwest European, and partly (in the case of the Oligocene) with the North German stages: this is how the well-known "Lattorfian – Rupelian – Chattian – Aquitanian – Burdigalian – Helvetian – Tortonian" set of terms was fitted to the stages of the Central Paratethys, with new stage names introduced only where all hope of correlation with Southwest Europe was lost owing to the complete isolation of the Paratethys (Sarmatian, Pannonian).

The development of correlational methodology has, however, made it clear that *the above names have often been used with incorrect content, on the basis of erroneous correlations*. It is wrong to speak of "our Tortonian", in case the formations in the Paratethys assigned to this term are older than the beds of the type section of Rio Mazzapiedi-Castellania, or to keep on calling Aquitanian

some deposits whose age has been proved to exceed that of the stratotype of the "Aquitanien". A scientific concept is expected to be unequivocal and clearly the terms Tortonian or Aquitanian must mean the same when referring to the Paratethys or Southwest Europe or any corner of the world, namely rocks formed within an interval of time defined by the stratotypes. The ambiguity of the terms in question was further enhanced by the fact that, precisely owing to the difficulties of correlation, one and the same formation was often placed into different stages by various authors. Since the local lithostratigraphic terminology is also highly lacunary, very few people besides the specialist could find their way through the ensuing complicated maze of terms. For instance, the Budafok formation was placed into the Chattian by Noszky sen., into the Aquitanian by Horusitzky and into the Burdigalian by Csepreghy-Meznerics. (Latest research has shown this formation to cover approximately the time span of the Aquitanian plus Burdigalian.)

All this is a full justification for considering the stratigraphic units of the Central Paratethys as independent stages and to express this state of facts by an appropriate terminology. New stages have to be defined on the basis of stratotypes, as postulated also by the fourth Congress of the CMNS: "The new units are likewise to be based on stratotype sections, to be chosen in such a manner that the boundaries are on, or close to, biostratigraphic zones." The new units are described in this sense in the series "Chronostratigraphie und Neostratotypen" (cf. Cicha et al. 1967).

The new stages are the following, in succession from the bottom upwards (Cicha et Seneš 1968, Papp 1968):

Egerian. Holostratotype Eger, North Hungary. Proposed by Seneš, Cicha, Papp, Báldi. Terminology used up to now: Chattian, Chatto-Aquitanian, Aquitanian, Upper Stampian; in the publications of the present author: Upper Oligocene.

Eggenburgian. Holostratotype: Loibersdorf (Niederösterreich). Proposed by Papp, Steininger, Seneš, Cicha. Terminology used up to now: lately mostly Burdigalian, earlier Lower Mediterranean, or Aquitanian too.

Ottnangian. Holostratotype: Ottnang (Oberösterreich). Proposed by Papp, Steininger, Seneš, Cicha. Terminology used up to now: lately Lower Helvetian, Helvetian s.str., Upper Burdigalian.

Carpathian. Holostratotype: Slup (Czechoslovakia). Proposed by Cicha and Tejkal in 1959. Terminology used up to now: lately Helvetian, Upper Helvetian, earlier also Burdigalian for some deeper-lying portions.

Badenian. Holostratotype: Sooss (Niederösterreich). Proposed by Kapounek, Papp, Turnovsky in 1960. Terminology used up to now: mainly Tortonian, for some of its older portions Grundian, Helvetian, Upper Mediterranean.

Sarmatian. Holostratotype: Nexing (Niederösterreich). Proposed by E. Suess in 1866.

Pannonian. Holostratotype: Vösendorf (Niederösterreich). Proposed by L. Telegdi–Roth in 1879.

Stratigraphic position and principal formations of the Egerian in Hungary

Of the stages enumerated above, I shall restrict discussion here to the Egerian. Leaving aside the details of research history, lithology and palaeontology, I shall attempt to hold the treatment at its most concise. In Hungary, the Egerian includes the Eger, Mór, Mány, Törökbálint and Kováčov formations, most of them in their entirety.

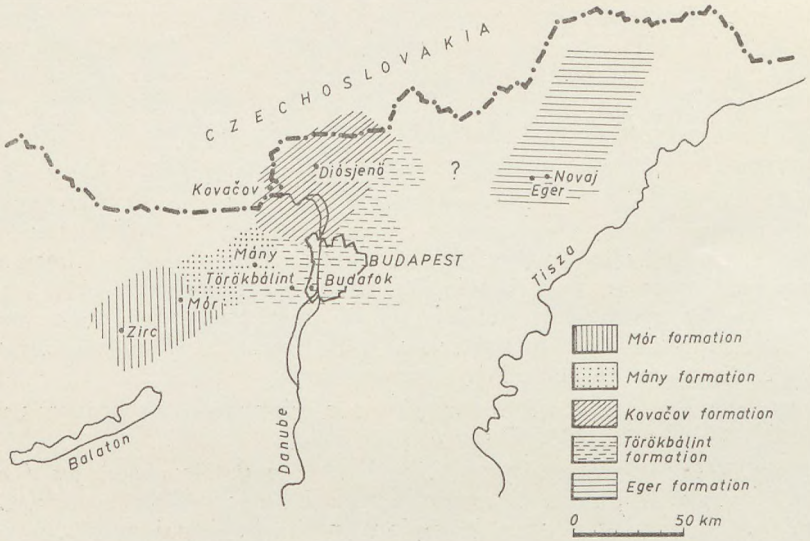

Fig. 1. Extent of the formations of the Egerian stage in Hungary

(1.) Eger formation

The best and most widely known disclosure of this formation is in the Wind Brickyard of Eger; it is the holostratotype of the stage. Another thoroughly studied section of the formation is that of the Nyárjas at Novaj near Eger, which latter will be described as a faciostratotype.

The section of the holostratotype (the disclosure of the Wind Brickyard at Eger) was described earlier (Báldi 1966). Concerning the section of the Nyárjas at Novaj cf. the papers by Báldi et al. (1961) and Drooger (1961). Taking into account also the other disclosures of the formation (Noszvaj–Nagyimány, Eger–Afrikadülő, Eger–Síkhegy, Eger–Vincellériskola (Verger School), Ostoros–Kerekhegy, the oil wells at Eger, Demjén, Bogács and Szomolya) the following comprehensive characterization can be given.

The Eger formation falls into four members, respectively four corresponding assemblage zones. The members are as follows.

a) *Glauconitic, tuffitic sandstone* which in the Novaj section and in some oil wells includes interbedded Lepidocyclina or lithothamnian limestone.

Thickness 20 to 40 m. Kenawy *(1968) demonstrated in it the Globigerina ampliapertura Zone.* The occurrence of *Miogypsina septentrionalis, Lepidocyclina morgani* and *L. tournoueri* (Drooger 1961, Báldi et al. 1961) is also of importance. Further forms of some frequency are *Operculina, Heterostegina, Flabellipecten burdigalensis, Chlamys csepreghymeznericsae, Megacardita arduini, Cerithium egerense, Diastoma grateloupi turritoapenninica, Pirula condita, P. concinna, Babylonia eburnoides umbilicosiformis, Volutilithes multicostata, Athleta rarispina.* The assemblage is complemented by some solitary corals, brachiopods, bryozoa and shark teeth.

b) *Molluscan clay.* 50 m thick. This member develops gradually from the preceding one. It contains a deep sublittoral-bathyal (120 to 300 m of sea depth) foraminifera and molluscan fauna, locally with species of *Schizaster* and fish scales. According to Kenawy (1968), *it belongs to the Globorotalia opima*

some deposits whose age has been proved to exceed that of the stratotype of the "Aquitanien". A scientific concept is expected to be unequivocal and clearly the terms Tortonian or Aquitanian must mean the same when referring to the Paratethys or Southwest Europe or any corner of the world, namely rocks formed within an interval of time defined by the stratotypes. The ambiguity of the terms in question was further enhanced by the fact that, precisely owing to the difficulties of correlation, one and the same formation was often placed into different stages by various authors. Since the local lithostratigraphic terminology is also highly lacunary, very few people besides the specialist could find their way through the ensuing complicated maze of terms. For instance, the Budafok formation was placed into the Chattian by Noszky sen., into the Aquitanian by Horusitzky and into the Burdigalian by Csepreghy-Meznerics. (Latest research has shown this formation to cover approximately the time span of the Aquitanian plus Burdigalian.)

All this is a full justification for considering the stratigraphic units of the Central Paratethys as independent stages and to express this state of facts by an appropriate terminology. New stages have to be defined on the basis of stratotypes, as postulated also by the fourth Congress of the CMNS: "The new units are likewise to be based on stratotype sections, to be chosen in such a manner that the boundaries are on, or close to, biostratigraphic zones." The new units are described in this sense in the series "Chronostratigraphie und Neostratotypen" (cf. Cicha et al. 1967).

The new stages are the following, in succession from the bottom upwards (Cicha et Seneš 1968, Papp 1968):

Egerian. Holostratotype Eger, North Hungary. Proposed by Seneš, Cicha, Papp, Báldi. Terminology used up to now: Chattian, Chatto-Aquitanian, Aquitanian, Upper Stampian; in the publications of the present author: Upper Oligocene.

Eggenburgian. Holostratotype: Loibersdorf (Niederösterreich). Proposed by Papp, Steininger, Seneš, Cicha. Terminology used up to now: lately mostly Burdigalian, earlier Lower Mediterranean, or Aquitanian too.

Chattian by K. Telegdi-Roth and Noszky sen., and with the Aquitanian of Southwest France by Gaál and Horusitzky and Seneš. Drooger held it to be Chattian on the basis of the occurrence of *Miogypsina septentrionalis*. My own studies of molluscs have led me to the conclusion (Báldi 1966) that it is contemporaneous with the Chattian stage, the "Tongriano" of Cassinelle, the Belluno and Schio beds and the Escornebéou—Peyrère niveau of the Aquitanian basin. This was confirmed by the plankton studies of Kenaway (1968), who stated the Eger formation to be Oligocene. Papp (1968) and Cicha et Seneš (1968) consider the Egerian a transitional stage between Oligocene and Miocene. The holostratotype at Eger is, however, according to all relevant data, Upper Oligocene in its entirety; the Eger formation does not pass the Oligocene—Miocene boundary. Besides the planktonic and larger foraminifera this is proved also by the molluscs. The molluscan fauna comprises 23 to 28 percent Oligocene and only 3 to 7 percent Miocene species (the rest are endemic or persistent). It is in the Eger formation that there appear first the following species, otherwise known as Miocene: *Limopsis anomala, Chlamys incomparabilis, Rostellaria dentata, Natica tigrina, Zonaria globosa, Euthriofusus burdigalensis, Strombus coronatus, Athleta ficulina, A. rarispina.*

(2.) Mór formation. Widespread in the Bakony Mountains from Mór to Zirc, built up of 40 to 400 m of clayey aleurite and clay, with interbeddings of biotitic sandstone and, at its base, with conglomerate intercalations and stringers or workable seams of lignite (Szápár). It unconformably rests on Mesozoic or Eocene rocks, and *underlies* Pleistocene, or marine Ottnangian and Badenian sands or limestones (Bántapuszta formation).

Its fauna is of exclusively fresh-water and oligohaline origin with *Brotia escheri, Viviparus cf. ventricosus, Unio inaequiradiatus, Pomatias antiquum, Coretus, Radix, Archaeozonites, Oestophora, Caracollina, Triptychia, Tropidomphalus, Parachlorea, Strophostoma* as the characteristic forms. There are also remains of vertebrates [*Anthracotherium* and a recent find of a jawbone of *Amphitragulus* (according to a preliminary identification by Hürzeler)].

This formation is considered Lower Oligocene by some and Miocene by others. Recent investigation has convinced me, however, that this formation is Egerian in full or for the most part and consequently Upper Oligocene. The following arguments are adduced:

a) The presence of *Amphitragulus* and *Caracollina, Triptychia, Tropidomphalus, Pomatias antiquum* and *Unio inaequiradiatus.*

b) Parachlorea, Strophostoma, Anthracotherium and *Pomatias antiquum* render improbable the Miocene age of the formation.

c) The formation laterally passes into the Mány formation which by its marine fauna is Egerian beyond doubt.

(3.) Mány formation. Occurring in the basins of the Vértes and Gerecse Mountains, it consists of 100 to 500 m of clayey aleurite and aleuritic clay, little-consolidated biotitic fine-grained sandstone, with a few intercalated conglomerates and stringers of lignite.

It unconformably rests on Triassic or Eocene rocks and likewise unconformably *underlies* Upper Badenian or Sarmatian clay or limestone.

Just like the previous formation, this one is also largely known from borehole cores. It passes laterally into the Mór formation to the West, into the Törökbálint formation to the East and into the Kováčov formation to the North-East.

From this formation I have described *four assemblage zones*, as follows (B á l d i 1967):

a) *Lowermost (Polymesoda) Zone of a dominant brackish-lagoonal facies* with the species *Polymesoda convexa, Ostrea cyathula, Gari protracta, Theodoxus pictus, Th. crenulatus, Hydrobia ventrosa, Melanopsis impressa hantkeni, Tympanotonus margaritaceus, Pirenella plicata* and *Congeria basteroti* ("Cyrena beds" of early literature). Accompanied by a few limnic interbeddings with *Viviparus* and *Brotia*.

b) *Diplodonta Zone.* Masses of *Taras (=Diplodonta) rotundatus, Pitar polytropa, Cardium bojorum, Turritella venus.* This is essentially *an alternation of shallow sublittoral (1 to 30 m of sea depth) beds and Polymesoda-bearing, brackish-lagoonal strata* (="Cyrena beds"), locally with the dominance of the latter. Limnic interbeddings are few and far between.

c) *Angulus Zone. Dominant shallow sublittoral facies, with frequent brackish-lagoonal interbeddings* with *Polymesoda.* Besides *Angulus nysti* and the already enumerated species of the *Diplodonta* Zone, the most frequent species are *Pitar beyrichi, Anomia ephippium, Cultellus budensis, Ensis hausmanni,* whereas the typical forms *Glycymeris latiradiata s.l.* and *Laevicardium tenuisulcatum* are more scarce.

d) *Incomparabilis Zone. Dominant medium-depth sublittoral facies* (30 to 120 m of sea depth) with scarce shallow sublittoral interbeddings. Lagoonal interbeddings are restricted to a few sections. This zone is encountered only in the eastern part of the formation area, indicating a transition towards the Törökbálint formation. In the latter this zone is greatly thickened and typical of the entire formation. Its more common species are *Chlamys incomparabilis (=textus), Laevicardium cyprium, Angulus posterus, Cardium heeri, Cardita orbicularis subparvocostata, Astarte gracilis degrangei, Cyprina islandica rotundata, Pholadomya puschi, Flabellipecten burdigalensis, Turritella venus, Drepanocheilus speciosus, Pirula concinna* and also *Dentalium, Bryozoa* and *Schizaster.*

The succession of the assemblage zones indicates a transgression. Unfortunately, part of the *Incomparabilis* Zone and its presumable cover (the regressive portion of the sedimentary cycle) were eroded during the Lower Miocene.

(4.) Törökbálint formation. Clayey aleurite and little consolidated fine-grained sandstone of 200 m mean thickness, with a few interbeddings of sand. Most extensive about Budapest, with lateral passages to the Mány formation to the West and the Kováčov formation to the North.

It *overlies* conformably the Kiscell clay, and *underlies* likewise conformably the Budafok formation. This latter contains the typical Lower Miocene species of the Eggenburgian stage *(Glycymeris fichteli, Laevicardium kübecki, Pecten pseudobeudanti, Chlamys gigas, Ch. holgeri, Ch. palmata, Turritella terebralis, Phalium subsulcosum, Galeodes cornuta, Tudicla rusticula,* etc.).

The abundant molluscan fauna of the Törökbálint formation was the subject of an earlier description (Báldi 1963, 1964). The most frequent species are: *Nucula comta, Nuculoma laevigata, Glycymeris latiradiata obovatoides, Pteria phalenacaea, Chlamys incomparabilis, Ostrea cyathula, Astarte gracilis degrangei, Cardita orbicularis subparvocostata, Phacoides borealis, Laevicardium cyprium, L. tenuisulcatum, Pitar beyrichi, Angulus nysti, Pholadomya puschi, Turritella venus, Drepanocheilus speciosus, Polinices catena achatensis, Pirula concinna, Turris laticlavia, T. duchasteli, Turricula regularis, Dentalium kickxi.* There are also Bryozoa and species of *Schizaster.*

The formation is *largely of medium-depth sublittoral* origin (30 to 120 m of sea depth) *with fairly numerous shallow sublittoral interbeddings* (1 to 30 m). Indications of brackish and limnic influences are visible only in the uppermost levels. Common species of these topmost levels are: *Glycymeris latiradiata s.l., Pecten arcuatus, Ostrea cyathula, Crassatella carcarensis, Linga columbella, Corbula carinata, Turritella venus, Tympanotonus margaritaceus, Pirenella plicata.* The occurence of *Globularia gibberosa sanctistephani* and that of *Egerea collectiva* is noteworthy.

According to Kenawy (1968) the Törökbálint formation *belongs to the Globorotalia opima opima Zone.*

Since the investigations of Hofmann and Fuchs, the Törökbálint strata have been considered equivalent to the Chattian stage. Between 1956 and 1960 they were held to be Aquitanian by Csepreghy–Meznerics and Seneš. Recent investigation of the molluscs and plankton proves an Oligocene age.

(5) Kováčov formation

200 to 500 m of clayey aleurite, sand, gravelly coarse sand with a few stringers of lignite (especially near the top).

It extends north of Budapest from the Pilis Mountains up to the Western Cserhát Mountains (Dorog Basin, Szentendre–Visegrád Mountains, Eastern Börzsöny and Western Cserhát).

It is characterized by the *dominance of a shallow sublittoral fauna* (sea depth 1 to 30 m) ("Pectunculus sands" in earlier literature), but there are also *fairly frequent littoral-brackish interbeddings* ("Potamides strata") and sometimes also lagoonal ones ("Cyrena beds"). The older portions include medium-depth sublittoral, the younger ones also limnic and even terrestrial faunae.

This formation *overlies* the Kiscell clay and is covered by the bryozoan limestone and Chlamys sandstone of the Carpathian. In the Cserhát Hills, however, its cover is the Budafok formation with sands containing *Anomia* and larger *Pectinids*, together with an *Eggenburgian* fauna.

The richest locality of the formation is Kováčov in South Slovakia, where molluscs were described by Seneš (1958). Its more important Hungarian localities are Kesztölc, Dömös, Leányfalu, Göd, Pomáz, Diósjenő, Becske, Dejtár. The most common and most typical species of the formation are, largely on the basis of the above localities: *Nucula schmidti, Anadara diluvii, Trisidos schafarziki, Glycymeris latiradiata subfichteli, Mytilus aquitanicus, Anomia ephippium, Ostrea cyathula, Crassatella carcarensis, Cyprina islandica*

rotundata, Taras rotundatus, Cardium bojorum, Laevicardium tenuisulcatum, Pitar polytropa, P. undata, Venus multilamella, Lutraria oblonga soror, Gari protracta, Solecurtus basteroti, Angulus nysti, Corbula carinata, Pholadomya puschi, Thracia pubescens, Turritella venus, T. beyrichi, Protoma cathedralis, P quadricanaliculata, Tympanotonus margaritaceus, Pirenella plicata, Diastoma grateloupi turritoapenninica, Aporrhais callosa, Drepanocheilus speciosus, Rostellaria dentata, Polinices catena, Ampullina crassatina, Globularia gibberosa sanctistephani, Bullia hungarica, Babylonia eburnoides umbilicosiformis, Athleta rarispina, Turricula regularis

Proposal concerning the introduction of a Kiscellian stage

The Egerian usually conformably overlies the Kiscell clay. The latter is currently held to be Rupelian. A control of the correctness of this assumption is a task of the future. It seems desirable, however, to introduce, for reasons of coherence, independently of the views on correlation that be, the concept of a Kiscellian stage, on the pattern of the new subdivision of the Neogene. Its holostratotype would be the best brickyard disclosure of Kiscell in Budapest, its faciostratotypes should be designated at Törökbálint and Eger. The lower and upper boundaries of the Kiscellian should be dated by planktonic foraminifera, all the more so since this formation is rich in plankton. For its upper boundary the cropping up of masses of *Globigerina ampliapertura* with the simultaneous disappearance of *Clavulinoides szabói*, as described by Kenawy (1968), seems appropriate. Its lower boundary would coincide with the lower limit of the fourth, *Globigerina*-rich assemblage zone of Majzon (1966)

REFERENCES

XXI. Intern. Geol. Congr., Copenhagen 1960. Statement of Principles of Stratigraphic Classification and Terminology. Report of the Intern. Subcommission on Stratigraphic Terminoy logy of the ICS.

Results of the fourth Assembly of the Committee for Mediterranean Neogene Stratigraphe (CMNS). Bologna 1967.

Andreánszky, G. (1966): On the Upper Oligocene Flora of Hungary. Analysis of the site at the Wind brickyard, Eger. Akadémiai Kiadó, Budapest.

Báldi, T., Kecskeméti, T., Nyirő, M. R. et Drooger, C. W. (1961): Neue Angaben zur Grenzziehung zwischen Chatt und Aquitan in der Umgebung von Eger (Nordungarn). Ann. Mus. Nat. Hung., 53, p. 67–132.

Báldi, T. (1963): Die oberoligozäne Molluskenfauna von Törökbálint. Ann. Mus. Nat. Hung., 55, p. 71–107.

Báldi, T. (1964): Über das Alter des „Pectunculussandes" von Törökbálint und das Problem der Oligozän–Miozän-Grenze. Ann. Mus. Nat. Hung., 56, p. 135–152.

Báldi, T. (1966): Die oberoligozäne Molluskenfauna von Eger und die Neuuntersuchung der Schichtfolge. Ann. Mus. Nat. Hung., 58. p. 69–101.

Báldi, T. (1967): A Mány–Zsámbéki-medence felsőoligocén makrofaunája. (German abstract: Oberoligozäne Makrofauna des Beckens von Mány–Zsámbék. Földt. Közl. 97, p. 437–446.

Báldi, T. (1968): Az európai neogén emeletek helyzetéről. (Hungarian. On the position of the Neogene stages of Europe.) Földt. Közl., 98, p. 285–289.

Cicha, I., Seneš, J. et Tejkal, J. (1967): M_3 (Karpatien). Die karpatische Serie und ihre Stratotypen. *(In* Chronostratigraphie und Neostratotypen, 1, Bratislava, p. 312.

Cicha, I. et Seneš, J. (1968): Sur la position du miocène de la Paratethys centrale dans le cadre du tertiaire de l'Europe. Geol. Sborn. 19, p. 95–116.

Csepreghy-Meznerics, I., et Seneš, J. (1957): Neue Ergebnisse der stratigraphischen Untersuchungen miozäner Schichten in der Südslowakei und Nordungarn. Neues Jb. Geol. Pal., Mh., 1, p. 1–13.

Csepreghy-Meznerics, I. (1962): Das Problem des „Chatt"-Aquitans in wissenschaftsgeschichtlicher Beleuchtung. Ann. Mus. Nat. Hung., 54, p. 57–71.

Drooger, C. W. (1961): Miogypsina in Hungary. Proc. Koninkl. Nederl. Ak. Wetensch., Ser. B, 64, p. 417–427.

Drooger, C. W. (1964): Problems of mid-Tertiary stratigraphic Interpretation. Micropaleontology, 10, p. 369–374.

Kenawy, A. I. (1968): Planctonic Foraminifera from the Oligocene and Lower Miocene of Hungary. Ann. Univ. Sci. Budapestinensis, Sect. geol., 11, p. 133–201.

Majzon, L. (1966): Foraminiferavizsgálatok. (Hungarian. Foraminifera studies.) Akadémiai Kiadó, Budapest, p. 939.

Papp, A. (1958): Nomenclature of the Neogene of Austria. Verhandlungen d. Geol. Bundesanst., p. 19–27. In co-operation with R. Grill, R. Janoschek, J. Kapounek, K. Kollmann, K. Turnovsky.

Reiss, Z. (1964): Significance of stratigraphic Categories – a Review. IUGS. C. on Mediterranean Neogene Stratigraphy, Proc. of the third Session in Berne; Brill, Leiden 1966, p. 9–17.

Seneš, J. (1958): Pectunculus-Sande und Egerer Faunentypus im Tertiär bei Kováčov im Karpatenbecken. Geol. Práce, Monogr, ser. p. 232.

Vadász, E. (1960): Magyarország földtana. (Hungarian. Geology of Hungary, 2. edit.) Akadémiai Kiadó, Budapest, p. 646.

OBERPLEISTOZÄNE TUNDRAPHASEN UND IHRE FEINGLIEDERUNG IM PROFIL MIT ÜBERRESTEN EINER MOUSTÉRIEN-KULTUR VON ÉRD BEI BUDAPEST

von
P. KRIVÁN
(Geologisches Institut der Eötvös-Universität, Budapest)
(Eingegangen dem 29. XI. 1968.)

SUMMARY

The Mousterian finds of Érd were embedded in the fill of two Rissian-Würmian valley-heads of parallel axes, sculpted in a Sarmatian limestone. The base of the fill is an autochthonous Riss-Würmian red earth. The deposition of the Mousterian remains covered the period from the end of the Riss-Würm interglacial to the end of the first, introductory (cryophile) part of the $Würm_I$ glaciation. The excellent long-range stratigraphic correlation possibilities of the Érd locality make the end of this episode contemporaneous with the "Brörup" phase of interstadial character. The relationship of the Érd and Tata Mousterian has also been clarified: the Tata Mousterian is younger, having come to exist at the end of the $Würm_{I\alpha}$ phase.

The introductory ice-forming (cryophile) phase of the $Würm_I$ can be subdivided on the basis of the fundamental profile of Tata and even more of the fundamental profile of Érd, which gives the most detailed subdivision of all, into 11 tundra episodes within the tundra phase "A" (Table 1). The introductory phase of the $Würm_I$ is trisected by two brief episodes of loess deposition, marking the brief episodes of glaciation preceding the Amersfoort "interstadial" and placed between the Amersfoort and Brörup "interstadials" (Figs. 1, 3). In the further course of this Würmian phase there are four longer tundra phases ("B", "C", "D", "E"). Of these, "D" and "E" divide up into three episodes each. The number of tundra phases in the Érd profile is five, with a total number of 19 episodes. The stratigraphy of the episodes is given in the comprehensive table.

Die morfogenetische Lage der Talausfüllung

Die die Kulturschichten enthaltende Talausfüllung detritischen Ursprungs lagert in einem Taltorso, entstanden entlang von zwei parallelen Bruchzonen von NNO-SSW-Streichen. Die dicht nebeneinander liegenden und auch in ihrer Entwicklung parallelen Täler, in 18 bis 22 m Länge erhalten und durch steile Talköpfe abgeschlossen, sind in die Oberfläche eines plattig-bankigen Sarmatkalkes eingeschnitten: die obenerwähnten Brüche und auch die Talachsen zeigen in die Richtung des Einfallens der Sarmatschichten, und die Talsohlen sind mit den Sarmatschichten isoklinal.

Obzwar die Kalkbank an der Talsohle ziemlich massiv war und die Neigung der Talsohle bei 6 bis 8° festlegte und auch die in den archäologischen Auf-

schlüssen bargelegten und die Talbildung bedingenden Brüche als geschlossen gelten müssen (selbst die sichtbaren Bruchspalten sind durch eine aus dem Detritus des Kalkes bestehende und durch eisenhaltige und kalkige Bindestoffe zementierte Ausfüllung verstopft), sind an der Talsohle anfängliche Karrformen, Karstformen (rudimentäre Schlünde) sichtbar. Diese Karstformen gehören zu den Produkten einer kurzfristigen epigenetischen Talentwicklung, welche von der Zeit des Rückgreifens eines Haupttales (das sich im Streichen des Sarmatkalkes, entlang von NNW-SSO streichenden Querbrüchen des Gebirges entwickelte) und die dadurch bedingte Köpfung der kleinen Talabschnitte bis zum Anfang der Talausfüllung dauerte.

Folglich hat die rückgreifende Einschneidung des heutigen Haupttales entlang der Querbrüche das einstige Haupttal geköpft und durch die Einteufung seiner Talsohle in seiner Entwicklung gehindert und endlich zu einem hangenden Seitental, einem Taltorso degradiert.

Die in ihrer Entwicklung gehemmte, morphologisch in Hängelage geratene Talkopfgruppe (heute beträgt der Unterschied zwischen den Talsohlenniveaus 8 m) wurde zeitweise durch eingeschwemmtes Material verdammt und die aufgestauten Gewässer hatten die Entstehung rudimentärer Karstformen zur Folge. Die Weiterentwicklung dieser Formen ist jedoch durch die bedeutend beschleunigte Einschwemmung von Spülmaterial und durch die Auffüllung der Täler gehemmt und abgeschlossen worden.

Später wurde die Talkopfgruppe mitsamt Taltorsos voll aufgefüllt und derart verhüllt, dass H u n y a d i (1962) bei der Bekanntgabe der Vertebratenfunde in der Talausfüllung unter Bezugnahme auf die Zusammensetzung der Fauna (Höhlenbär!) beim Anblick der mit einem kalkigen Bindemittel zementierten Sarmatkalkplatten im Hangenden der detritischen fossilführenden Schicht, die sowieso eine dem Einfallen der anstehenden Sarmatschichten parallele Neigung aufwiesen, von einer Höhlenbildung, von der Entstehung einer Felsnische schreiben konnte.

Die Talfüllung und ihre paläoklimatologische Aussage

Die Schichtenreihe der Talfüllung besteht aus detritischen Bildungen von teils auto-, teils allochthonem Skelett. Die ersteren stammen vom sarmatischen Rahmen der Talgruppe her, die letzteren aus dem Lösskomplex. Beide Typen von Detritus kommen als Skelett auch in pleistozänen und rezenten Böden vor. In ihrer Dynamik sind jedoch die Bodenbildungsprozesse über Sarmatschutt denen der Lössböden gleich — eben weil der Löss aus dem sarmatischen Rahmen bedeutend Kalk aufnehmen konnte — und ist eindeutig rendzinisch veranlangt. Als Ausnahme soll das älteste Glied der Schichtenreihe angeführt werden, ein rötlichbrauner Waldboden, der, über dem sarmatischen Detritus entwickelt und in Fetzen und Flecken erhalten, mediterrane klimatische Einflüsse erkennen lässt.

Der Skelett der Kulturschichten ist aus dem in Körner zerfallene Verwitterungsergebnis des Sarmatkalkes zusammengehäuft: er besteht überwiegend aus Körner unter 0,1 mm ∅. Sein Kalkgehalt schwankt zwischen 75 und 85% und die Dominanz des Kalkes bleibt selbst in den Eluvionszonen der Bodenbildung erhalten.

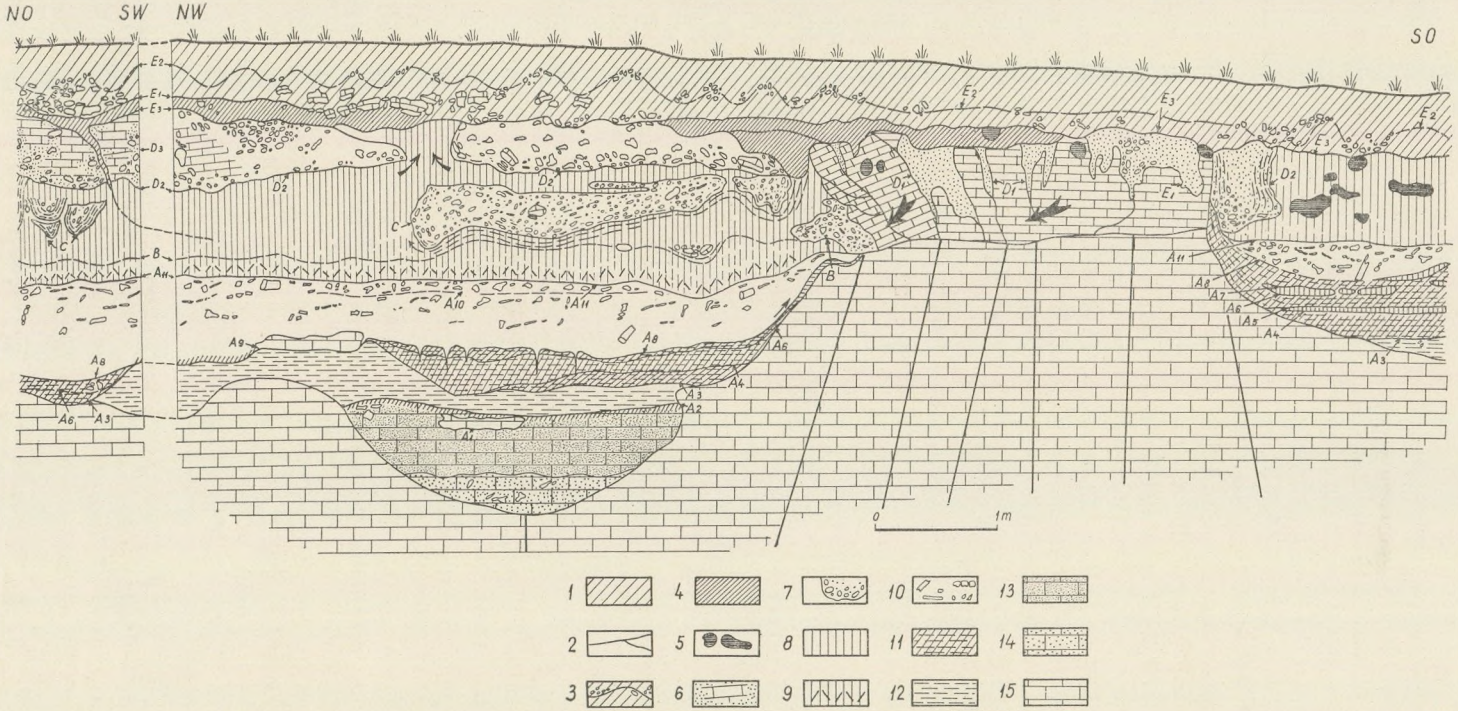

Abb. 1. Zusammenfassender Transversalschnitt durch das Würm-Fundamentalprofil von Érd. Die Deutung der Ablagerungen und der Ausfüllungsprozesse des Tales sowie die Zeichenerklärung sind in der Tabelle gegeben

1: Rendzina, 2: Eisblättigkeit und Eislinsen, 3: Girlandentundra von Sarmatkalk, 4: Rudimentäre Rendzina, 5: Krotowina, 6: Grobdetritus und Blöken von Saramatkalk, 7: Tundra mit Eissäcken, 8: Löss, 9: Löss mit Detritus von Sarmatkalk, 10: Knochen, 11: Rendzina über feinkörnigem Sarmatkalkdetritus, 12: Feinkörnigen Sarmatkalkdetritus, 13—14: Sarmatkalkdetritus, 15: Sarmatkalk.

Es soll bemerkt werden, dass die Anhäufung dieses Skelettes ein ziemlich langsamer Prozess der Übereinanderlagerung von Schichten war, der noch gerade mit der Anhäufung des archäologischen Materials Schritt halten konnte. Der parallele Fortschritt der Aufhäufung und Eindeckung des archäologischen Materials war andererseits ein sehr glücklicher Umstand für die feinstratigrafische Gliederung der Schichtenreihe und für die Rekonstruktion der Ereignisreihe und der paläoklimatologischen Entwicklung.

Die groben Zerkleinerungsprodukte, Steinblöcke des Sarmatkalkes wurden in die Schichtenreihen der Taltorsos nur in den Tundraphasen eingebaut, entlang von eigenartigen, unverkennbaren Tundra-Transportflächen.

Abgesehen von zwei dünnen Zwischenlagerungen liegen die Lössbildungen im Hangenden der Kulturschichten. Nach ihrer Korngrössenverteilung sind sie als lehmig-aleuritische Lössabarten anzusprechen, mit etwa 50% der Körner in den obengenannten Fraktionen. Die Zahl der Körner über 0,1 mm ist verschwindend klein, höchstens einige %. Diese Ergebnisse beziehen sich auf von Kalk befreites Material.

Der hauptsächlich lokal entstandene Kalkgehalt der Lössbildungen schwankt zwischen 35 und 55%, örtlich mit schwacher Auslaugung bzw. Anreicherung.

Die als Skelett der Kulturschichten fungierenden Verwitterungsprodukte des Sarmatkalkes liegen unten mit einer Ablagerungsgrenzfläche über dem rötlichbraunen Boden und über dem keine Kulturreste enthaltenden zusammengeschwemmten Kalkdetritus, der die rudimentären Schlünde im mittleren Talabschnitt ausfüllt. Die Aufschwemmungen des Kalkdetritus sind zuerst durch eine kolluviale Ablagerungsgrenzfläche, dann durch neun periglazial-solifluidale Grenzflächen der Abtragung und Ablagerung gegliedert, sowie durch drei rudimentäre Rendzinalagen (unter den Periglazial-Solifluidalflächen 2., 4., 8.) und zwei Lösschichten (unter den Flächen 5. und 7.)

Die Schichten im Hangenden der Kulturschichten gestatten eine ähnlich feine Gliederung.

Bei der stratigrafischen Einfügung der Kulturschichten kommt den nicht zu stark ausgeprägten Solifluidalflächen, welche als kleine Schwankungen innerhalb einer und derselben Tundraphase angesehen werden dürfen und folglich zusammen mit den Lösslagen und den Episoden der Bodenbildung eine vollständige und eingehende Gliederung der Zeitspanne ihrer Bildung ermöglichen, eine wichtige Bedeutung zu. Diese Solifluidalprozesse haben neben einer minimalen Austragung von Material (nicht Durchbewegung!) gar keine Umhäufung der Siedlung bewirkt, die Herde oder die originelle Lagerung der Kulturreste nicht im mindesten gestört. Daraus folgt, dass die Gesamtheit der Kulturschichten archäologisch eine einzige und einheitliche Schichtenentwicklungsgeschichte im autochthonen Zustand darstellt.

Die Reihe der Kulturschichten wird oben durch die Periglazial-Solifluidalfläche Nr. 10 abgeschlossen, die auch der Zusammenschwemmung des sarmatischen Detritus ein Ende bereitet. Darüber liegen bereits Lössbildungen mit mehrfacher tundrischer Umhäufung und Anhäufung (Eislinsen, Eiskeile, Eissäcke als Tundraerscheinungen, Solifluidalflächen), welche die periglazialen Ereignisse der letzten Vereisungsphase in grosser Auflösung darstellen.

Zusammenfassend lässt sich feststellen, dass die mediterrane Klimaphase vor der Ablagerung der Kulturschichten (rötlichbraune Erde) in eine langdauernde ozeanische, feucht-kühle, niederschlagsreiche Phase überging, die schwache, aber häufig sich wiederholende subarktische Züge aufweist, und zweimal durch kontinentale, kalt-trockene Episoden (Lössbildung) unterbrochen wurde. Diese Klimaphase spielte die Rolle der sog. eisbildenden Phase, die der fortdauernden Lössbildung vorangeht und diese einleitet. Wenn wir die zwei lössbildenden Episoden dieser eisbildenden Phase ihrer klimatischen Bedeutung gemäss als zwei kurze Stadialen auffassen, so sollen die Schichten zwischen ihnen einerseits und zwischen der jüngeren und der darauffolgenden höheren Lösschicht bzw. die über diesen Schichten vorliegenden begrabenen Bodenrudimente anderseits als die Bildungen je einer Interstadiale aufgefasst werden.

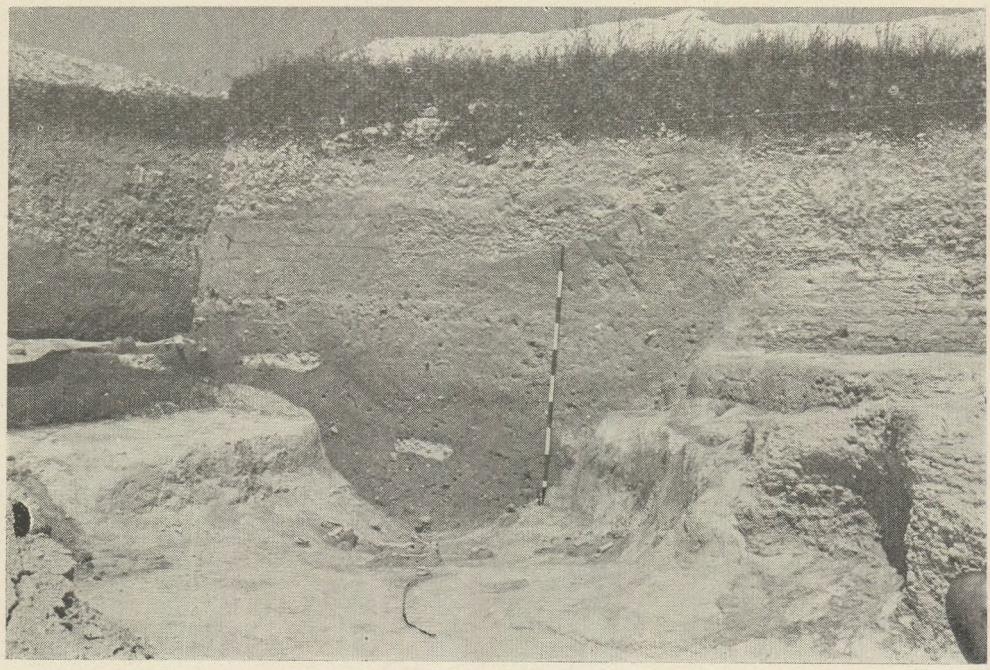

Abb. 2. Schaubild des Transversalschnittes

Später ist dann die durch die Stabilisierung der Lössbildung bewiesene kontinental-kalt-trockene Klimaphase durch eine kurze niederschlagsreiche ozeanische Klimaepisode abgewechselt worden, mit subarktischem Klima in der Umgebung (Eiskeile); die Lössbildung hörte für längere Zeit auf, und es trat die tiefgreifendste tundrisch bedingte Umhäufung der hangenden Schichtenreihe ein, als Ergebnis einer weiteren subarktisch-tundrischen Klimaphase (eine von Tundraphasen eingerahmte Interstadiale: die Tundraphasen schliessen einerseits eine Vereisungsphase ab, andrerseits führen sie eine neue Vereisungsphase ein).

Da die Talfüllung in den vorangehenden Klimaphasen bereits fast die jetzige Höhe des Reliefs erreichte, und Talköpfe und Taltorsos dadurch morfologisch verhüllt worden sind, ergaben die weiteren Klimaphasen nur reduziertere, kondensiertere Schichtenreihen. Diese lassen jedoch noch weitere zwei Lössbildungsphasen (Kontinental-Trockenklima) und zwei ozeanische Phasen mit anschliessenden und eine weitere Gliederung zulassenden subarktischen ozeanischen Phasen (Eiskeile-Säcke, Eislinsen-Eisblättrigkeit) erkennen.

Stratigrafische Einfügung der Talfüllung

Die durch die oben skizzierte Analyse aufgeschlossene paläoklimatische Ereignisfolge der Talausfüllung gestattet istet Kenntnis der Ereignisse des Würm in Ungarn auch eine stratigrafische Einfügung der Schichtenreihe. Bei dieser Tätigkeit wurden die Ergebnisse der ungarischen Lösstratigrafie herangezogen, sowie die Fundamentalprofile, die die Anfangs- bzw. Endphase der Würmeiszeit in grösster Auflösung zeigen· der Profilteil für die Anfangsphase aus dem Profil des oberpleistozänen Süsswasserkalkes von Tata und das feinstgegliederte Profil der Endphase, die Schichtenreihe der Aueterrassen der Donau bei Szekszárd.

Beide Profile sind durch C^{14}-Altersangaben kalibriert.

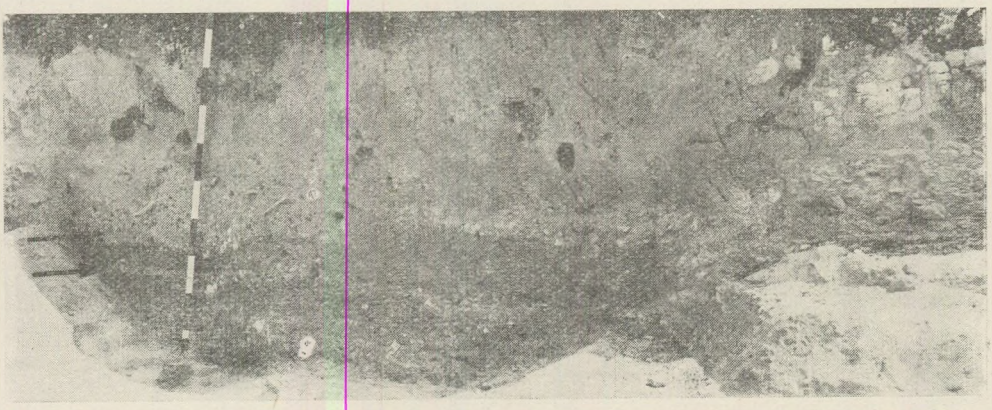

Abb. 3. Transversalschnitt der Lösslagen, die die Anfangsphase des $Würm_I$ in der südlichen Talausfüllung gliedern (vor der Amersfoort-„Interstadiale"; zwischen den beiden „Interstadialen" Amersfoort und Brörup; durch Pfeile angedeutet)

Da Verfasser die Schichtenreihe des Fundamentalprofils von Tata früher bereits korrekt eingefügt und mit der aus den Würm-Fundamentalprofilen der Niederlanden abgeklärten Gliederung parallelisiert hatte, ist er nun in der Lage, auch das Profil von Érd mit dem Tata-Profil zu parallelisieren.

Die Ergebnisse dieser Tätigkeit sind aus der angeschlossenen Tabelle zu ersehen.

Danach liegen die Schichten mit Moustérien-Kultur, die die Talkopf- und Taltorsogruppe von Érd ausfüllen, in der Zeitspanne zwischen dem Ende der Riss-Würm-Interglaziale und dem Ende der „Brörup-Interstadiale".

Tabelle 1.

Schichtenreihe der Talfüllung (Ereignisreihe der Ablagerung)	Bezeichnung der Grenzflächen der Ablagerung	Alter der Schichten	
Rendzina		Holozän	
Eisblättrigkeit und Eislinsen. Ruhende Tundra mit Kalkplatten	E_3	$Würm_3$	$Dryas_2$
Rudimentäre Rendzina			Alleröd
Girlandentundra mit Grobdetritus aus Sarmatkalk	E_2		$Dryas_1$
Rudimentäre Rendzina			Bölling
Tundra mit Fissäcken, mit einer aus Sarmatkalk entstandenen feinkörnigen schwach rendzinisierten Ausfüllung	E_1		$Dryas_0$
Tundra mit Eiskeilen und Säcken mit der gleichen Ausfüllung wie oben	D_3	$Würm_2 - Würm_3$	
Rudimentäre Rendzina über mit Sarmatkalkdetritus vermengtem Lösskelett			
Tundra mit Fissäcken, tiefgreifende solifluidale Umhäufung mit fein- und grobkörnigem Detritus und Blöcken von Sarmatkalk	D_2		
Tundra mit Eiskeilen und Säcken mit aus Sarmatkalk entstandener feinkörniger Ausfüllung	D_1		
Löss		$Würm_2$	
Tundra mit Eissäcken, mit Fein- und Grobdetritus aus Sarmatkalk	C	$Würm_{1\beta} - Würm_2$	
Löss		$Würm_1$	$Würm_{1\beta}$
Tundra mit Eissäcken, ausgefüllt mit einem Gemisch von Löss und Detritus von Sarmatkalk	B		$Würm_{1\alpha} - Würm_{1\beta}$
Löss mit Detritus von Sarmatkalk	A_{II}		(Moustérien von Tata)

Tabelle I.

	Schichtenreihe der Talfüllung (Ereignisreihe der Ablagerung)	Bezeichnung der Grenzflächen der Ablagerung		Alter der Schichten
Schichten	Löss mit Sarmatkalkdetritus	A_{10}	Eisbildende Phase von $Würm_I$	$Würm_{I\alpha}$
	Feinkörniger Sarmatkalkdetritus mit wenig Löss	A_9		
	wie oben	A_8		
	Rendzina über feinkörnigem Sarmatkalkdetritus			Brörup
	Feinkörniger Sarmatkalkdetritus mit wenig Löss	A_7		
	Löss	A_6		$Würm_{I\alpha-1}$
	Feinkörniger Sarmatkalkdetritus mit wenig Löss	A_5		Amersfoort
	Löss	A_4		$Würm_{I\alpha-2}$
	Rudimentäre Rendzina über feinkörnigem Sarmatkalkdetritus			
	Feinkörniger Sarmatkalkdetritus	A_3		
Feinkörniger Sarmatkalkdetritus		A_2		
Kultur-	Rudimentäre Rendzina über feinkörnigem Sarmatkalkdetritus			
	Feinkörniger Sarmatkalkdetritus	A_1		
	wie oben			
Feinkörniger Sarmatkalkdetritus				
Rötlichbrauner begrabener Boden		Riss – Würm		

LITERATUR

Hunyadi, L. (1962): Az érdparkvárosi gerinces ősmaradvány-lelőhely (Die Vertebraten-Fundstätte von Érdparkváros), Földtani Közlöny 92, 4, pp. 460–463.

Gábori-Csánk, V. (1968): La station du Paléolithique moyen d'Érd – Hongrie. Akadémiai Kiadó, Budapest.

AN UNDIFFERENTIATED STRATOVOLCANIC MARGINAL FACIES OF THE INTRA-CARPATHIAN VOLCANIC GIRDLE (CSERHÁT HILLS, NORTHEAST HUNGARY)

by
T. PÓKA
(Geochemical Research Laboratory of the Hungarian Academy of Sciences)
Manuscript received the 8th November 1968

ZUSAMMENFASSUNG

Der Mitteltorton-Vulkanismus im Cserhát-Gebirge weist in mineralogisch-petrografischer und magmachemischer Hinsicht eine eigenartige Einheitlichkeit auf. Das Gestein der Gänge und kleineren Eruptionszentren und des durch diese gespeisten doppelten Lavadecke-Systems, die zusammen die Randzone des Mátra-Vulkanismus bilden, ist von wenigen Ausnahmen abgesehen von Orto-Charakter und durchweg Pyroxenandesit.

Die verschiedenen Ausbildungen unterscheiden sich kaum im durchschnittlichen An-Gehalt der Plagioklase, jedoch reagieren die Pyroxene in ihrer Phasenzahl und chemischen Zusammensetzung schon empfindlicher auf Unterschiede in den Abkühlungsverhältnissen. Der Pyroxenandesit ist in mineralogischer Zusammensetzung und Petrochemismus (mit einem Durchschnittswert, der saurer ist als normaldioritisch) der mittleren Andesitgruppe des Mátra-Gebirges verwandt. Sowohl die petrografischen als auch die tektonischen Analogien beweisen, dass Mátra und Cserhát einst ein zusammenhängendes Stratovulkansystem bildeten und dass die heutige bedeutende geomorfologische Absonderung der beiden Gebirge durch nachtortonische, junge tektonische Bewegungen, insbesondere durch ein NNO-SSW streichendes Bruchsystem bedingt ist.

Introduction

Among the volcanic mountains of the Intra-Carpathian volcanic girdle, the Middle Tortonian volcanics of the Cserhát Hills stand out with their peculiar mineralogical, petrographical and magma chemical uniformity and with the relatively favourable state of disclosure of the marginal and root zones of the volcanic formation. It was these features that attracted the attention of Hungarian workers as early as the end of the last century. The volcanism and in part also the general geology of the area was treated, without any detailed knowledge of the conditions existing in the adjacent Mátra Mountains, by Schafarzik (1892) in a manner considerably in advance over the average output of that age. It was his monograph that served as a basis of further research, because it correctly established in the broad outline the ex-

tent and the age of the individual geological formations and also the age (Tortonian) of the volcanism. In 1917 Hollós contributed to the knowledge of the Cserhát by describing the geology of the andesite dykes of Csörög; in 1930, Reichert gave a description of the pyroxene andesite of Szanda Hill.

In 1940 was published the geological monograph of Noszky sen. (1940) with a geological map of 1 to 75 000 scale, a fundamental and comprehensive description of the area, still valid today except for some slight modifications in the subdivision of the Tertiary. This work established among others the volcanological types (dykes, "stocks", lava sheets) of the Central or "true" Cserhát and their disposition in space.

Vendl in 1932 gave a detailed petrographic description of six types of Cserhát pyroxene andesites. Some of his data were made use of for comparative purposes in the present paper. The asphalt-bearing pyroxene andesite dyke of Sulyom Hill at Nagybátony was described by Jugovics in 1948.

In latter years, the structural considerations (concerning dyke and fault swarm orientation) of Balkay (1960) and the detailed analyses of Csalagovits (1965), Buda (1966) and Árkai (1967) into the volcanics at Szanda and Herencsény and into the southernmost fault swarm, respectively (which dealt in some detail also with the interaction of the sedimentary host rock and the volcanics) were the publications of importance concerning the Cserhát Hills.

Szádeczky-Kardoss et al. in 1967 gave a comprehensive review of the Tertiary volcanism of the Carpathian Basin, into which they fitted also the Cserhát on the basis of available literature.

A reinvestigation of the Cserhát volcanics has lately been initiated with the double aim

(1) of elucidating the causes of the peculiar lack of petrographic and chemical differentiation,

(2) of establishing general geological and structural connections between the Mátra Mountains and the Cserhát Hills.

Geology

It is but geomorphologically that the Cserhát Hills constitute a well-defined unit, because geologically the Cserhát is just a continuation of the Mátra, with a dyke system forming part of the base of the Mátra volcano, and with a more or less bipartite area of lava flows of relatively small extent and thickness (200 m) fed by this dyke system. The lava flows are more substantial in the east and south than in the north and west and also their erosion was somewhat one-sided owing to the general southwesterly tilting of the Cserhát Hills base. As a result, in the western and northern part of the area erosion has laid bare a number of dykes of WNW-ESE strike (plus some of NNW-SSE strike in the North Cserhát) which today constitute long unbroken ridges lending a somewhat peculiar aspect to the landscape. In these parts of the region the dykes tended to swell into centres of eruption at the points of intersection of a fault

system presumably preceding volcanism. The depth of erosion to our time was just sufficient to disclose some of these centres (Szanda, Bercel, Hollókő, Zsunypuszta). Farther north, erosion is deeper by 100 to 200 metres, the crystallinity of dyke rocks is higher, and tamped-down portions of dykes whose top parts never attained the surface are laid bare in increasing numbers. The northern and western endings of the dykes are non-structural; they disappear tapering in the Tertiary deposits, as a sign of the gradual weakening of volcanism in that direction. A simplified geological map of the Cserhát with the sampling localities indicated is shown as Fig. 1.

In the following we shall in our description of the investigations and their results refer to the symbols given in Table I.

TABLE I.

List of sampling localities

I. Eastern member of Szécsény dyke pair
(Andesite dyke 12 km long, 5 to 20 m wide. Rock: holocrystalline-porphyric hypersthenic augite andesite)

II. Western member of Szécsény dyke pair
(Andesite dyke 10 km long, 2 to 20 m wide. Rock: locally amygdaloidal, slightly porphyric "amafic" andesite)

III. Rimóc dyke swarm (dykes of 5 to 15 m width)
(a) Rimóc-South, Pusztavár, *(b)* Rimóc-South, south flank of Vakarás Hill, *(c)* Rimóc-South, top of Vakarás Hill, *(d)* Hollókő, small quarry in south flank of Szár Hill.
(Rock: Augite andesite with pigeonite-rimmed hypersthene)

IV. East end of Sipek dyke swarm
(Rock: Holocrystalline porphyric hypersthenic augite andesite)

V. Dyke swarm of Mohora-Cserhátsurány (after the description by Gy. Buda).
(a) North dyke, *(b)* South dyke.

VI. Szanda dyke (5 to 10 m wide).
(Rock: holocrystalline porphyric augite andesite with pigeonite-rimmed hypersthene)
(a) West flank of Peres Hill, *(b)* top of Peres Hill, *(c)* East flank of Peres Hill.

D. Southernmost dyke swarm of the Cserhát Hills (after the description by P. Árkai).
(a) North dyke (Cseke Hill), bronzitic augite andesite.
(b) South dyke (Pokol Valley). "Amafic" andesite.

N Orthopyroxene andesite dykes of the Cserhát Hills dyke swarm at Nagybátony, at the feet of the Mátra Mountain.
(a) Augite andesite dyke (Nagybátony West, Sulyom Peak)
(b) Older bronzitic and hypersthenic augite andesite dyke, Nagybátony-South, Nagyparlag Peak. Strike WNW-ESE.
(c) Younger hypersthenic augite andesite dyke of ENE-WSW strike.

VII. Eruption centre of the Szanda (0.5 by 0.2 km).
(Rock: holocrystalline porphyric hypersthenic augite andesite.)
(a) Averaged sample.
(b) Great quarry of the Szanda, lower horizon of columnar jointing
(c) Great quarry of the Szanda, upper horizon of laminar parting
(d) Lower (columnar) horizon of the Vár Hill at Szanda
(e) Upper (laminar) horizon of same.

VIII. Eruption centre of Bercel (1.5 by 3 km)
(Rock: holocrystalline porphyric hypersthenic augite andesite)
(a) Hollókő, Vár Hill
(b) Hollókő, Szár Hill, great quarry
(c) Hollókő, Szár Hill, along the fault (hydro-metaandesite)

IX. Eruption centre of Hollókő (0.25 by 2.0 km)
(Rock: holocrystalline porphyric augite andesite with pigeonite-rimmed hypersthene)

X. Őr Hill at Nagylóc (lava flow 50 m thick)
("Amafic" andesite of vitreous matrix)

XI. Lava flow of the Zsuny Hills (cca 100 m thick) and the exposure of the centre of eruption feeding it in the quarry at Zsunypuszta
(a) Lower level of centre of eruption
(Rock: hypersthene-pigeonite andesite of "doleritic" texture)
(b) Upper level of centre of eruption
(Rock: holocrystalline porphyric, hypersthenic-pigeonitic augite andesite)
(c) Middle level of lava sheet (scoriaceous, vitreous hypersthenic augite andesite)
(d) Uppermost level of lava sheet (oxyandesite with 20 percent goethite)

XII. Lava flow of Buják (about 30 m thick)
(Rock: scoriaceous, vitreous hypersthenic augite andesite)
(a) Buják, top of Kálvária Hill
(b) Buják, Kálvária Hill, NW flank (locality investigated by A. Vendl; most acid volcanic rock found so far in the Cserhát Hills – according to Vendl, the sample was taken close to a big partly remelted sandstone inclusion which suggests its acidity (64 percent SiO_2) to be due to a local cause)

XIII. Lava flow of the Kozárd plateau, about 50 m thick.
(Rock: hypersthenic augite andesite with a vitreous matrix)

E. Lava flow of the Ecskend Plateau at Acsa (from the description by P. Árkai).
(Rock: hypersthenic augite andesite with vitreous matrix)

We have measured the composition of plagioclase and pyroxene phenocrysts as well as of the same minerals in the matrix by universal-stage methods for all rock types. Moreover, there were prepared of all basic types chemical analyses (by B. Simó) and trace element analyses (by Mrs B. Nagy). In the composition of the plagioclases in the Cserhát Hills pyroxene andesites, as represented by the statistic average An content of the plagioclases in the individual types of rock, there is no substantial difference. On the other hand, the data summarized in Table II show that the maximal and minimal An contents of the individual generations of plagioclases are rather far apart in function of the rates of cooling

Fig. 1.

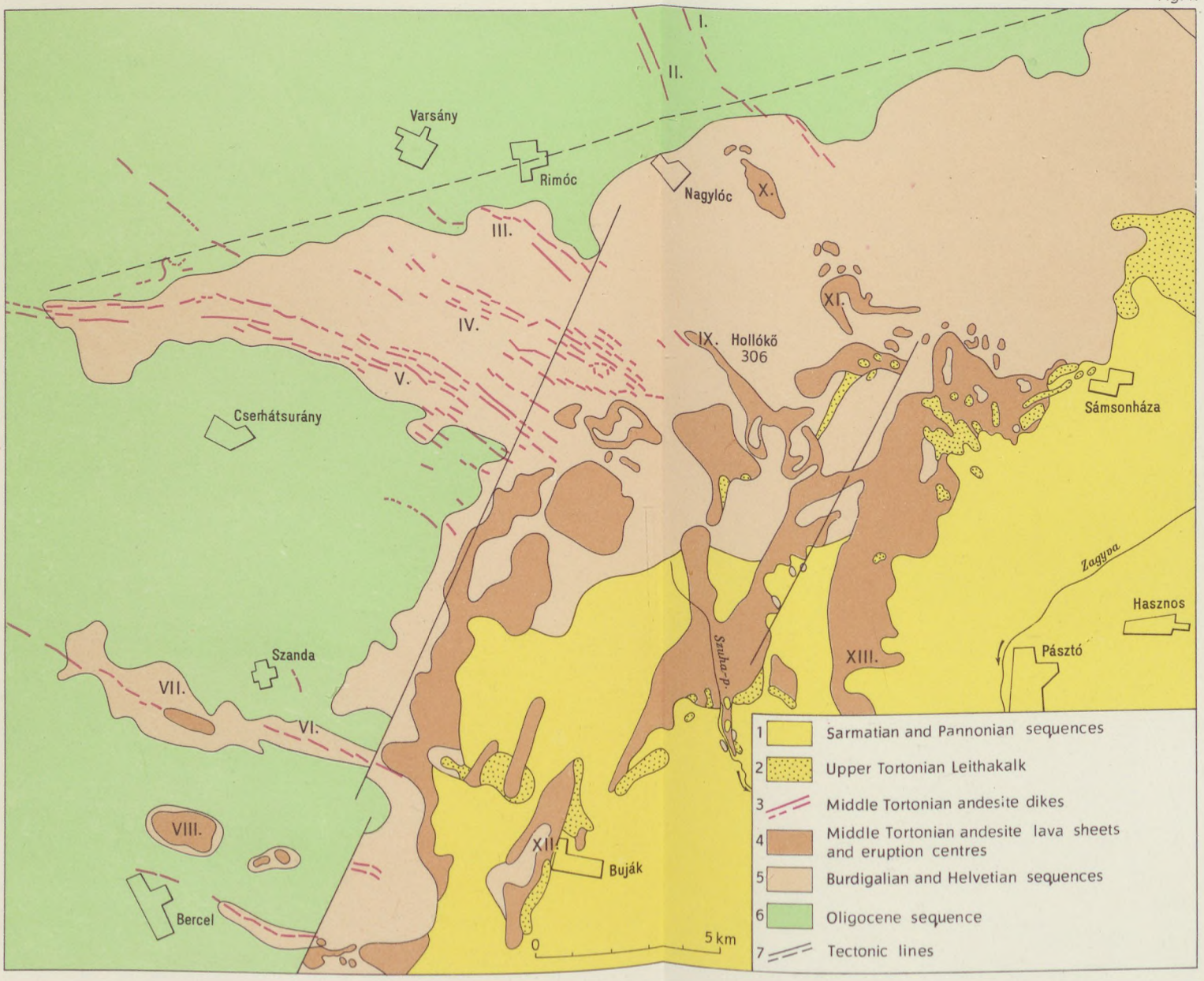
I.
II.
Varsány
Rimóc
Nagylóc
X.
III.
IV.
XI.
IX. Hollókő
306
V.
Cserhátsurány
Sámsonháza
Zagyva
Hasznos
Szuha-p.
Pásztó
XIII.
Szanda
VII.
VI.
VIII.
XII.
Buják
Bercel
0
5 km
1 Sarmatian and Pannonian sequences
2 Upper Tortonian Leithakalk
3 Middle Tortonian andesite dikes
4 Middle Tortonian andesite lava sheets and eruption centres
5 Burdigalian and Helvetian sequences
6 Oligocene sequence
7 Tectonic lines

Table II.

Anorthite content of plagioclase in pyroxene andesites

Sample symbol	Phenocrysts			Matrix			Rock average	Anorthite range
	max.	min.	weighted av.	max.	min.	weighted av.		
	all data in percent							
(A) Dykes								
I.	90	60	74	69	34.5	52.5	63.2	55.5
II.	90	57	74	69.5	56.0	63.0	68.5	34.0
III.	84.6	70.5	77.5	70.2	53.5	62.7	70.1	31.1
D.	80	—	63.7	—	50	55	59.3	30.0
N.	80	57.5	66.5	63	42.5	54.5	60.5	37.5
average	85	61	71	68	47	58	64.5	38
(B) Centres of eruption								
VII.	82.5	68.7	77.0	63.5	53.5	60.5	68.7	28.0
IX.	79.1	62.6	71.0	66.0	50.0	57.5	69.2	29.1
average	81	66	74	65	52	59	68	29
(C) Lava flows								
X.	90	57	77	70	64	65	71	26
XI.	75	52	66	55	50	52	59	25
XII.	86	78.5	80	75	65	69	74.5	21
XIII.	85	67.5	77	70	62	65	71	23
E.	—	—	66.2	—	—	57	61.6	—
average	84	64	73	68	60	62	68	24

In the dykes, the An content of plagioclase phenocrysts changes by 24 percent in the course of cooling; that of the plagioclase crystals in the matrix changes by 21 percent. This suggests cooling to have been fairly uniform.

In the pyroxene andesite dykes, the difference between the two changes is just 3 percent, that is, there is an almost continuous passage from one set of crystals to the other.

In the centres of eruption the An content of the phenocrysts changes 15 percent, that of the plagioclases in the matrix 13 percent. Hence, the cooling rate is faster than in the case of the dykes, but still fairly uniform. (Also, the texture graphs of the two rocks are similar, each with two marked maxima.)

The An content range of plagioclase phenocrysts in the lava flows hardly differs from that in the dykes, which shows that most of the plagioclase phenocrysts had already formed in the volcanic vent. However, in the matrix plagioclases of the lava flows the An range is only 8 percent, indicating a more rapid cooling.

The plagioclases of the pyroxene andesites of various solidification are, then, of the same chemical nature on the average, precisely owing to the general lack of differentiation in the original melt, but the An percentage ranges of the individual generations of plagioclases vary rather widely as a function of rates of cooling (Fig. 2.).

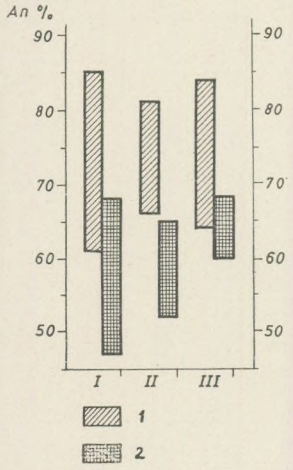

Fig. 2. Range of An content (in percent) in the plagioclase generations of pyroxene andesites of various facies

1 – phenocrysts, 2 – in matrix, I. – dykes, II. – eruption centres, III. – lava flows

Pyroxenes exhibit a greater variety of composition than plagioclases do. (Their composition has been determined by universal-stage methods, by the intermediary of the parameters 2V, z/c and birefringence).

On the basis of the number and composition of the pyroxene phases we have described three fundamental types of pyroxene andesite.

(1) A rock containing a single-phase pyroxene is the "amafic" andesite which contains only in its matrix a high-calcium augite. This type constitutes both some dykes and the upper horizons of lava flows. Its origin is due to a very fast initial rate of cooling, due in turn to a rapid surge of the melt.

In some cases, e.g. in the case of the western member of the double dyke at Szécsény, most of the dyke remained tamped down and took in a considerable amount of water vapor from the host rock, which was a sandy-clayey sediment saturated with water. The high volatile content prevented the early formation of mafic constituents; such could develop only in the matrix, in the form of augite and nontronite-montmorillonite. Most of the Ca and Fe entered solid phases only at hydrothermal temperatures, in the forms of amygdaloid druses (calcite and siderite).

(2) Most frequent in the Cserhát Hills is a basically augitic two-pyroxene-phase andesite with hypersthene or sometimes bronzite. Also, this type occurs both as dykes and lava flows. The orthopyroxenes contain 23 to 40 percent Fs. There is a general tendency for the Fe content of the augite in the matrix to grow hand in hand with that of the orthopyroxenes.

(3) As a third pyroxene phase, pigeonite apears in the form of wreaths around the hypersthene crystals of the augite-based hypersthene andesite. In the three-pyroxene-phase andesites, the augite of the matrix is usually very rich in Ca or Fe. The Fe contents of pigeonite and augite grow hand in hand. Slow cooling makes it possible for Ca to enter the orthopyroxene lattice: consequently, a substantial portion of the Fe content crystallizes in the augite of the matrix.

The pyroxene andesite of the centre of eruption feeding the lava flow of the Zsuny Hills is of a peculiar type. At the lower level of the disclosure there is a coarsely crystalline pyroxene andesite of "doleritic" texture with hardly any porphyric constituents; there are two pyroxene phases (hypersthene and pigeonite, both iron-rich), of equal grain size, filling out the interstices of the plagioclase plates. The typically one-peak grain size distribution curve and the nature of

the pyroxene phases reveal this centre of effusion to have been a long-lived one with lots of heat supply. This is further confirmed by the fact that the plagioclases in the rock cannot be separated into generations either, neither by size nor by An content. Higher up in the profile, a more rapid cooling gave rise to a more porphyric texture and there appears iron-rich augite as the third pyroxene phase in the matrix.

The average compositions of the pyroxenes in andesites with one, two and three pyroxene phases respectively are represented in Fig. 3.

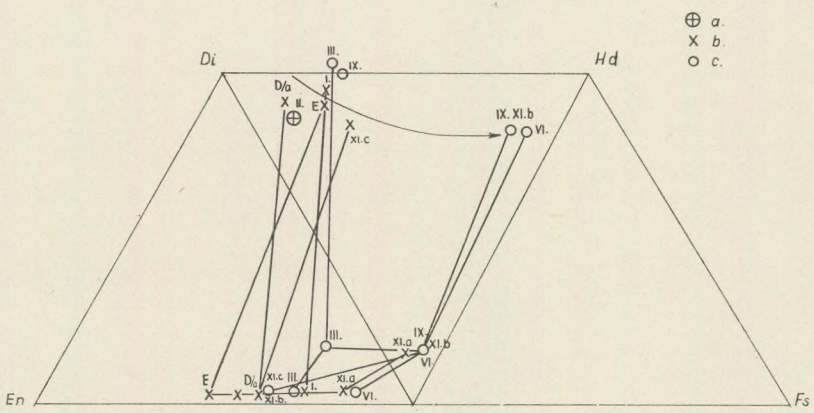

Fig. 3. Chemical composition of pyroxenes in pyroxene andesites
(a) in andesites of one pyroxene phase,
(b) in andesites of two pyroxene phases,
(c) in andesites of three pyroxene phases

The chemical analyses of the various types of rock exhibit but insignificant differences, indicating the melt to have been rather slightly differentiated. (Table III.)

Since the Niggli values are fairly sensitive even to slight differences, they lend themselves better to the comparison and grouping of the individual volcanic facies than the analyses themselves. The mean *si* parameter is least in the dykes (154), being 164 for the centres of eruption and greatest, 175 for the lava flows. Chemism is dioritic in the mean in the case of dykes and centres of eruptions, and tonalitic in the case of the lava flows. Accordingly, the *qz* parameter is least for the dykes (+10.3), greater for the centres of eruption (+11. 2) and greatest for the lava flows (+23.9). As confronted with the insignificant changes in *al*, *fm*, *c* and *alk*, the change in *si* is due to the apperarance of free quartz and glass in the matrix. The distribution of *si* over the entire scale of Cserhát volcanics shows a nearly dioritic average (slightly displaced towards a more acid composition). (Fig. 4.)

The diagram of AFM values (Fig 5) contains for comparison also the mean AFM values of the lower and middle andesite group of the Mátra Mountains. The good agreement between the average AFM values of the Cserhát volcanics and the middle Mátra group proves that the Cserhát volcanics are in their

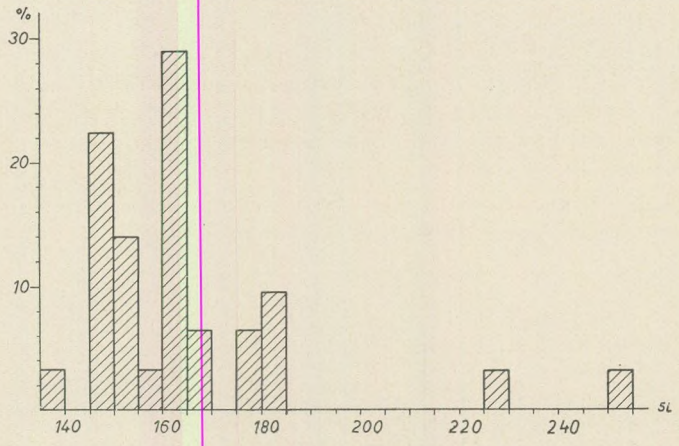

Fig. 4. Distribution of the si parameter (Niggli) in the Cserhát Hills volcanics

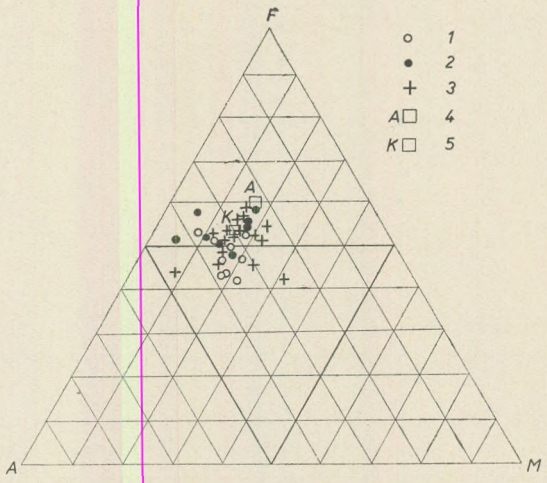

Fig. 5. AFM diagram of Cserhát Hills volcanics

1 — dykes, 2 — centres of eruption, 3 — lava flows, 4 — lower (A) and middle (K) andesite group of the Mátra Mountains

bulk similar to the most intense middle phase of volcanism in the Mátra Mountains and represent the same stage of differentiation.

Spectral analyses of more than 200 samples of Cserhát pyroxene andesites were prepared by Mrs B. Nagy at the Institute of Petrography and Geochemistry of the Eötvös University. The weighted averages of the individual elements and the mean values published for them in the relevant literature are shown in Fig. 6.

Of the lithophile elements, Li, Ba and Sr are enriched by one order of magnitude. The pegmatophile and chalcophile elements agree with the averages, whereas the siderophile elements show lower-than-average values.

Table III

CHEMICAL COMPOSITIONS AND NIGGLI VALUES OF CSERHÁT HILLS PYROXENE ANDESITES

Sample symbol	I.	II.	III.				IV.	V.		VI.			D.		N.			VII.					VIII.	IX.			X.	XI.			XII.		XIII.	E.
			a.	b.	c.	d.		a.	b.	a.	b.	c.	a.	b.	a.	b.	c.	a.	b.	c.	d.	e.		a.	b.	c.		a.	b.	c.	a.	b.		
Analyst	(1)	(1)	(3)	(1)	(3)	(1)		(3)	(3)	(1)	(1)	(1)	(2)	(2)	(3)	(1)	(1)	(4)	(1)	(1)	(1)	(1)	(2)	(3)	(1)	(1)	(1)	(1)	(1)	(1)	(1)	(3)	(3)	(3)
SiO_2	51.34	54.64	52.76	54.81	53.06	52.62	52.23	52.29	48.76	55.02	55.08	54.73	55.51	56.42	54.59	52.72	52.78	56.19	56.11	55.36	55.00	55.83	53.28	52.80	54.66	54.14	56.20	54.29	54.64	56.32	54.21	64.23	52.41	56.02
TiO_2	1.07	1.65	0.98	1.19	1.14	1.43	1.34	2.90	3.03	1.40	1.81	1.85	0.92	1.24	0.81	0.58	0.98	1.21	0.88	1.96	1.84	1.37	0.56	1.05	1.63	1.49	1.84	1.59	1.67	1.26	1.43	0.67	1.20	1.05
Al_2O_3	20.64	17.83	17.82	20.72	19.18	20.63	20.56	19.09	17.15	16.90	15.31	18.18	15.14	15.44	18.10	21.85	19.53	18.05	18.23	18.21	18.26	17.86	19.70	19.44	21.15	21.33	18.49	19.16	17.40	17.42	22.12	16.00	17.34	16.23
Fe_2O_3	3.47	3.41	1.86	4.29	3.99	2.07	3.96	2.30	4.30	3.99	5.27	2.18	1.97	2.66	2.60	2.06	3.48	1.73	1.55	2.80	1.44	1.96	2.41	3.47	2.16	4.05	1.14	3.67	3.79	7.49	3.48	2.74	3.45	2.49
FeO	4.09	4.78	7.15	1.30	4.33	5.14	3.23	4.32	4.12	5.25	4.81	4.90	5.00	6.90	5.27	4.81	5.11	5.88	4.99	3.65	4.72	5.42	5.07	5.15	4.13	1.55	4.73	4.21	5.22	0.50	2.18	4.22	7.81	7.51
MnO	0.01	0.65	0.11	0.01	0.12	0.20	0.08	0.12	0.13	0.28	0.11	0.14	0.12	0.13	0.06	0.04	0.09	0.15	0.15	0.37	0.06	0.08	0.09	0.11	0.00	0.21	0.00	0.09	0.15	0.07	0.04	0.18	0.13	0.09
MgO	2.93	2.79	2.48	1.05	2.57	2.67	2.51	3.30	2.11	1.94	2.61	2.55	4.96	2.52	2.54	3.07	3.29	3.18	2.88	2.66	3.10	2.47	2.79	2.33	2.31	0.96	2.28	2.65	2.86	0.86	1.27	0.83	3.55	2.91
CaO	9.34	6.75	9.49	8.67	7.99	8.41	8.67	9.52	9.97	8.89	8.82	8.56	8.30	6.20	7.84	9.00	8.00	7.82	8.57	8.29	9.23	8.28	9.35	8.70	9.23	7.75	7.80	7.32	6.82	3.74	9.11	3.88	9.47	7.07
Na_2O	1.85	2.30	3.64	3.10	3.40	2.50	2.50	2.51	1.89	3.05	3.05	3.02	2.50	2.88	3.41	2.22	2.88	2.73	3.02	3.05	2.90	3.21	2.73	4.71	2.05	2.20	1.90	2.61	2.40	1.90	2.25	2.28	3.27	4.09
K_2O	1.45	2.05	0.99	2.75	2.43	1.93	2.06	1.71	1.77	2.75	2.00	2.75	2.03	2.77	1.54	1.30	1.56	2.19	2.60	2.50	2.25	2.50	1.97	1.12	1.38	1.75	2.20	2.14	2.25	2.75	1.50	3.79	1.21	1.50
H_2O^+	1.12	1.67	0.33	1.15	0.19	1.10	0.90	1.40	2.43	1.07	0.33	1.02	2.90	2.05	2.07	0.08	0.35	0.20	1.33	1.12	1.40	1.12	0.72	0.21	1.26	2.10	2.03	0.72	1.65	3.53	0.83	0.25	0.22	0.13
H_2O^-	1.40	1.02	1.75	1.32	2.31	0.74	1.44	0.59	2.22	0.23	0.27	0.40	0.84	0.85	0.19	1.41	0.73	0.78	0.17	0.60	0.10	0.25	1.20	1.26	0.06	1.72	0.43	1.13	0.64	3.68	1.17	1.24	1.34	0.59
P_2O_5	0.16	0.20	0.59	0.15	0.32	0.13	0.18	0.30	0.45	0.11	0.12	0.12	0.17	0.21	0.57	0.10	0.12	0.10	0.13	0.13	0.13	0.13	0.39	0.24	0.15	0.14	0.23	0.17	0.20	0.14	0.11	0.25	0.19	0.33
CO_2	0.68	0.00	–	0.07	–	0.00	0.00	0.14	0.57	0.13	0.17	0.03	0.06	0.00	0.13	0.94	0.82	0.14	0.08	0.03	0.06	0.07	0.16	–	0.00	0.00	0.17	0.05	0.00	0.00	0.00	–	–	–
si	146	180	147	166	151	152	155	149	145	159	160	162	152	167	162	146	149	164	164	160	160	166	152	145	176	180	178	163	181	212	223	255	135	162
ti	2.3	3.8	2.0	2.7	2.4	3.1	2.9	6.2	6.8	3.1	4.0	4.0	2.2	3.4	1.7	1.3	2.1	2.7	1.9	4.5	4.0	3.1	1.19	2.2	3.6	3.7	4.4	3.6	3.8	4.7	3.7	2.0	2.3	2.3
p	0.2	0.2	0.7	1.8	0.4	0.2	0.2	1.7	0.5	1.7	1.7	1.8	0.3	0.3	0.2	0.3	0.2	0.1	1.6	1.7	1.7	1.8	0.47	2.3	0.2	0.2	0.3	0.5	0.3	0.3	0.3	0.4	0.2	0.4
al	34.5	32.5	29.0	36.8	32.0	35.0	35.0	32.0	30.3	28.8	26.2	31.5	25.5	27.5	32.0	36.0	32.0	31.0	31.5	31.0	31.0	31.0	33.0	31.5	36.5	41.5	34.5	33.7	31.2	39.0	40.8	37.5	26.5	27.5
fm	29.2	34.2	31.0	17.9	30.0	28.8	27.5	29.0	29.5	30.2	34.5	28.3	39.2	37.0	30.0	28.5	33.0	32.5	28.2	27.2	28.2	28.6	27.0	28.5	25.3	19.8	26.2	30.7	35.2	31.0	29.3	27.5	37.5	36.5
c	28.3	22.5	28.5	31.0	24.5	26.0	27.0	29.0	31.8	27.3	27.3	26.8	24.7	19.7	25.0	27.0	24.0	24.5	26.7	28.7	28.0	26.0	28.5	25.5	29.2	27.5	26.5	23.7	22.0	15.5	15.9	16.5	26.0	22.0
alk	7.7	10.8	11.5	14.3	13.5	11.8	10.8	10.0	8.9	13.6	12.2	13.8	10.6	15.8	13.0	8.5	11.0	12.0	13.5	13.2	12.5	14.0	11.0	14.5	8.5	10.4	12.6	11.8	11.5	14.5	14.2	18.5	10.0	14.0
k	0.34	0.37	0.15	0.37	0.32	0.34	0.35	0.30	0.38	0.37	0.30	0.37	0.38	0.40	0.22	0.29	0.28	0.33	0.36	0.35	0.34	0.34	0.32	0.14	0.30	0.34	0.53	0.35	0.38	0.45	0.49	0.52	0.20	0.20
mg	0.42	0.37	0.33	0.26	0.37	0.40	0.39	0.48	0.31	0.29	0.32	0.39	0.53	0.27	0.37	0.45	0.41	0.35	0.44	0.42	0.48	0.38	0.36	0.33	0.40	0.24	0.41	0.38	0.37	0.15	0.17	0.18	0.37	0.35
c/fm	0.97	0.66	0.91	0.17	0.81	0.90	0.98	1.00	1.07	0.90	0.79	0.95	0.63	0.53	0.82	0.96	0.72	0.75	0.95	1.05	0.99	0.91	1.03	0.89	1.16	1.10	0.98	0.77	0.63	0.50	0.54	0.60	0.70	0.60
qz	+15.2	+36.8	+1.0	+8.8	−3.0	+4.8	+1.0	+9.0	+9.8	+4.6	+11.2	+6.8	+9.8	+3.8	+10.0	+12.0	+6.5	+16.0	−25.6	+7.2	+10.0	+10.0	−7.2	−13.0	+42.0	+34.8	+27.6	+15.8	+35.0	+54.0	+66.2	+81.0	−5.0	+6.0
A	24.0	28.5	29.0	46.5	35.0	31.0	31.8	30.0	25.7	34.0	28.0	37.5	27.6	31.8	32.4	26.3	27.3	31.2	37.4	37.6	35.8	36.7	31.5	35.0	28.6	37.4	33.5	28.4	28.2	34.5	35.0	43.5	23.3	30.3
F	55.0	53.5	56.0	44.5	49.5	50.5	50.7	46.5	59.3	54.5	57.0	45.7	42.0	54.0	51.0	51.0	52.6	48.4	43.4	43.8	42.6	47.5	50.0	51.5	52.0	53.4	48.0	53.6	54.4	59.0	52.0	50.5	58.5	54.0
M	21.0	18.0	15.6	9.0	15.5	18.5	17.5	23.5	15.0	11.5	15.0	16.8	30.4	14.2	16.6	22.7	20.1	20.4	19.2	18.6	21.6	15.8	18.5	13.5	19.4	9.2	18.5	18.0	17.4	6.5	12.0	6.0	18.2	15.7

(1) = Simó, B.
(2) = Csajághy, G.
(3) = Vendl, A.
(4) = Kolecsinszky, K.

The enrichment of trace elements is invariably greater in the dykes than in the lava flows, by as much as an order of magnitude in the case of some elements (Ba, Sr, Cu, Pb). The scatter of the individual elements is shown in Fig. 7.

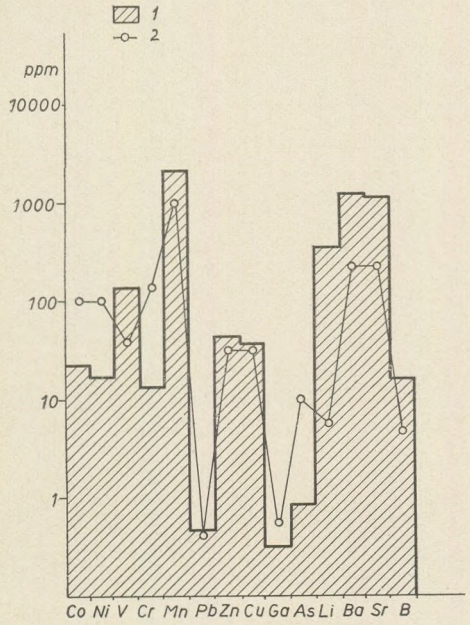

Fig. 6. Distribution of trace elements in the Cserhát Hills pyroxene andesites

1 — weighted average content of the element in ppm, 2 — average values published in literature

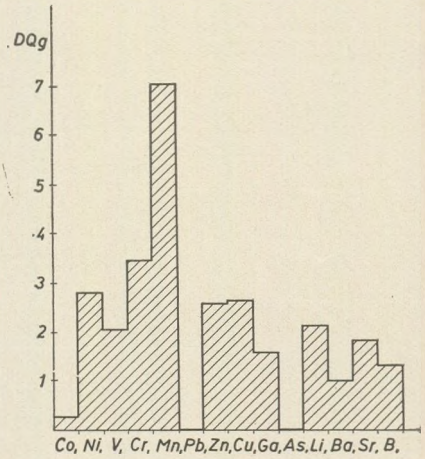

Fig. 7. Scatter of trace elements in Cserhát Hills pyroxene andesites

Conclusions

The above-characterized mineralogical, petrographical and magma chemical uniformity of the stratovolcanic complex of the Cserhát Hills can be interpreted on the assumption of the rapid and almost simultaneous surge of a magma agreeing in composition with the average composition of the entire Mátra-Cserhát volcano. This surge took place along the steep and profound marginal faults of the volcanic region. In the course of the uprising of the magma, no differentiation and/or contamination could take place, nor could the magma take in substantial amounts of water from the sedimentary host rock. This is why the relatively dry and undifferentiated magma largely produced varieties of orthoandesite, the composition of whose pyroxenes was affected first of all by the conditions of cooling.

Besides the agreement in mineral composition and chemical constitution the correspondence of the Cserhát volcanics including the dyke swarms to the middle (and to a small extent to the upper) andesite group of the Mátra Moun-

tains is confirmed also by an agreement of magnetic pole positions evinced by the latest palaeomagnetic measurements of Márton and Szalay.

The fault system of mostly WNW-ESE, subordinately NNW-SSE strike of the Cserhát Hills dykes also fits into the radial dyke pattern of the Mátra Mountains. According to Kubovics (1966) the dykes of the Northern Mátra are mostly of NNE-SSW and ENE-WSW strike, as opposed to NW-SE and E-W strikes in the Western Mátra. In the northern foreland of the Mátra, the strikes are transitional between the two areas: WNW-ESE, ENE-WSW and NNW-SSE. The radial dyke pattern with its centre in the Mátra region is shown in Fig 8.

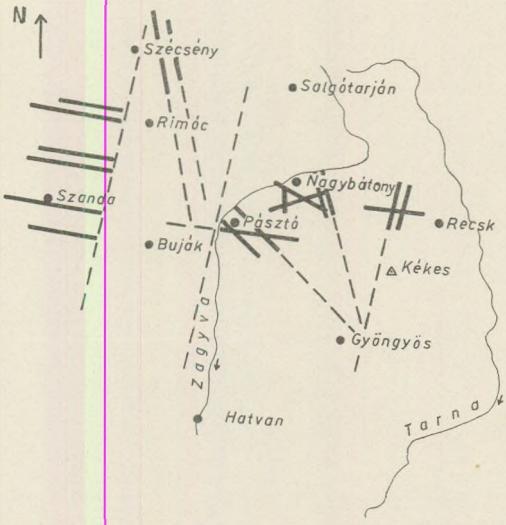

Fig. 8. The fault systems of Mátra and Cserhát Montains.

The formerly coherent stratovolcanic unit of the Mátra and Cserhát was dissected by faults of NNE-SSW strike during the Attican, Rhodanian and Walachian phases of orogeny. The concomitant ample vertical displacements then resulted in the development of a separate geomorphological unit in the Cserhát region.

REFERENCES

Árkai, P. (1967): Correlation of quantitative petrographic characteristics of pyroxene andesites in the volcanic complex of the Southwestern Cserhát Hills. Annales Univ. Sec. Geol. XI.

Balkay, B. (1960): The tectonism of the Cenozoic volcanism in Hungary. Ann. Univ. Sci. Bud. Sec. Geol. III.

Buda, Gy. (1960): A középső-cserháti piroxénandezittelérek vizsgálata (Middle Cserhát pyroxene andesites), D. Sc. Thesis.

Csalagovits, I. (1965): Geological and petrological conditions of the Szanda – Bercel area. Annales Hist. Nat. Musei LVII.

Hollós, A. L. (1917): A csörögi andezit-telérek földtani viszonyai (Geology of the Csörög andesite dykes), Földtani Kčzlöny.

Kuno, H. – Nagashima, K. (1952): Chemical composition of hypersthene and pigeonite in equilibrium in magma. Am. Miner. vol. 37.
Kubovics, I. (1966): Az ÉNy és ÉK Mátra földtani és vulkanológiai viszonyai (Geology and volcanology of the Northwest and Northeast Mátra). Candidate's thesis.
Noszky sen., J.: (1940): Cserhát. In the series Magyar tájak földtani leírása.
Poldervaart, A. (1957): The relationship of orthopyroxene to pigeonite. Min. Mag. 28.
Poldervaart, A. – Hess, H. H. (1955): Pyroxenes in the crystallisation of basaltic magma. Jour. Geol. 59.
Póka, T. – Simó, B. (1956): Die Rolle des Nebengesteins in der Entwicklung der subvulkanischen Facies. Ann. Univ. Sci. Bud. Sec. Geol. X.
Reichert, R. (1930): A Szanda-hegy piroxénandezitje (The pyroxene andesite of Szanda Hill). Földtani Közlöny.
Schafarzik, F. (1892): A Cserhát piroxénandezitjei (The pyroxene andesites of the Cserhát), Földtani Int. Évi Jelentései.
Szádeczky-Kardoss et al. (1967): Die Neovulkanite Ungarns. Acta Geologica XI.
Szádeczky-Kardoss, E. (1967): Elgondolások a kárpáti medencerendszer mélyszerkezeti és magmatektonikai vizsgálatához. (Some ideas on the deep-structure and magmatotectonic investigation of the Carpathian basins.) MTA X. Oszt. Közl. I.
Vadász, E. (1952): Magyarország földtana (Geology of Hungary), Akadémiai Kiadó, Budapest.
Vendl, A. (1932): A Cserhát piroxénandezitjei (The pyroxene andesites of the Cserhát). Mat. és Term. Tud. Ért.

ОБ ИЗМЕНЕНИЯХ ПАРАМЕТРОВ ИОНОСФЕРЫ НАД Г. БЕКЕШЧАБА ЗА ВРЕМЯ ЧАСТИЧНОГО ЗАТЕМНЕНИЯ СОЛНЦА 20-ГО МАЯ 1966 г.

Э. ФЛОРИАН
(Геофизический институт Университета им. Л. Этвеша, г Будапешт)
(Поступила. 15. 1. 1968)

SUMMARY

Changes in ionosphere parameters largely arose during the second half of the eclipse. The decrease in critical frequencies for the *F1*- and *F2* layers was twice the decrease for the *E* layer. The drop in electron concentration was twice as much for *F1* and three times as much for *F2* as for *E*. The recombination coefficient varied from 1.5 to $2.5 \cdot 10^{-8}$ $cm^3 sec^{-1}$. A slope in the *F1* layer could be demonstrated.

Измерения, проведенные на станции по изучению ионосферы в г. Бекешчаба (46°40′ север, 21°10′ восток) позволили изучать три слоя (*E*, *F1* и *F2*) ионосферы во время *частичного* затемнения Солнца, характеризующегося следующими астрономическими данными для г. Бекешчаба:

первый контакт	–	$09^{ч}21^{м}$
максимальная фаза		$10^{ч}42^{м}$
последний контакт	–	$12^{ч}05^{м}$

по среднеевропейскому времени. При максимальной фазе Луна покрыла 0,758 часть поверхности Солнца.

Основой для сопоставления берутся, как правило, средние величины различных параметров, полученных по 5 дней до и после данного дня. В рассматриваемом случае 19 мая, по техническим причинам, не были проведены измерения. С учетом количества солнечных пятен для сопоставления использовались результаты измерений, проведенных 17, 18, 21, 22, 23 и 24 мая.

Изменение высоты слоев

Мощные слои ионосферы (*F1* и *F2*) характеризуются значительно большей плотностью атмосферы у подошвы слоя по сравнению с кровлей. В густом воздухе намечается большая частота рекомбинации. Следовательно, при снижении интенсивности радиации Солнца нижняя поверхность мошных слоев поднимается. Для тонкого слоя *E* такое поднятие осуществляется в

столь незначительной мере, что оно не может быть зарегистрировано нашей аппаратурой, при помощи которой можно выявить изменения высоты до ±5 км. Слой *E* ионизируется сравнительно равномерно накаливаюшей фотосферой Солнца, испускающей лучи с длиной волн 900—1000 Å, и так интенсивность ионизирующей радиации является пропорциональной радиационной поверхности Солнца. Слой *F1* обусловливается частично, а слой *F2* — полностью солнечными лучами, характеризующимися меньшими длинами волн и приходящими с активных частей Солнца. Следовательно, в данном случае увеличение высоты этих слоев зависит не от поверхности Солнца, а от покрытости активных частей. Это обстоятельство хорошо видно по Рис. 1, на которой тонкими линиями показан суточный ход средней высоты слоев *F1* и *F2* ($\overline{h'F}$ и $\overline{h'F2}$), а жирными линиями — изменения, имевшие место во время потемнения Солнца (*h'F* и *h'F2*). На фигурах стрелками отмечается время первого и последнего контактов и максимальной фазы.

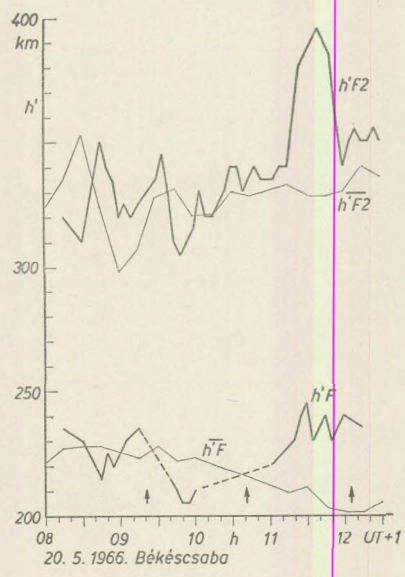

Рис. 1. Изменение виртуальной высоты слоев *F1* и *F2* за время затемнения Солнца. Тонкими линиями показаны средние величины, полученные в контрольные дни, а стрелками — начало, конец и максимальная фаза затемнения

В отношении слоя *F2* намечаются значительные изменения во времени даже средней высоты. Это тоже свидетельствует о неравномерности радиации активных участков. Интересно заметить, что изменение высоты как слоя *F1* так и слоя *F2* происходит только после максимальной фазы, почти в одно и то же время. Следовательно, в рассматриваемые дни эти слои получили ионизирующую радиацию главным образом с активных участков, поверхность которых была покрыта Луной только во второй половине затемнения Солнца.

Максимальное виртуальное поднятие высоты составляло 40 км в слое *F1*, представляющей собой низы области *F* и 70 км в слое *F2*.

Изменение предельной частоты

Максимальная радиочастота, еще отражающаяся в вертикальном направлении с некоторого слоя, представляет собой *предельную частоту*. Как это и ожидалось, за время затемнения Солнца этот параметр претерпел значительное изменение во всех слоях.

При затемнении Солнца снижение предельной частоты происходит наиболее равномерно в слое *E*, поскольку это снижение зависит от непокрытой

поверхности Солнца. Жаль, что точное определение предельной частоты слоя *E* часто затрудняется за счет плавающих в данном слое кусков густых, так называемых *E*-спорадических облаков (*Es*). По таким причинам не получена полностью правильная кривая снижения предельной частоты слоя *E* на станции г. Бекешчаба. Предельные частоты слоев *F1* и *F2* уже заведомо не могут иметь правильного хода в связи с неравномерной радиацией активных участков Солнца.

На Рис. 2. показаны отклонения предельных частот за время затемнения Солнца от средних величин (*Δ*Mc). При затемнении намечалось одновременное снижение предельных частот слоя *E* на 0,50 Mc, а слоев *F1* и *F2* соответственно на 0,79 и 0,80 Mc. Одновременность и близкие величины снижения свидетельствуют о том, что в день затемнения Солнца последние два слоя вызывались в основном одним и тем же активным участком и что данный участок был покрыт Луной только после максимальной фазы.

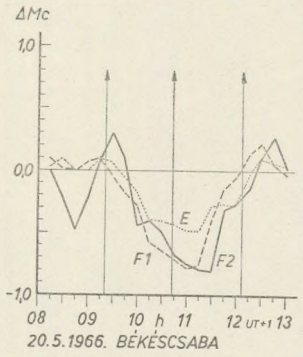

Рис. 2. Отклонения величин предельных частот слоев *E*, *F1* и *F2* за время затемнения Солнца от средних величин, подсчитанных по данным контрольных дней

Для сравнения приводятся подобные данные, полученные в других местах и в другие времена. J. A. Gledhill (1959) сообщил величины изменения предельных частот за время кольцевого затемнения Солнца, происшедшего 25 декабря 1954 г. над городами Кейп Таун и Йоханнесбург. Здесь были намечены снижения частоты равные 0,5—0,6 Mc для слоя *E*, 1,0—1,2 Mc для слоя *F1* и 1,2—1,6 Mc для слоя *F2*. В данном случае снижение предельной частоты следовало за степенью покрытия диска Солнца лучше, чем в 1966 г. в г. Бекешчаба. C. M. Minnis (1959) изучал изменения предельной частоты, наблюдавшиеся за время затемнения Солнца 14-го декабря 1955 г. над Сингапуром. Здесь в слое *E* намечалось снижение равное 0,5 Mc, в слое *F1* — 1,0 Mc. Место наблюдения располагается недалеко от экватора, в связи с чем можно было наблюдать и за слоем *F1* 1/2, в котором маскимальное снижение составляло также 1,0 Mc. На поверхность, покрытую в то время только наполовину, по всей вероятности, сильно влияло несколько активных центров, так как в предельной частоте слоя *F2* почти не намечалось снижение.

Изменения плотности электронов

Максимальная плотность электронов слоев ионосферы (N_e) вычисляется по Ф. Rawer и K. Suchy (1967) по формуле

$$N_e = 1{,}2404(\mathrm{fo})^2 10^4$$

где fo — предельная частота данного слоя в Mc.

На Рис. 3 показана плотность электронов слоев *E*, *F1* и *F2*, подсчитанная по вышеуказанной формуле. Средние величины показаны тонкой линией,

а величины, наблюденные за время затемнения Солнца — жирными линиями. Средняя плотность электронов слоя E составляет около 1,5, слоя $F1$ – 2,8, а слоя $F2$ – $6{,}0 \cdot 10^5$ см^3.

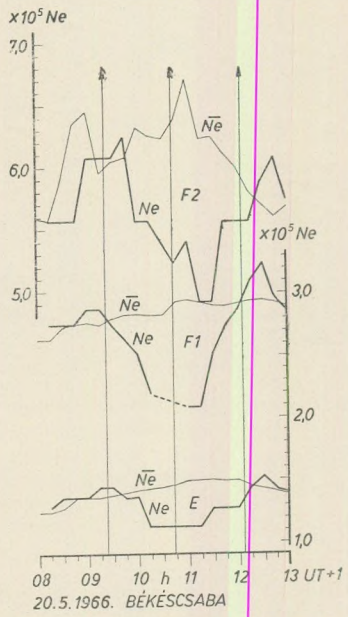

Рис. 3. Изменение плотности электронов за время затемнения Солнца в слоях E, $F1$ и $F2$. Тонкими линиями отмечены средние величины за контрольные дни

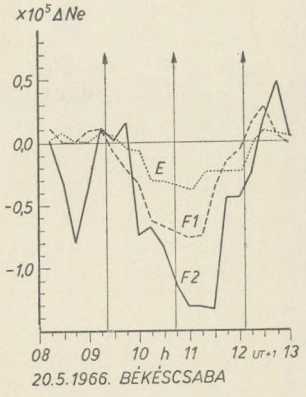

Рис. 4. Отклонение величин плотности электронов во времени от средних величин, за время затемнения Солнца

На Рис. 4 приведены суммарные величины отклонений (ΔN_e), полученные за время затемнения Солнца. Из фигуры видно, что наибольшее снижение концентрации электронов за максимальной фазой затемнения Солнца характерно для слоя $F2$ ($1{,}33 \cdot 10^5$ см$^{-3}$). В данном слое уменьшение плотности в три раза больше, чем в слое E и в два раза больше, чем в слое $F1$. В слое E максимальное уменьшение составляло $4 \cdot 10^4$ см$^{-3}$.

Уменьшение плотности электронов для различных слоев во время затемнения Солнца вычислялось рядом исследователей. Так M. E. Szendrei и M. W. McElhinny (1956) определили уменьшение плотности $1 \cdot 10^5$ в слое $F1$ и $0{,}6-0{,}8 \cdot 10^5$ см$^{-3}$ на различных высотах слоя $F2$ по данным, полученным на станции Грехемстоу, 25 декабря 1954 г. G. Nestorov и J. Taubenheim (1962), вычислили уменьшение плотности электронов слоя E за время полного затемнения солнца над г. Нессебар и частичного над г. Софией с использованием данных, полученных за время затемнения Солнца 15 февраля 1961 г. По их расчетам при полном затемнении (над г. Нессебар) снижение плотсности электронов составило $6 \cdot 10^4$ см$^{-3}$, а над Софией – $5{,}5 \cdot 10^4$ см$^{-3}$. Подобные величины были получены для этих же местностей К. Б. Серафимовым (1964).

Вычисление коэффициента рекомбинации

Величины коэффициента рекомбинации за время затемнения Солнца, а также их изменения были вычислены по методу C. M. Minnis (1955). По его мнению коэффициент рекомбинации для слоя $E(\alpha_E)$ может быть получен с использованием соотношения

$$\alpha_E = \frac{fq_0 \cos^{0,25}\chi - \frac{dE_e}{dt}}{N_e^2}.$$

где f – непокрытая за время затемнения поверхность Солнца, q_0 – степень возбуждения ионов, x – зенитное расстояние Солнца и N_e – количество электронов на 1 см³ во время t.

В рассматриваемом случае размер непокрытой поверхности Солнца был определен по фотоснимкам, полученным в обсерватории „Урания" недалекого города Мишкольц и переданным в наше распоряжение профессором д-ром Дь. Сабо. Ход покрытия поверхности Солнца показан на Рис. 5. Величины полтности электронов для различных времен t, а также величины q_0 взяты из более точной кривой плотности электронов, приведенной на Рис. 3.

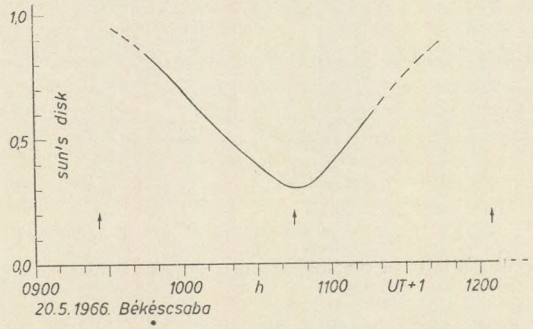

Рис. 5. Изменение размера непокрытой поверхности Солнца за время затемнения, по фотоснимкам Мишкольцской обсерватории „Урания"

Так, коэффициенты рекомбинации могли быть точно вычислены для четырех времен, как это видно по Рис. 6. В первую половину затемнения рассматриваемый коэффициент оказался гораздо меньшим (1,78 – 1,63 – 1,24 · 10^{-8} см³сек$^{-1}$) по сравнению со средней величиной (4 · 10^{-8} см³сек$^{-1}$), а после максимального покрытия наблюдалось увеличение коэффициента (2,05 · 10^{-8} см³сек$^{-1}$).

К. Б. Серафимовым (1964) найдена увеличенная на порядок величина коэффициента по случаю затемнения Солнца, наблюденного в 1961 г. над территорией Болгарии. Во время затемнения Солнца в 1952 г. над гг. Картум и Ибадан C. M. Minnis (1958) вычислил величину 1,2 –

$-1{,}4 \cdot 10^{-8}$ см^{3}сек$^{-1}$. G. Nestorov и J. Taubenheim (1962) считали наиболее вероятной величину коэффициента α_E равную $1 \cdot 10^{-7}$ см^{3}сек$^{-1}$ для затемнения Солнца в 1961 г. над территорией Болгарии.

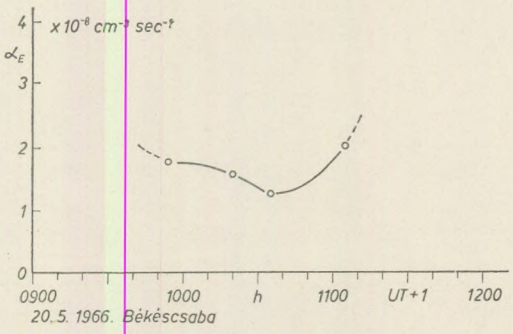

Рис. 6. Изменение величины коэффициента рекомбинации за время затемнения Солнца

В соответствии с вышеизложенным наиболее характерной особенностью затемнения Солнца в мае 1966 г. было происхождение изменений в более высоких слоях после максимального покрытия поверхности Солнца. Объяснение этого явления можно найти в публикации Афинской национальной обсерватории (1966), в которой приведена карта Фраунгофера от 20 мая 1966 с указанием направления и времени прохождения Луны. На западной стороне Солнца, вблизи 300-го градуса периметра располагается активная область, обозначаемая буквой *D*. Вероятно, что данная область, покрытая в последнюю очередь, была центром максимальной ионизации слоев *F1* и *F2*.

Погрешности наблюдения над слоем F1

По мнению C. M. Minnis (1958), E. И. Bramley (1956), J. A. Gledhill (1959) и других исследователей наблюдения над слоем *F1*, проведенные во время затемнения Солнца, не могут дать точных данных о предельной частоте и концентрации электронов, поскольку при наклонном впадении радиоволн предельная частота увеличивается. Поднятие будет максимальной по линии, по которой на поверхности Земли намечается максимальное покрытие Солнца. С удалением поднятие уменьшается, но именно в этих местах подошва пласта оказывается наклонной. Следовательно, можно говорить о *наклоне* нижней поверхности слоя *F1*. По результатам ряда измерений E. N. Bramley (1956) сообщает о наличии углов наклона около 4—5 градусов.

Поскольку при наклонном впадении к приемной аппаратуре поступает более высокая предельная частота, чем при вертикальном, количество частиц (N_e), подсчитанное по предельной частоте в указанных местах, не может быть правильным, а является завышенным.

По мнению C. M. Minnis (1958) необходимо сопоставить ходы предельных частот для слоев *E* и *F1*. В нормальных случаях, когда подошва обоих слоев параллельна поверхности Земли и когда применяемые радиоволны отражаются в вертикальном направлении, *отношение двух предельных частот является постоянным*. Следовательно, если нанести пункты, получаемые в таких случаях из величин предельных частот *foE* и *foF1* в линейную систему координат, то регрессионная прямая этих пунктов проходит через начало координат, или же — с учетом разброса — по крайней мере вблизи его.

При наличии затемнения Солнца точки отражения образуются у наклонной подошвы слоя *F1* и у подошвы слоя *E*, высота которого не изменяется, в связи с чем *изменяется отношение предельных частот foE* и *foF1*. Вследствие этого получаемая таким образом прямая ряда точек проходит дальше от начала координат. И так метод C. M. Minnis позволяет выявить погрешности, но не позволяет определить величину погрешности и даже угол наклона. Однако вероятно, что при помощи вышеуказанного метода можно определить численное значение наклона и тем самым и возникающей погрешности.

Данные, получаемые *по линии* проекции *максимального затемнения Солнца* на Землю должны отображать параллельность подошв слоев *E* и *F1*, так как в данном месте слой *F1* должен характеризоваться максимальным поднятием его высоты. Прямые, получаемые по измеренным здесь данным, должны проходить через начало координат, или же близко к нему. Прямая, получаемая по данным наблюдения, провод мого очень далеко от этой линии, должна иметь подобный ход. Последний случай не требует дополнительного пояснения. Если имеется возможность выявить наличие предыдущего случая, то при использовании достаточного количества данных о затемнении Солнца, можно вычислить отношение угла между прямыми к углу наклона, следовательно, также и предельную частоту и исправленную величину концентрации электронов.

Вышеизложенные соображения подтверждаются прямыми, полученными предлагаемым методом по данным затемнений Солнца в 1961 и 1966 гг. Город Бекешчаба располагается довольно далеко от линии полного затемнения Солнца, наблюденного в 1966 г. в Греции, чтобы намечалась значительная наклонность над ней и на подошве слоя *F1*. К сожалению нет возможности привести здесь прямые, составляемые одновременно по данным, полученным в Греции. Однако в нашем распоряжении имеются подробные данные о затемнении Солнца, происшедшем 15 февраля 1961 г. и характеризующемся полным затемнением над г. Нессебар (42°42′ север, 27°43′ восток) как из Будапешта (1961), так и из Нессебара (1961). Так, на Рис. 7. приводятся прямые, построенные по измерениям *foE* и *foF1*, проведенным в 1966 г. в г. Бекешчаба и в 1961 г. в гг. Будапешт и Нессебар. Сплошными тонкими линиями показано отношение величин *foE* и *foF1* по данным контрольных дней, а пунктирными жирными линиями — то же за время затемнения Солнца. Для г. Бекешчаба и Будапешт, где предполагается наличие значительной наклонности, намечается большой угол между прямыми (20° и 18° соответственно), в то время, как по данным, полученным в Нессебаре при полном затемнении Солнца, этот угол составляет всего 4 градуса.

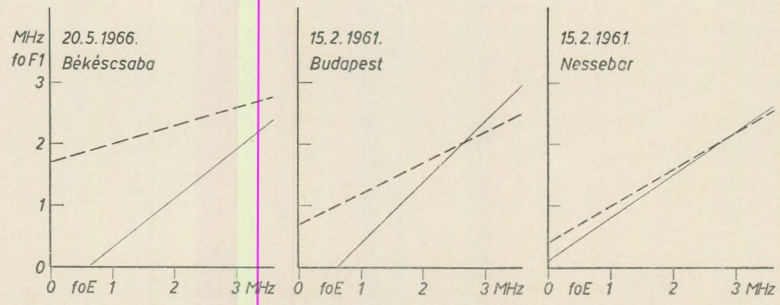

Рис. 7. Регрессионные прямые, полученные по данным *foF1* и *foE* за время затемнения Солнца показаны жирными линиями, а те же прямые по контрольным данным — тонкими линиями. Величины углов между отдельными прямыми позволяют судить о наклоне слоя *F1*.

Данная фигура довольно убедительно свидетельствует о том, что по размеру углов между полученными вышеизложенным образом прямыми можно судить о размере угла наклона. Таким образом, там, где имеются подробные данные по ряду затемнений Солнца, было бы целесообразно определить численное соотношение углов.

ЛИТЕРАТУРА

Gledhill, J. A. (1959): The behaviour of the ionosphere over Cape Town and Johannesburg during the annular solar eclipse of 25 December 1954. Journ. of Atm. and Terr. Physics, Vol. 16, Nos. 3/4, pp. 367–375.

Minnis, C. M. (1959): Ionospheric changes at Singapore during the solar eclipse of 14 December 1955. Journ. of Atm. and Terr. Physics, Vol. 13, Nos. 3/4, pp. 346–350.

Rawer, K. and Suchy, K. (1967): Radio Observations of the Ionosphere. Encyclopedia of Physics, Sect. 33. p. 268. Springer, Berlin.

Szendrei, M. E. and McElhinny, M. W. (1956): Recombination and attachment in the *F1* and *F2* layers during the solar eclipse of 25 December 1954. Journ. of Atm. and Terr. Physics, Vol. 9. Nos. 2/3, pp. 118–130.

Nestorov, G. and Taubenheim, J. (1962): Untersuchungen an der ionosphärischen E-Schicht während der totalen Sonnenfinsternis 15 Februar 1961. Journ. of Atm. and Terr. Physics, Vol. 24. pp. 633–642.

Serafimov, K. B. (1964): Ionisations-Neutralisations-Bilanz in der E-Schicht nach Angaben von der totalen Sonnenfinsternis am 15. Februar 1961. Pure and Applied Geophysics, Vol. 57. pp. 133–142.

Minnis, C. M. (1958): The interpretation of changes in the *E*- and *F1*-layers during solar eclipses. Journ. of Atm. and Terr. Physics. Vol. 12. pp. 272–282.

Bramley, E. N. (1956): Tilts in the ionosphere during the solar eclipse of 30 June 1954. Journ. of Atm. and Terr. Physics. Vol. 8. pp. 98–104.

Minnis, C. M. (1955): Ionospheric behaviour at Khartum during the eclipse of 25th February 1952. Journ. of Atm. and Terr. Physics, Vol. 6. pp. 91–112.

Contribution From The Ionospheric Institute of The National Observatory of Athens. Scientific Report No. IIA009, August 1966.

Ionospheric Data, Budapest, 1961, Országos Meteorológiai Intézet.

Stündliche Werte der Ionosphärendaten, Nesseber (1961). Heinrich Hertz Institut. Berlin.

Gledhill, J. A. (1959): The behaviour of the ionosphere over Cape Town and Johannesburg during the annular solar eclipse of 25 December 1954. Journ. of Atm. and Terr. Physics, Vol. 16. pp. 367–375.

A COMPLEX INTERPRETATION OF GEOPHYSICAL DATA ON THE DEEP STRUCTURE OF HUNGARY, I.

by

KARATAEV, G. I., SHEOHKOV, B. N., STEGENA, L.

(Institute of Geology and Geophysics, Siberian Department of the Academy of Sciences, USSR, — Insitute of Physics of the Earth, Academy of Sciences, USSR, — Geophysical Institute of Eotvös University, Budapest)

Received: 10 July 1967

ZUSAMMENFASSUNG

Die Bouguer-Anomalien (G), die magnetischen Anomalien (Z), das Oberflächenrelief (R), die seismischen Oberflächenwellen (U), die zeitlichen Höhenänderungen (N), die geothermischen Tiefenstufen (T), die tellurischen Ströme (C) und die Tiefe des Grundgebirges (B) werden analysiert, zusammen mit den Daten H_{Conrad} und H_{Moho} von drei seismischen Tiefsondierungsprofilen (*dss*), zwecks der Bestimmung von H_{Moho} für das ganze Gebiet von Ungarn. In diesem ersten Teil der Arbeit sind die Korrelationen zwischen diesen Daten, sowie die Standard-Gleichungen mit den Fehlern nach der Methode der kleinsten Quadrate gegeben.

In Hungary, in the last decade or so the study of various sets of geophysical data has been given a great deal of attention. There are contour maps of the following geophysical parameters: Bouguer anomaly (G), vertical magnetic anomaly (Z), relief of the ground surface (R), group velocities of seismic surface waves (U), variation in repeated high-precision levellings (N), geothermal reciprocal gradient (T), telluric currents (C), depth of the basement (B).

Furthermore, in 3 profiles, deep seismic soundings (*dss*) have been carried out, and the depths of the Conrad (H_c) and Moho (H_M) interfaces have been determined along these profiles.

We can assume that there exists a correlation between all these parameters If this is so, one can calculate H_M from the *dss* profiles for the whole territory of Hungary.

A method of the analytic description of large volumes of geophysical data concerning crustal structure

It is known that the gravity anomalies correlate to some degree with the M interface. This is so because at the M interface there is a discontinuity in ϱ (about 0.3 to 0.5 g/cm^3). A similar correlation is obtained also between the M interface and the relief of the ground surface.

It is known also that the gravity anomaly reflects to a large degree the resultant of the following influences: the variation of the thickness of the sedimentary layer, the heterogeneity of the basement, the variation of the thicknesses of the crustal layers, the heterogeneity of the upper mantle. The magnetic anomalies are, after all, also connected with these influences.

As a consequence, geophysicists use with some success the maps of magnetic anomalies in the study of the sedimentary layer and of the basement material. Hence if such a correlation yields a reliable enough inference concerning the structure of the upper layers, one can exclude from the observed gravity anomalies the influence of the geological factor.

We see that the depth of the M interface (H_M), the observed gravity (G) and magnetic (Z) anomalies, the thickness of the sedimentary layer (B) and the relief of the ground surface (R) are connected with one another. This connexion can be described by the following equation (K a r a t a e v, 1966):

$$H_M(r) = \alpha_0 + \int_{R_0} q_1(r-r')G(r')\,dr' + \int_{R_0} q_2(r-r')Z(r')\,dr' + \int_{R_0} q_3(r-r')B(r')\,dr' + \int_{R_0} q_4(r-r')R(r')dr'. \quad (1)$$

(R_0 — area of integration).

The terms $q_i(r-r')$, ($i = 1, 2, 3, 4$) are unknown weighting functions; the r are the coordinates of the points where the geophysical or geological parameters have been determined.

Furthermore, crustal thickness and dispersion of velocity of seismic surface waves are functionally connected. Thus we can add to equation (1) terms accounting for the dispersion of surface waves, for example in the form $\alpha_1 U_1 + \alpha_2 U_2 + \ldots$ where $U_1, U_2, \ldots$ are the velocities for various periods.

It is further known that the rates of recent crustal movement correlate with neotectonism (M e s h c h e r y a k o v, 1963). As there exists some correlation between the M interface and the neotectonism, we can suppose that the relief of M indirectly (through neotectonism) correlates with the recent rates of crustal movement. Similarly, an indirect correlation may exist between neotectonic and geothermal conditions and also between geothermics and H_{Moho}. Magnetotelluric deep sounding will yield first of all the depth of the basement (and of the low-velocity layer). There exists a correlation between depth of basement and Moho depth, and thus there may exist an indirect correlation between C and depth of Moho, too.

Thus we can include in our mathematical model of the Earth also the rates of recent crustal movement, the geothermal conditions and the results of magneto-telluric deep sounding, for example in the following form:

$$\alpha N + \beta T + \gamma C.$$

The above considerations imply that the elements just mentioned (the relief of the ground surface, the rates of recent movements, dispersion of surface waves, gravitational and magnetic anomalies, thickness of the sedimentary layer, geothermal gradients, electrical conductivity) are to some degree

connected (directly or indirectly) with the depth of the M interface. We can try to describe this connection analytically, either for all elements, or only for some of them. The importance of such a description is evident:

1. We can study in a quantitative way the degree of correlation between these various elements and the thickness of the crust, and the influence of each element upon the M surface.

2. We can obtain some quasi-analytic form of the connexion between these elements, in whose possession we can predict any parameters of the crust (for example H_M).

In a first approximation we may seek the analytic form of the connexion between the elements as follows:

$$H_M(r) = \alpha_0 + \alpha_1 G(r) + \alpha_2 Z(r) + \alpha_3 B(r) + \alpha_4 R(r) + \alpha_5 N(r) + \alpha_6 U_1 + \alpha_7 U_2 + \alpha_8 U_3 + \alpha_9 U_4 + \alpha_{10} T(r) + \alpha_{11} C(r). \tag{2}$$

We can then investigate the equations

$$H_M(r) = \alpha_0 + \sum_{i=1}^{11} \alpha_i f_i[\lambda_{ni}(r)] \tag{3}$$

where $\lambda_{n1} = G$, $\lambda_{n2} = Z$ are some functions known beforehand (for example $f_1(G) = G^2$ or $f_2(Z) = e^{-Z}$, and so on).

The nature of the function $f_i(\lambda_{ni})$ can be inferred from the analysis of two values: H_M and λ_{ni}, $i = 1, 2, \ldots 11$ for all elements. In our calculations we shall take that function which gives minimum error.

Should equation (3) not prove satisfactory because of a too great error, we shall analyse an equation of the following type:

$$H_M(r) = \alpha_0 + \sum_{i=1}^{11} \int_{R_0} q_i(r - r') f_i[\lambda_{ni}(r')] dr'. \tag{4}$$

For these calculations it is necessary to possess the experimental data H_M, G, ... These are known along the profiles of *dss*.

If we introduce the experimental data in our formula, we must add $\varepsilon(r)$ to the left-hand side; formula (2) can then be rewritten to read

$$H_M(r) + \varepsilon(r) = \alpha_0 + \alpha_1 G(r) + \ldots + \alpha_{11} C(r). \tag{5}$$

If we solve a system of n such equations for n points $(r_1, r_2, \ldots r_n)$ we can, using the method of least squares, obtain the unknown parameters α and the mean square error ε of H_M as calculated from $G, Z, \ldots C$.

Provenience of data.

Fig. 1. shows the maps of the various data used by us. The authors are as follows:

G: Renner, 1959
Z: Posgay, 1967
R: Schmidt, 1961
U: Shechkov, 1968
N: Bendefy, 1965
T: Stegena, 1964
C: Ádám – Verő, 1967
B: Kőrössy, 1964
dss: Mituch, 1966, 1967.

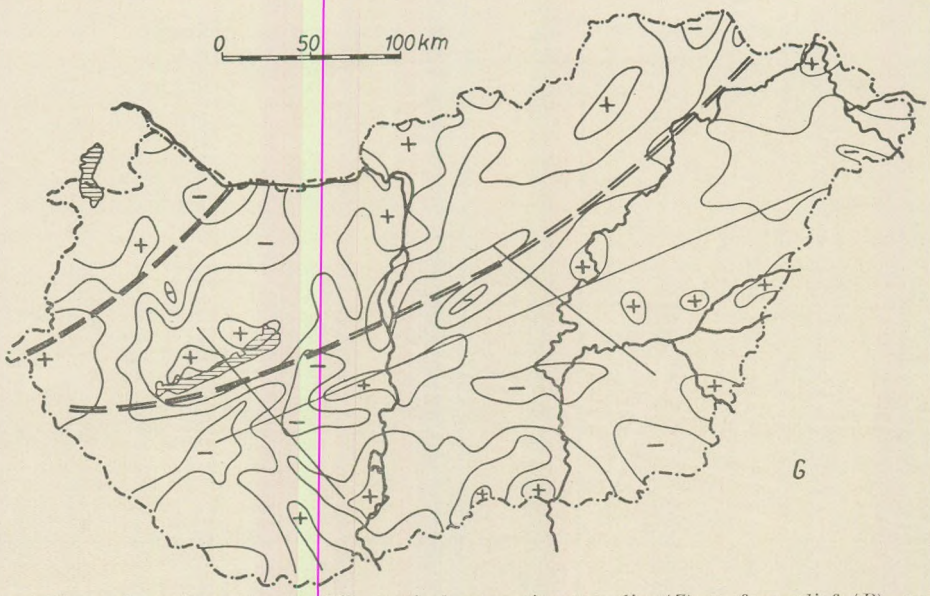

Fig. 1. Maps of gravity anomalies (*G*), vertical magnetic anomalies (*Z*), surface relief (*R*), variation in repeated high-precision levellings (*N*), geothermal reciprocal gradient (*T*), telluric currents (*C*), depth of the basement (*B*), group velocities of seismic surface waves (*U*) and results of deep seismic soundings (*dss*), used in this work

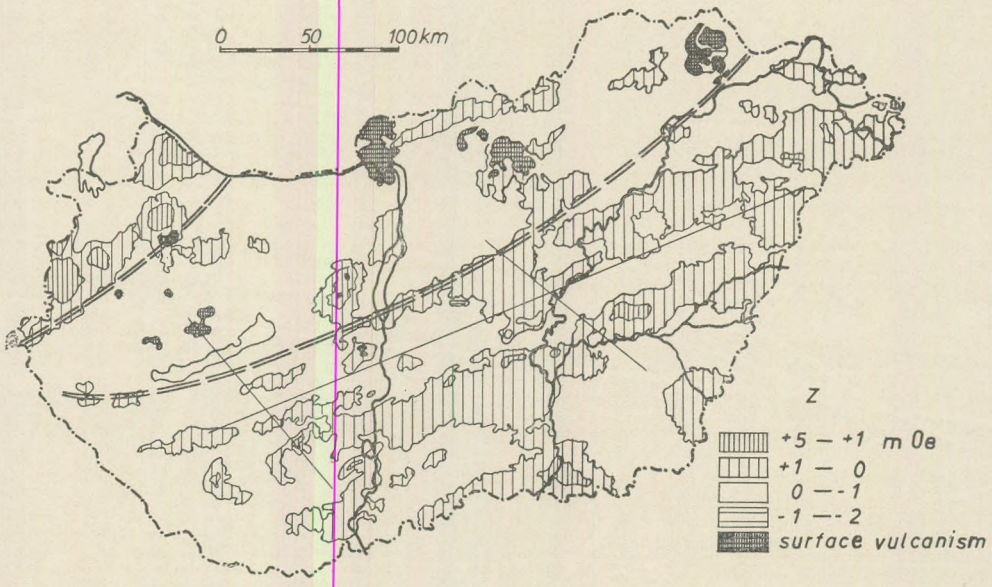

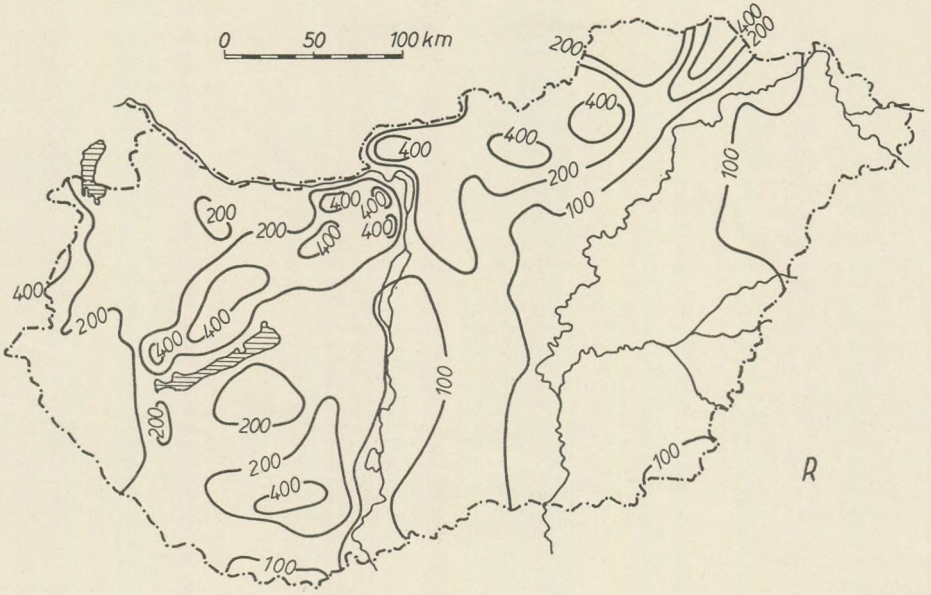
0 50 100 km
R

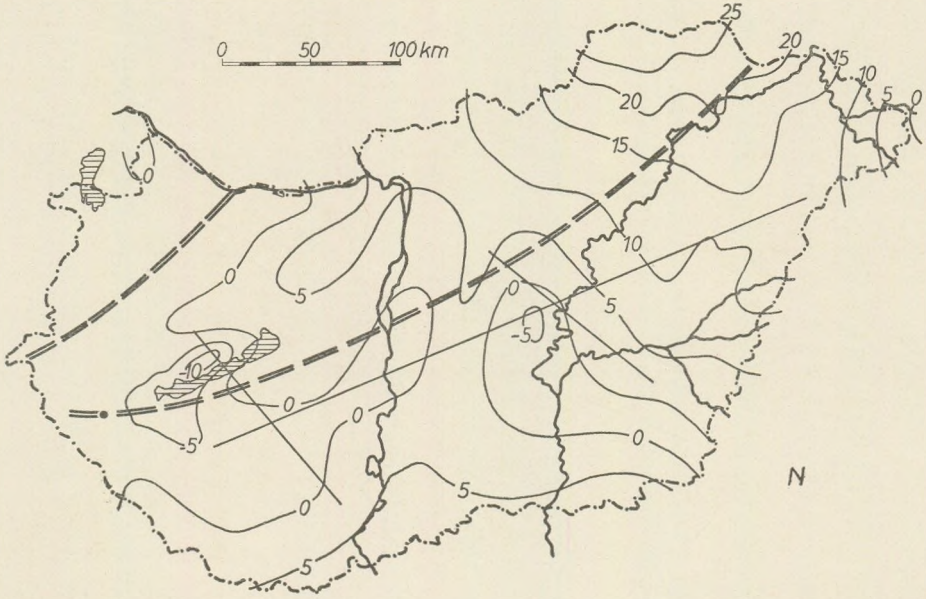
0 50 100 km
N

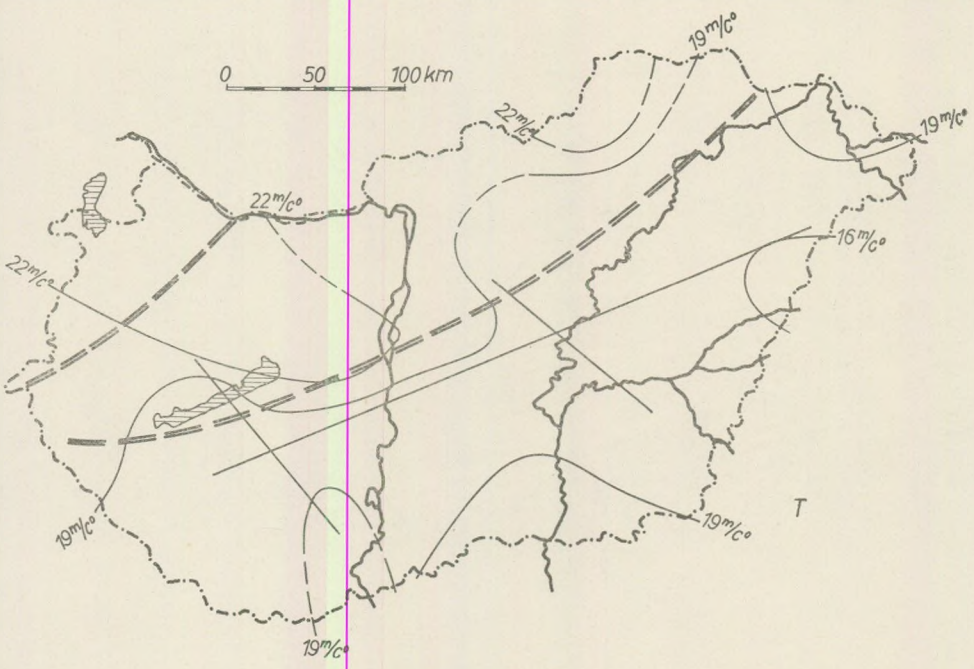

Fig. 1. Maps of gravity anomalies (*G*), vertical magnetic anomalies (*Z*), surface relief (*R*), variation in repeated high-precision levellings (*N*), geothermal reciprocal gradient (*T*), telluric currents (*C*), depth of the basement (*B*), group velocities of seismic surface waves (*U*) and results of deep seismic soundings (*dss*), used in this work

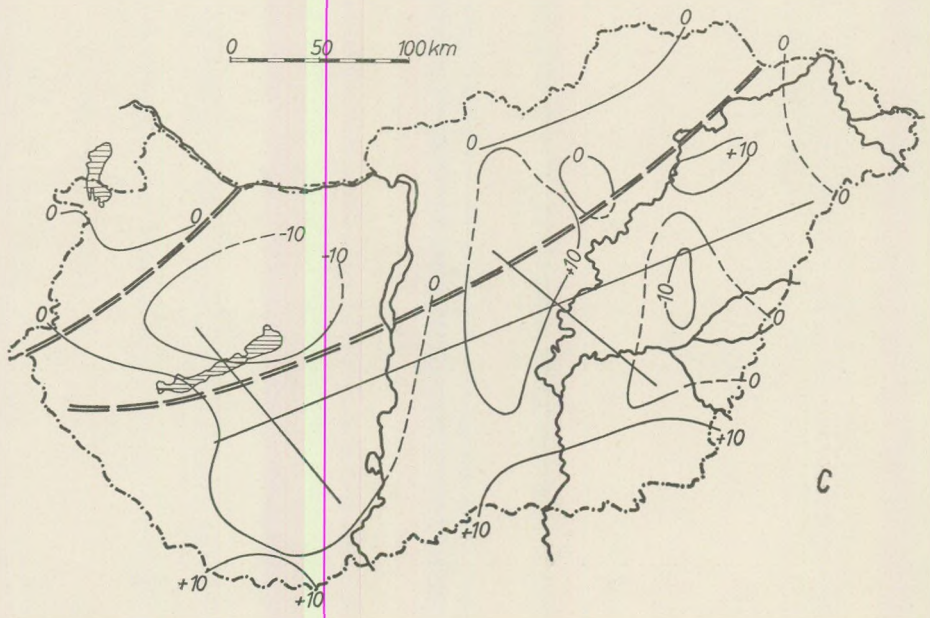

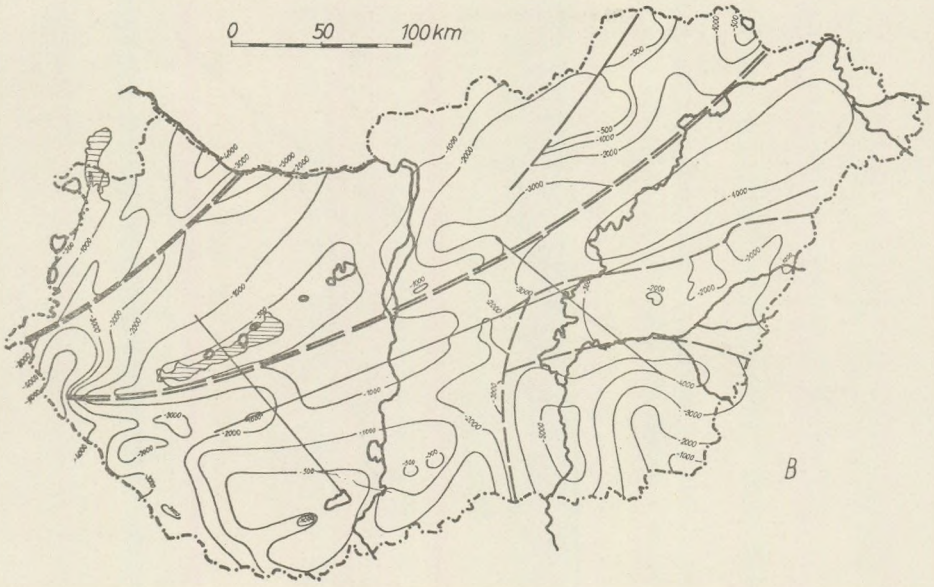
0 50 100km
B

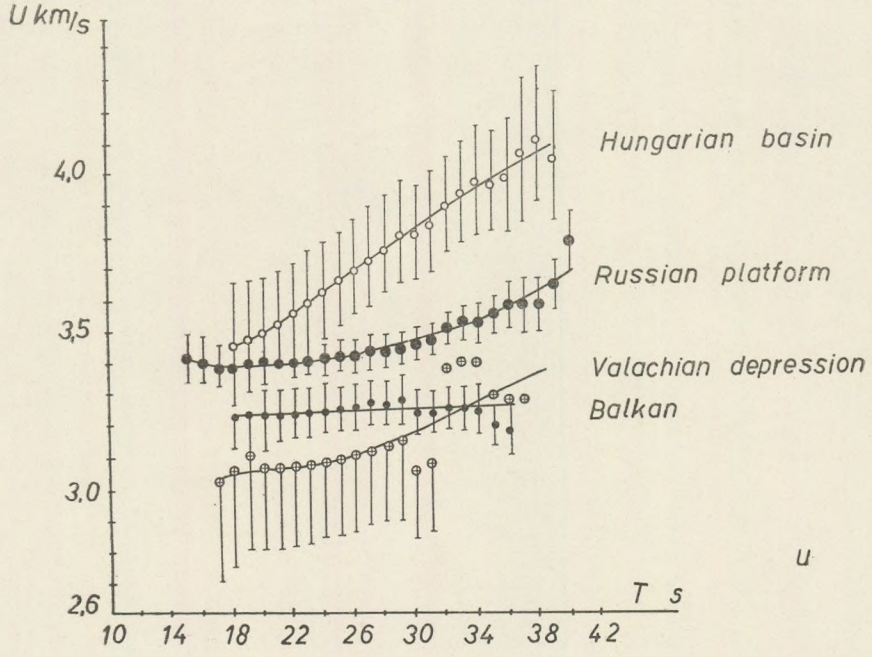
U km/s
4,0
3,5
3,0
2,6
10 14 18 22 26 30 34 38 42
T s
Hungarian basin
Russian platform
Valachian depression
Balkan
u

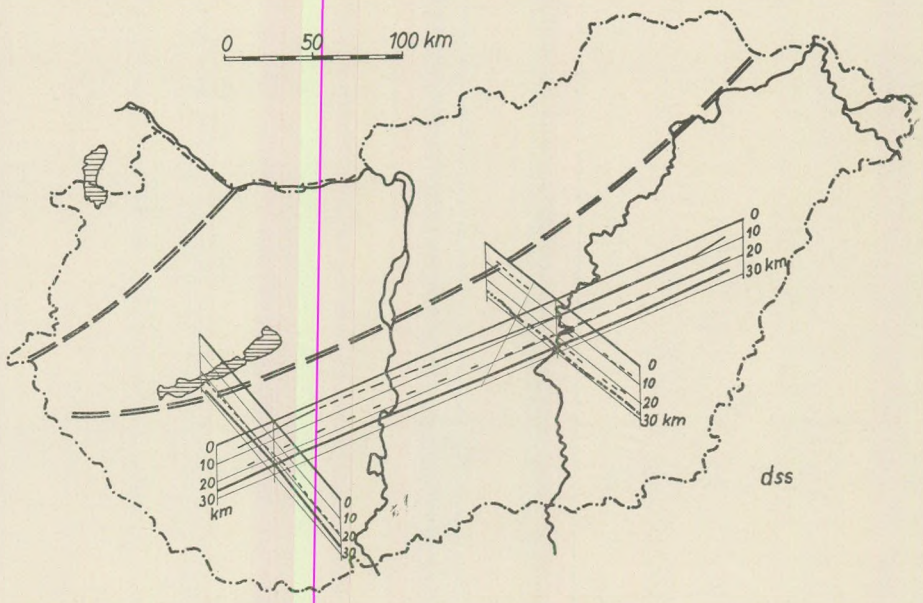

Using these maps, we read out the values at the grid points of a grid of 10 km spacing. This grid was different for the profiles I, II and III, as shown in Fig 2. In Fig. 1. dss the double lines separate the geological super-provinces of Hungary; Tertiary depressions (*A*) form the Hungarian Mountains (*B*).

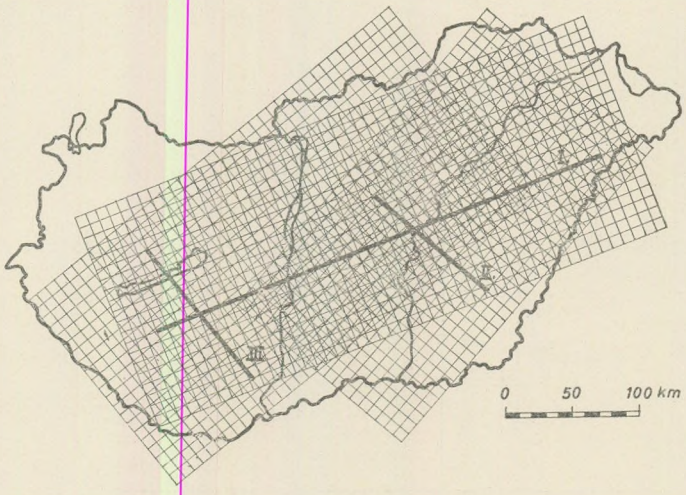

Fig. 2. Seismic *dss* profiles and the read-out grids

Calculations of standard equations using the *dss* profiles

The calculations were performed on the computers of the Siberian Department of the Academy of Sciences, USSR.

At first, we tried to obtain standard relations for the profiles I, II and III, separately for the geological areas A and B.

These calculations have implied that:

1 For area B it is not possible to get good enough standard relations, as the data of *dss* are too scanty.

2. In area A, it is not possible to calculate H_c from the data available, as the standard error is too great (~ 10 km).

3. In area A, the standard errors of the equations connecting H_M with Z, R and G do not exceed 1.3 km:

$$26\,348 - 0.0092Z_0 - 0.0084\Sigma_1 Z + 0.0018\Sigma_2 Z + 0.0027\Sigma_3 Z + 0.0004\Sigma_4 Z + \\ + 0.0042\Sigma_5 Z + 0.0048\Sigma_6 Z = H_{M,0}; \quad \varepsilon = 1.3 \text{ km}$$

$$29\,509 - 0.0192R_0 - 0.0043\Sigma_1 R + 0.0007\Sigma_2 R - 0.0015\Sigma_3 R + 0.0021\Sigma_4 R + \\ + 0.0009\Sigma_5 R - 0.0001\Sigma_6 R = H_{M,0}; \quad \varepsilon = 1.2 \text{ km}$$

$$28\,420 - 0.0130G_0 + 0.0498\Sigma_1 G - 0.0328\Sigma_2 G + 0.0170\Sigma_3 G - 0.0107\Sigma_4 G - \\ - 0.0358\Sigma_5 G - 0.0383\Sigma_6 G = H_{M,0}; \quad \varepsilon = 1.2 \text{ km}$$

Fig. 3. shows the measured values of H_M along *dss* profile I, and, as examples, the depths calculated from the equations for R and Z.

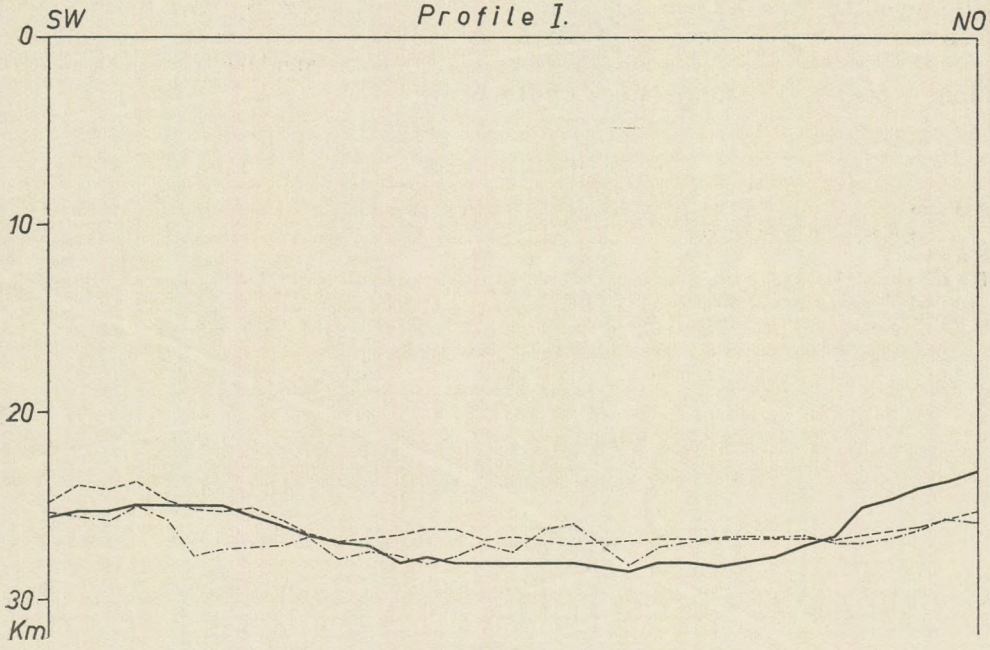

Fig. 3. The measured depths (solid line) and the calculated depths of Moho

4. These preliminary calculations have shown that the joint analysis of various geophysical data in order to determine H_M, using those data that give separately a small enough error, is an entirely feasible undertaking. Hence, we proceeded to calculate the standard equations for the following 15 combinations of data (Table I.)

Table I.

Combinations of data, used to determine the standard equations for H_M, and the standard errors·

$H_M = f(G, Z, R, N)$	1.080
$H_M = f(R, N, T, C)$	1.088
$H_M = f(R, N)$	1.090
$H_M = f(G, Z, R, N, U)$	1.118
$H_M = f(G, Z, R. N. T, C, U)$	1.124
$H_M = f(R, N, T, C, U)$	1.129
$H_M = f(R. N, U)$	1.130
$H_M = f(G, Z, T, C)$	1.433
$H_M = f(G, Z, T, C, U)$	1.487
$H_M = f(T\ C)$	1.535
$H_M = f(G, Z)$	1.536
$H_M = f(G. Z, R, N, T, C)$	1.573
$H_M = f(T, C, U)$	1.590
$H_M = f(G, Z, U$	1.592
$H_M = f(U)$	1.633

As shown in Table I, the best value of H_M is obtained using the combination G, Z, R, N (gravimeter, magnetometer, relief and time variation in precision levelling, geothermal data and telluric currents; R, N relief, time variation in precision levelling, geothermal data and telluric currents.

In part II, using the above equations we shall calculate the depth of the Moho interface for the territory of Hungary.

REFERENCES

Ádám, A. – Verő, J. (1967): Latest results of electromagnetic measurements in Hungary Geofizikai Közlemények XVI. 1 – 2. Fig. 9.

Barta, Gy. (1957): Geomagnetism (in Hungarian). Budapest.

Bendefy, L. (1965): Grundlegende Probleme der Erforschung der rezenten Erdkrustenbewegung. Gerl. Beitr. z. Geophysik 74. 6.

Karataev, G. I. (1966): Korrelyazionnaja shema geologicheskoj interpretazii gravitazionnykh i magnitnikh anomaliy. Nauka, Novosibirsk.

Kőrössy, L. (1964): Tectonics of the basin areas of Hungary. Acta Geol. VIII.

Meshcheryakov, Yu. A. (1963): Vekovyji dvizenija zemnoj kory. Sb. „Sovr. dviz. zemn. kory", 1.

Mituch, E. (1966): Recent progress in the seismic deep sounding of Hungary using continuous broadside shooting system. Geofizikai Közlemények. XV. 1 – 4.

Mituch, E. (1967): Seismic investigation of the Earth's crust and recent progress in Hungary. Geofizikai Közlemények XVI. 1 – 2.

Posgay, K. (1967): A comprehensive survey of geomagnetic masses in Hungary. Geofizikai Közlemények XVI. 4.

Renner, J. (1959): Final elaboration of the measurements of the Hungarian national network of gravity bases. Geofizikai Közlemények VIII. 3.

Schmidt, E. R. (1961): Hydrogeologis her Atlas Ungarns. Budapest, p. 1.

Shechkov, B. N. (1968): Kharakteristika tektonicheskih blokhov Eurasii po dispersii poverhnostnih voln. I. Izv. ANSSSR, Fizika Zemli (in press).

Stegena, L. (1964): Geothermic maps of Hungary. Geofizikai Közlemények XII. 2.

PALAEOMAGNETIC INVESTIGATION OF MAGMATIC ROCKS FROM THE MECSEK MOUNTAINS, SOUTHERN HUNGARY

by

P. MÁRTON – E. SZALAY-MÁRTON

(Geophysical Institute of Eötvös University and State Institute of Geophysics, Budapest)

(Received: 5. 12. 1968)

SUMMARY

The paper presents the results of the palaeomagnetic investigation of 12 Lower Cretaceous and one Helvetian magmatic rock outcrops in the Mecsek Mountains. Of the thirteen, eight outcrops turned out to lend themselves to palaeomagnetic evaluation. Of these, six Cretaceous ones exhibit reverse magnetization, whereas one Cretaceous and one Helvetian locality are directly magnetized.

After the application of a correction for tilt the mean directions of magnetization cluster about two azimuths and inclinations, respectively: (1) $\bar{D}_1 = 349.3°$; $\bar{I}_1 = 51.2°$; (2) $\bar{D}_2 = 83.1°$; $\bar{I}_2 = 62.0°$. The deviation in D is significant. The pair $\bar{D}_1$, $\bar{I}_1$ agrees well with the values $\bar{D}_E$, $\bar{I}_E$ computed for the sampling localities from the mean virtual Eurasian Cretaceous pole (cf. the 20 data in Table I): $\bar{D}_E = 6.9°$; $\bar{I}_E = 54.9°$. The deviation of Group 2 from Group 1 (or, what amounts to the same, from the mean European direction) suggests a clockwise rotation by about 90°, about a vertical axis, of Group 2. This can be readily correlated with the involved changes of strike in the Mecsek Mountains geology. We have established rotation corrections for the individual localities on the basis of the geological map and determined the position of the Lower Cretaceous virtual geomagnetic pole as $\Phi = 81.0°$ and $\Lambda = 172.5°$ as a mean of all the seven evaluable Lower Cretaceous localities.

Introduction

Prior to an evaluation of palaeomagnetic data it is necessary to investigate whether the routine methods of such evaluation are applicable to the region and geological age involved: this investigation has to cover both geophysical and geological aspects.

The method of evaluation is based on the assumption of an axial geocentric dipole, i.e. on the assumption that on a long-range average (a few times 10^4 years or 10^5 years) the geomagnetic field can be described as the field of a magnetic dipole which is concentric with the Earth and whose magnetization is coaxial with Earth rotation. This assumption can be regarded as proved for geological ages not too long past (the Neogene, Quaternary and Recent times).

According to the actually accepted dynamo theory of geomagnetism, the equivalent geocentric dipole is (approximately) coaxial with rotation. Provided the geomagnetic field was during the geological ages sustained by the dynamo effect, the mean direction of the virtual geomagnetic poles (VGP's) averaged over a sizable coherent area (a continent) will point out at the same time also the direction of the axis of rotation. For the dipole hypothesis to be tenable, it is necessary that the scatter of the VGP's as computed from sufficiently reliable palaeomagnetic data should not exceed the actual scatter of VGP's. Concerning geological periods long past (the Mesozoic and Palaeozoic) the data should relate to one continent because together with the displacement of one continent relative to another the VGP directions will move also.

VGP data for the Eurasian Cretaceous (Table I, Fig. 12) reveal a scatter not exceeding that computed from present-day observatory data. (C o x and D o e l l, 1961.) Hence, the Cretaceous geomagnetic field can be treated as a

Table I. Eurasian VGP data

Location	Reference	Palaeomagnetic pole	
		$A°$	$\Phi°$
Britain			
1. Sussex	Nairn 1960	334.0	86.0
2. Sussex	ibid.	182.0	84.0
Rumania			
3. Ovidiu	Costa-Foru et al. 1964	121.0	83.0
4. Cuza-Voda	ibid.	131.0	85.5
Czechoslovakia			
5. Sluhy, Vrbatuv Kostelec	Bucha et al. 1963	158.22	78.95
Korea			
6. South Korea	Kienzle et al. 1966	140.6	73.9
Soviet Union			
7. Hissar	Khramov 1967	164.0	72.0
8. Hissar	ibid.	182.0	72.0
9. Hissar	ibid.	177.0	81.0
10. Hissar	ibid.	145.0	81.0
11. Ferghana	ibid.	332.0	75.0
12. Ferghana	ibid.	176.0	69.0
13. Ferghana	ibid.	176.0	65.0
14. Ferghana	ibid.	178.0	65.0
15. Ferghana	ibid.	178.0	65.0
16. Azerbaidzhan	ibid.	202.0	53.0
17. Tadzhikistan	ibid.	315.0	83.0
18. Turkmenia	ibid.	167.0	60.0
19. Primorlya	ibid.	146.0	58.0
20. Taimyr, Krasnovar	Vlasov – Nikolaichik 1964	334.0	73.0
Common mean direction*		170.1	78.0

* Fischer's statistical parameters: $k = 27.1$; $\alpha_{95} = 6.5°$

Fig. 1.


Szászvár
Mága
N
Mecseknádasd
Márévári-völgy
2 4 7
3
9 10 11
6
8
KOMLÓ
13
Zobák-psz.
12
5
Hosszúhetény
1
Zengővárkony
0 1 2 3 km
a
b
c
d
e
f
g
h
i
j
k
l
m
n
o
p
1

dipole in palaeomagnetic considerations. The scarcity of European data (five in all) has led us to consider as the VGP direction valid for the Mecsek Mountains magmatites (and consequently as the direction of the pole of the geomagnetic field that magnetized them at the time of their origin) the mean Eurasian VGP direction $\Phi = 78.0°$, $\Lambda = 170.1°$.

Magnetization of the rocks was detected by means of astatic magnetometers on cubes of 2.5 cm edge. The magnetometer of MA-21 type was used in two sensitivity settings: $c = 0.34\gamma$ per scale division and $c = 0.059\gamma$ per sc.d The sensitivities of the magnetometers built at our Laboratory are $c = 0.8\gamma$ per sc.d. and $c = 0.7\gamma$ per sc.d. respectively.

In order to remove secondary magnetization we applied A.C. demagnetization in 100 Oe steps. The statistical analysis of the magnetic directions of partially demagnetized sample groups was performed by the method of Fisher (F i s h e r, 1953). Original magnetization was established as the mean direction for which scatter was minimal.

Tilt correction was applied to the mean RM direction of each sampling locality separately, under the assumption of horizontal fold axes.

Geology

The magmatic rocks investigated all occur in the Eastern Mecsek, in the topography feature called the Zengő range. Sampling localities were plotted on the geological map of E. V a d á s z (1935) (Fig. 1): the relevant data are summarized in Table II. Sample groups 1 to 8 were collected under personal cooperation from I. Bilik, groups 9 to 12 under personal cooperation from I. Viczián.

The sampling area (Fig. 1) is a perisyncline with a sedimentary sequence ranging from the Liassic to the Middle Cretaceous. At its middle between Kisújbánya and Jánosipuszta there are Malm and Cretaceous deposits penetrated by trachydolerite lavas. The perysincline topographically constitutes a basin closed to the east by inward-dipping older Jurassic strata. Between Hosszúhetény and Pécsvárad the Lower and Upper Liassic constitute an anticline with Lower Liassic at its core. Sampling locality 5 is situated on the north flank of this anticline. This flank slopes down to Kisújbánya and consists of Dogger, Malm and Cretaceous strata. Sampling localities 1, 12 and 13 are connected with this anticline. North of Kisújbánya the perisyncline ends alsó with Dogger, Malm and Cretaceous strata dipping westward and southward. In the Máza valleyhead, Lower Liassic crops out with a phonolite (Localities 9, 10, 11). This flank is delimited to the north by a big east-west fault. To the southwest of this fault there is the Márévár anticline, an upright fold with a Middle Dogger core and involved plications of Dogger-Malm and trachydolerite in its flanks. "*The axis of this anticline is, as distinct from the usual east-west direction, oriented southwest-northeast*". (V a d á s z, 1935). Localities 2, 3, 4 and 7 are situated on the external (northwest) flank of this anticline. This flank continues beyond a fault between Komló and Jánosipuszta (Localities 6 and 8). A dislocated portion of the external flank constitutes the Magyaregregy – Nagymányok range whose fundamental feature is a Mesozoic complex

Table II. Mecsek Mountains sampling localities with characteristic parameters

Age	Sampling locality	Formation	Tectonic position	Tilt correction
			azimuth/angle of dip	azimuth/angle of tilt
			in degrees	
Lower Cretaceous	1. Zengővárkony	trachydolerite lava agglomerate	N-NW/30 – 50*	165/40
	2. Márévár valley	trachydolerite lava agglomerate	305/30*	125/30
	3. Márévár valley	trachydolerite dyke	?	–
	4. Márévár valley	trachydolerite lava	305/30*	125/30
	5. Hosszúhetény	trachydolerite dyke	N-NW/35 – 45*	165/40
	6. Jánosi Nagy valley	trachydolerite lava	310/30*	130/30
	7. Márévár valley	trachydolerite lava agglomerate	305/30*	125/30
	8. Jánosi puszta	trachydolerite lava agglomerate	120 – 150/30 – 40*	315/35
	9. Máza valley-head	amphibolitic teschenite	S/40**	360/40
	10. Máza valley-head	phonolite lava	S/45**	360/40
	11. Máza valley-head	phonolite dyke	S/45**	360/40
	12. Kövesdtető	phonolite lava	40/48**	220/48
Helvetian	13. Komló	amphibole andesite	–	–

* oral communication by I. Bilik
** oral communication by I. Viczián

overthrust upon the Mediterranean deposits (Miocene). The Zengő Range perisyncline merges to the west in the Komló profile into a single anticline, whereas to the east it passes into the imbricated and dislocated north flank of the southern anticline; that is, it has a spindle-like shape tapering towards the east and west.

The Mecsek Mountains trachydolerite volcanism is placed into the Valanginian and Hauterivian stages of the Cretaceous on the basis that it penetrates the Jurassic, with inclusions and, indeed, enormous blocks of Jurassic limestone in the lava and also in the tuffs, and that the volcanics are overlain by a littoral deposit consisting almost entirely of reworked trachydolerite and containing Hauterivian, Barremian and Aptian fossils.

The age of the phonolite cannot be directly established but since it is regarded as the acid product of differentiation of the phonolitic magma, it is also placed into the Cretaceous.

Trachydolerite eruption took place in connexion with the late part of the Neo-Cimmerian phase of orogeny — which also caused the uplifting of the Mesozoic deposits above sea level — and spread over the Jurassic surface, partly on dry land and partly in a shallow sea. The folding of the mountains took place only subsequently, in the Austrian phase of orogeny.

The amphibole andesite of Komló is an isolated body of volcanic rock. It is not underlain by any deposit younger than Mesozoic. The oldest deposit overlying it is the Lower Helvetian congerian complex. Its age is subject to discussion (Helvetian? Eocene?)

Of the cycles of dislocations that affected the deposits described above, the Austrian phase developed the principal elements of the entire Mecsek structure and the Rhodanian phase brought about imbrications, overthrusts and normal faults, the latter partly parallel, partly perpendicular to the main strike of the mountains. The folds have not, except for the marginal ones along the feet of the mountains, resulted in intense vertical disclocations. The faults parallel to the strike (longitudinal faults) are partly connected with the folding of the mountain, partly with strike-slip dislocations. There are numerous transversal faults (faults perpendicular to the strike of the mountains) which "*effected sinuosities in the strike of the strata, that is, they also brought about largely horizontal dislocations*" (V a d á s z, 1935).

Results

The uncorrected palaeomagnetic results are shown in Table III. The individual groups of samples invite the following comments.

Table III. Direct measurement results

Legend: N/N_0 ratio of evaluated to collected samples
$\overline{D}$ mean declination
$\overline{I}$ mean inclination
k Fisher's precision parameter
$\alpha°$ radius of the confidence circle at the 0.95 confidence level

Sampling locality	N/N_0	$\overline{D}°$	$\overline{I}°$	k	$\alpha°$	Demagnetization step yielding minimum scatter, in Oe
1. Zengővárkony	0/5	—	—	—	—	—
2. Márévár valley	0/9	—	—	—	—	—
3. Márévár valley	4/5	350.4	+51.5	27.0	18.0	100
4. Márévár valley	4/5	227.7	−60.1	60.0	12.0	0
5. Hosszúhetény	5/6	298.7	−39.1	36.0	12.8	200 – 300
6. Jánosi Nagy valley	6/6	205.4	−73.3	50.0	9.6	0
7. Márévár valley	0/7	—	—	—	—	—
8. Jánosi puszta	0/2	—	—	—	—	—
9. Mája valleyhead	3/3	—	—		—	200
10. Mája valleyhead	2/2	216.1	−45.9	17.0	13.9	100
11. Mája valleyhead	3/6	—	—	—	—	100
12. Kövesd-Peak	0/9	—	—	—	—	—
13. Komló	10/10	82.4	+61.8	112.0	4.2	0

1. Zengővárkony, Dezső-Rezső valley; trachydolerite pillow lava. $\overline{I}_n = 180 \cdot 10^{-5}$ cgs, $\overline{Q}_n = 0.8$. The deviations between the individual values within the group are rather slight for both parameters. The direction of original

remanent magnetism exhibits a great-circle distribution which includes the actual field vector, suggesting remagnetization in the actual field. A.C. demagnetization brings about random changes in both the direction and magnitude of RM except for two samples (Figs. 2a,b). No mean RM direction can be established.

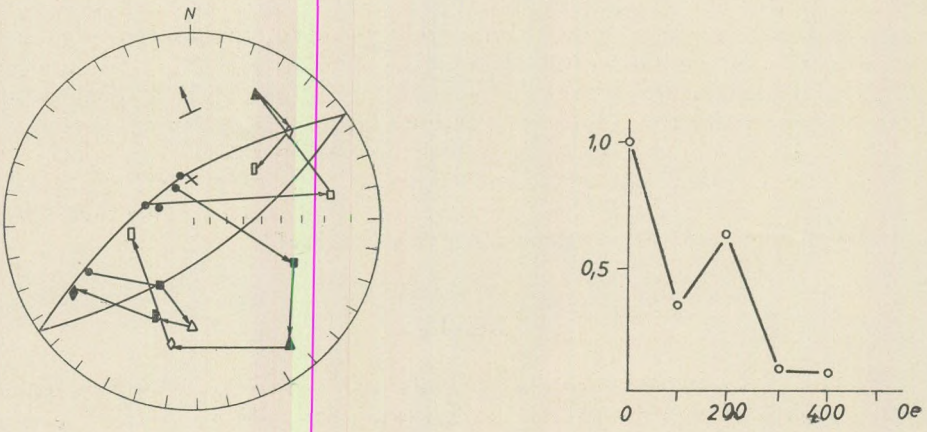

(a) (b)

Fig.2. Zengővárkony, Dezső-Rezső valley (1)

(a) The behaviour of the direction of RM in the course of AC demagnetization

Legend:

+ : present field direction
* : mean palaeomagnetic field direction
● : direction of initial RM

Directions of RM after demagnetization at field strengths of:

■ : 100 Oe
▲ : 200 Oe
◆ : 300 Oe
▮ : 400 Oe

(filled symbol: normal magnetization; empty symbol: reverse magnetization)

→ dip direction (for numerical value see Table II.)

(b) The behaviour of the intensity of RM in the course of AC demagnetization, referred to the original value as unit. (Alternating-field demagnetization graph)

2. Márévár valley, trachydolerite lava (agglomerate). Both the initial RM intensity (I_n) and the Koenigsberger ratio (Q_n) exhibit strong fluctuation, the former in the range of 47 to $760 \cdot 10^{-5}$ cgs, the latter in the 0.1 to 10.8 range. The directions of the initial RM are randomly scattered (Fig. 3a). The RM direction in samples of high Q_n is relatively stable during demagnetization; in samples of low Q_n it varies randomly. The RM directions of samples showing the same direction of magnetization after the individual stages of demagnetization are far apart, with both normal and reverse directions occurring. Variation of intensity is as on the example shown as Fig. 3b. No mean RM direction can be given.

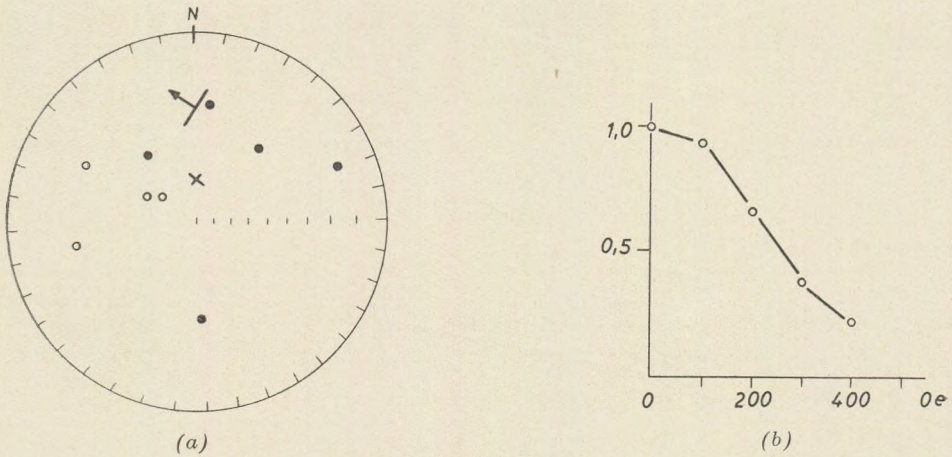

Fig. 3. Márévár valley (2)
(a) Original RM direction. Legend as in Fig. 2a
(b) Alternating-field demagnetization graph

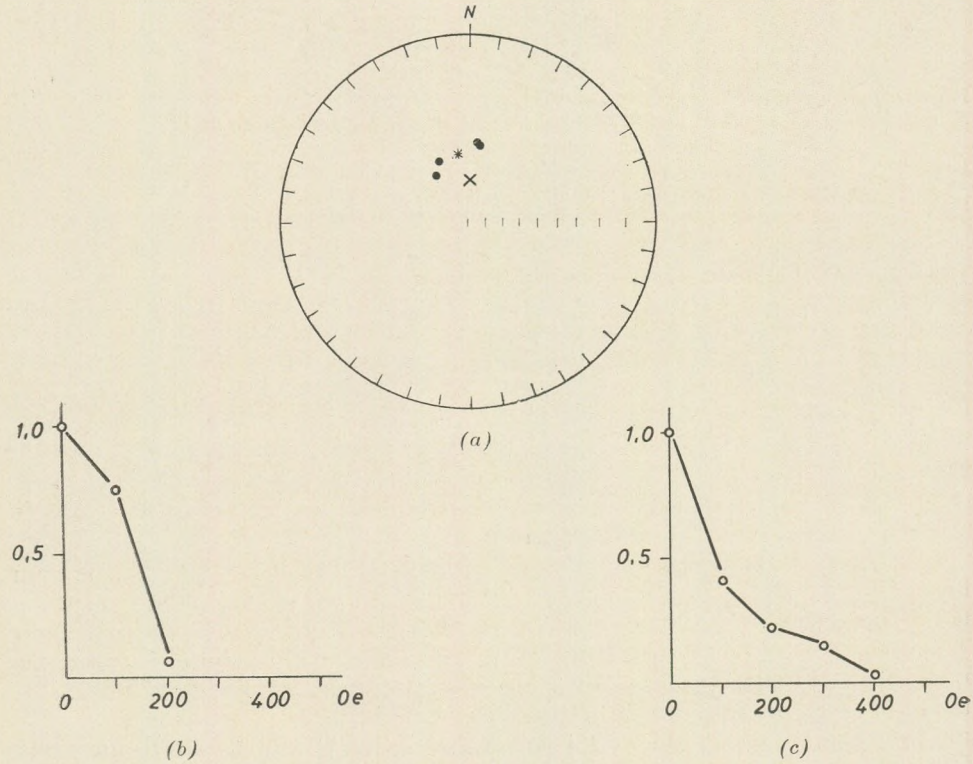

Fig. 4. Márévár valley (3)
(a) RM directions subsequent to 100 Oe demagnetization. Legend as in Fig. 2.
(b), *(c)* types of alternating-field demagnetization graphs

3. Márévár valley, trachydolerite dyke. $\bar{I}_n = 160 \cdot 10^{-5}$ cgs, $Q_n = 0.7$. The mean RM direction was computed from the 100 Oe demagnetization value (Fig. 4a). RM practically disappeared after the application of a 200 Oe alternating field in Samples 812 and 817, and after 400 Oe in samples 815 and 817 (Figs. 4b,c).

4. Márévár valley, trachydolerite lava. $\bar{I}_n = 2600 \cdot 10^{-5}$ cgs, $Q_n > 4$ for all samples. The mean RN direction was determined from the initial RN directions (Fig. 5a), because the demagnetization of the samples (Fig 5b) does not affect the RM direction.

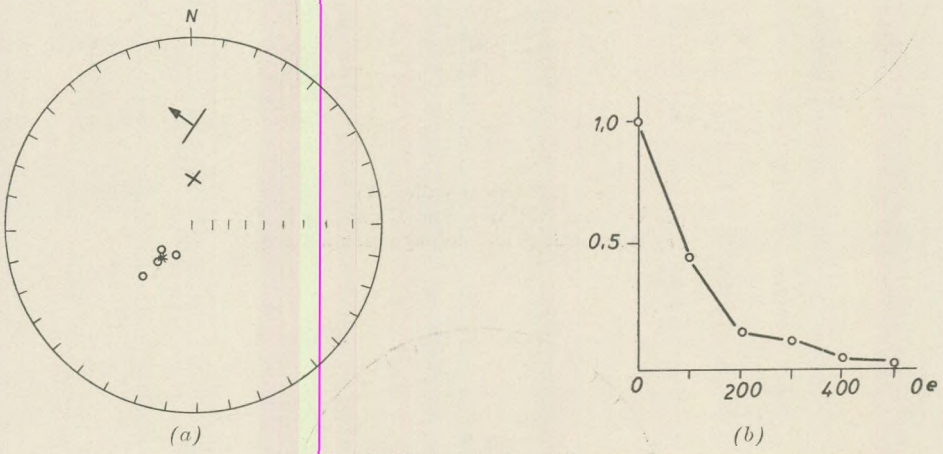

(a) (b)

Fig. 5. Márévár valley (4)
(a) Initial RM direction. Legend as in Fig. 2.
(b) Alternating-field demagnetization graph

5. Trachydolerite dyke, Hosszúhetény. $\bar{I}_n = 74 \cdot 10^{-5}$ cgs, $Q_n = 0.32$. Figs. 6b,c show two typical demagnetization graphs. The mean RM direction was computed after 200 Oe demagnetization for the samples of one type and after 300 Oe for the other type (Fig. 6a), because the secondary-magnetization component is harder in the second type.

6. Jánosi Nagy Valley, trachydolerite lava. $\bar{I}_n = 2198 \cdot 10^{-5}$ cgs, $Q_n =$ $= 10$ to 50. RM intensity decreases about uniformly during demagnetization, dropping to about 5 percent of the initial value after the application of 300 Oe. (Fig. 7b.) The direction of magnetization is unaffected. The mean RM direction was determined from the initial values (Fig. 7a).

7. Márévár valley, trachydolerite lava. $\bar{I}_n = 174 \cdot 10^{-5}$ cgs. In the course of magnetic washing, the direction of RM is displaced in both types of samples, those with higher Q_n ($\div$ 1) and also those with lower Q_n ($\div$ 0.4). The parameters of confidence of the mean RM direction belonging to the minimal scatter (subsequent to 100 Oe demagnetization) are unfavourable enough: $k = 8$, $\alpha =$ $= 25.0°$ (Figs. 8a,b).

8. Jánosi puszta, trachydolerite pillow lava. Owing to the unfavourable conditions of disclosure, this sample group consists of just two samples insufficient for an independent evaluation.

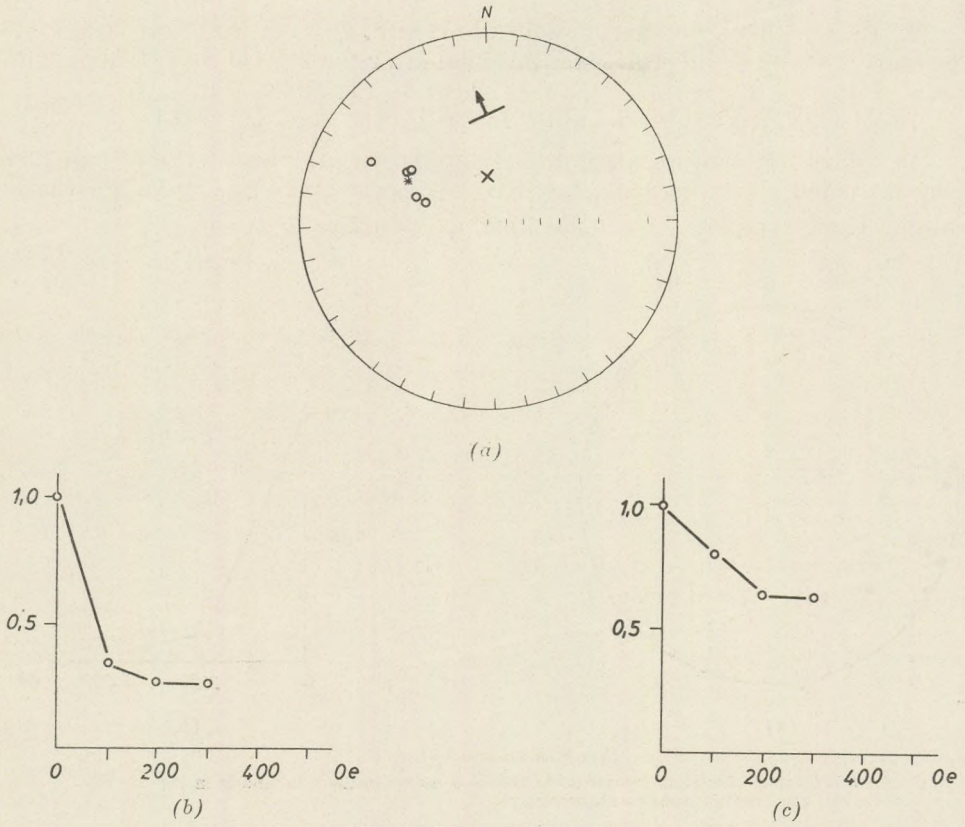

Fig. 6. Hosszúhetény (5)

(a) RM directions subsequent to 200 and 300 Oe demagnetization, respectively. Legend as in Fig. 2.
(b), *(c)* Types of alternating-field demagnetization graphs

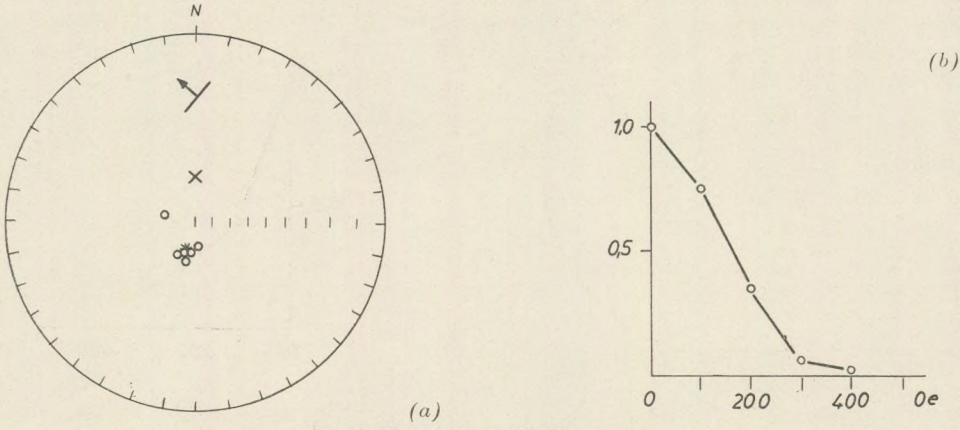

Fig. 7. Jánosi Nagy Valley (6)

(a) Initial RM direction. Legend as in Fig. 2.
(b) Alternating-field demagnetization graph

9. Máza valleyhead, amphibolic teschenite. $\bar{I}_n = 44 \cdot 10^{-5}$ cgs, $Q_n \div 0.3$. The scatter of the RM directions is minimal after the 200 Oe step of demagnetization. Intensity varies in the manner shown in Fig. 9b.

10. Máza valleyhead, phonolite. $I = 0.58 \cdot 10^{-5}$ cgs, $Q_n = 0.4$.

11. Máza valleyhead, phonolite dyke. Three samples of this group have been discarded for exceedingly low Koenigsberger ratios ($Q_n < 0.1$). For the remaining three samples, $\bar{I}_n = 0.39 \cdot 10^{-5}$, $\bar{Q}_n = 0.27$.

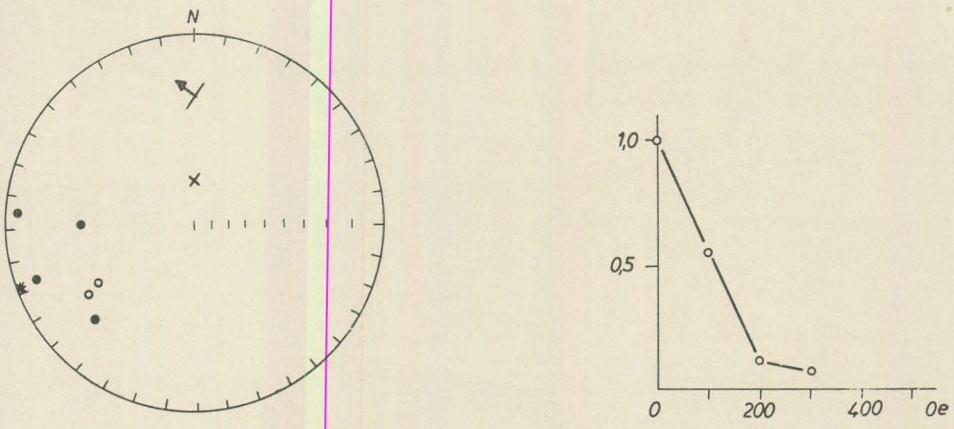

(a) (b)

Fig. 8. Márévár Valley (7)

(a) RM values of minimal scatter (after 100 Oe demagnetization). Legend as in Fig. 2.
(b) Alternating-field demagnetization graph

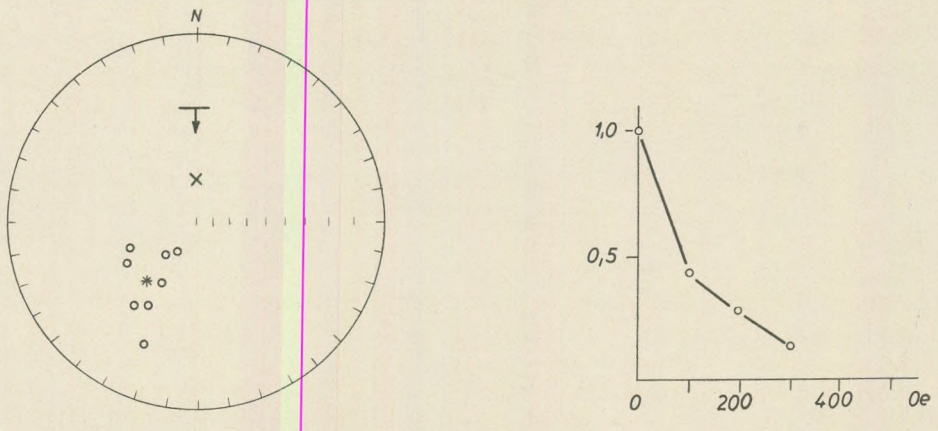

(a) (b)

Fig. 9. Máza valleyhead (9 to 11)

(a) RM directions after 200 Oe demagnetization for Group 9 and after 100 Oe for Groups 10 and 11. Legend as in Fig. 2.
(b) Alternating-field demagnetization graph typical of group 9.

Both groups (10 and 11) were demagnetized up to 600 Oe (alternating), but the measurement to a sufficient accuracy of the RM values remaining after 100 Oe would require a higher sensitivity than that of the instruments now at our disposal. For these two groups, we determined the mean RM direction from the data measured after 100 Oe demagnetization, as these yield a smaller scatter than the original RM directions. For the volcanic complex of the Mája valleyhead, we computed the mean RM direction from the totality of the data for localities 9, 10 and 11 (Fig. 9a).

12. Kövesdtető, phonolite. The low intensity as compared to the sensitivity of our instruments ($\bar{I}_n = 0.41 \cdot 10^{-5}$ cgs) and the irregular behaviour – presumably also due to insufficient accuracy of measurement – on RN demagnetization forbid for the time being the palaeomagnetic evaluation of this group of samples.

13. Komló, amphibole andesite. $\bar{I}_n = 122 \cdot 10^{-5}$, $\overline{Q_n} = 1.0$. In the course of magnetic washing, the direction of RM does not change; the variation of its intensity is as in Fig. 10b. The mean RM direction was computed from the initial values (Fig. 10a).

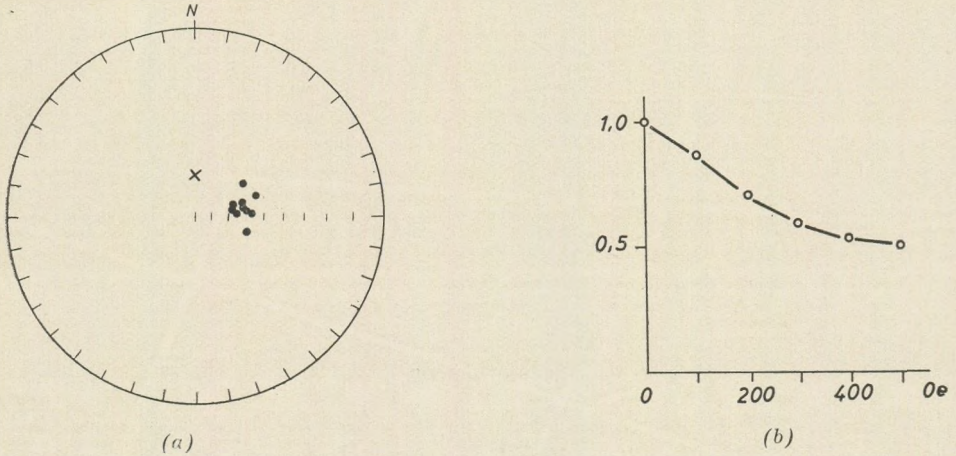

Fig. 10. Komló (13)
(a) Initial RM direction. Legend as in Fig. 2.
(b) Alternating field demagnetization graph

The significant deviations in mean RM directions are due to dislocations of the volcanic rocks in the course of geohistory, subsequent to their RM magnetization. On the assumption that the strike of the sedimentary complex in which the volcanic rock is embedded is the tilt axis, the tilt correction if any can be performed on the basis of the data representing the actual structural situation listed in Table II. The data corrected for tilt about a horizontal strike axis as summarized in Table IV and plotted in Fig. 11 (sets of three data) cluster about two points, $\bar{D}_1 = 349{,}3$; $\bar{I}_1 = 51.2$ and $\bar{D}_2 = 83.1$; $\bar{I}_2 = 61.0$. The mean difference between the two groups is significant in the declination value.

Table IV. Mean palaeomagnetic directions of evaluated sample groups after tilt correction

Sampling locality	$\bar{D}°$	$\bar{I}°$
Márévár valley (3)	350,0	+ 51.5
Márévár valley (4)*	180.0	− 53.0
Hosszúhetény (5)	255.5	− 56.0
Jánosi Nagy valley (6)	158.0	− 51.5
Máza valleyhead (9 to 11)	274.0	− 64.5
Komló (13)*	82.4	+ 61.8

* without tilt correction

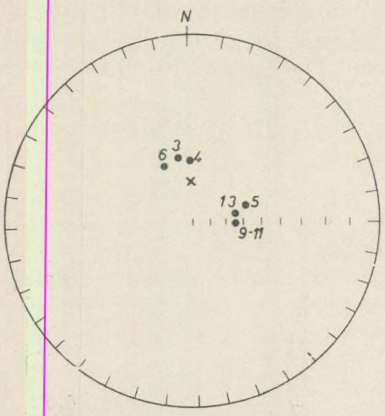

Fig. 11. Mean D and I values for normal magnetization after tilt correction for the palaeomagnetically evaluable localities

Conclusions

1. Conclusions as to the origin of natural remanent magnetization can on the basis of the data measured so far be drawn from the intensity values, Q_n numbers, the behaviour of the individual samples under AC demagnetization, and the consistency of data within the individual sample groups. It turns out that the original TRM of the saple groups 4, 6 and 13 is preserved without change. In sample groups 3, 5, 9, 10 and 11 the original TRM was partly effaced since the origin of the rock, and secondary components of magnetization came to exist (IRM, VRM) which can be effaced by magnetic washing. In the rock of locality 1, secondary magnetization is dominant. The RM of the lava agglomerates 2, 7, and 8 is both in direction and magnitude the resultant of several effects. The original thermoremanent magnetization can be considered owing to the dislocations undergone in the course of cooling as the resultant of PTRM's of various orientation, and the resultant magnetization cannot by the very nature of its origin reflect the geomagnetic field of the time of cooling.

2. Of the sample groups evaluated (3, 4, 5, 6, 9, 10, 11, 13), 3 and 13 exhibit normal magnetization, the rest are reversed. Hence, the main period of volcanism (the Valanginian stage) is characterized by a geomagnetic zone of negative polarity. Sample group 3 (trachydolerite dyke) suggests with its normal magnetization a distinct magnetic episode.

3. Applying the tilt correction established for the external flank of the Márévár anticline (Table II) to the sample group 3, the mean direction subsequent to the correction becomes inconsistent with the Cretaceous field direction, whereas without correction there is no such inconsistency. Hence, this dyke was emplaced subsequent to the folding of the anticline, its normal magnetization being younger than the reverse one of the other magmatites.

4. The mean value of the tilt-corrected means of sample groups 4 and 6 and of the uncorrected mean of group 3, $\bar{D} = 349.3$; $\bar{I} = 51.2$ fits the mean direction $\bar{D}_E = 6.9$; $\bar{I}_E = 54.9$ computed for the Mecsek Mountains from the Eurasian set of data (Table I). These rocks are in their original position except for the tilt. The tilt-corrected data of the sample-groups 5 and 9 to 11 differ mostly in declination from $(\bar{D}_E, \bar{I}_E)$. The deviation gives a clockwise rotation of the latter rocks about a vertical axis relative to the Márévár anticline. Also the emplacement of the Komló andesite (Group 13) preceded this rotation.

5. The rotations about a vertical axis revealed by the palaeomagnetic data have the same general tendency as the deviations in strike from the strike of the Márévár anticline, which can be read off the geological map at the sampling localities 5, 9 to 11 and 13. The rotations determined by palaeomagnetic means interpret at the same time also the deviations in strike. Conversely, the deviations of the strikes measured at the localities 5, 9 to 11 and 13 give a further possibility of correcting the main palaeomagnetic vectors of these groups. The twist corrections are 45° for 5, 55° for 9 to 11 and 95° for 13, all counterclockwise.

Table V lists the VGP values obtained after tilt and/or twist correction for each sample group. The pair $\Phi = 81.0$; $A = 172.5°$ obtained as the mean of the first five (Fig. 12) is considered as the VGP coordinate pair valid for the Lower Cretaceous. The VGP yielded by sample group 13 will have to

Table V. VGP coordinates obtained after tilt and/or twist correction

Sampling locality	$A°$	$\Phi°$	Geomagnetic pole
Márévár valley (3)	225.0	75.5	northern
Márévár valley (4)	196.0	77.5	southern
Hosszúhetény (5)	112.5	66.5	southern
Jánosi Nagy valley (6)	254.0	69.0	southern
Máza valleyhead (9 to 11)	92.0	63.5	southern
Mean (3, 4, 5, 6, 9 to 11)*	172.5	81.0	
Komló (13)	258.0	79.0	northern

* computed from the mean directions corrected for tectonic position of the sample groups, with $\bar{D} = 4.8°$, $\bar{I} = 57.4°$

be interpreted in more detail after the clarification of the precise age of this geological body

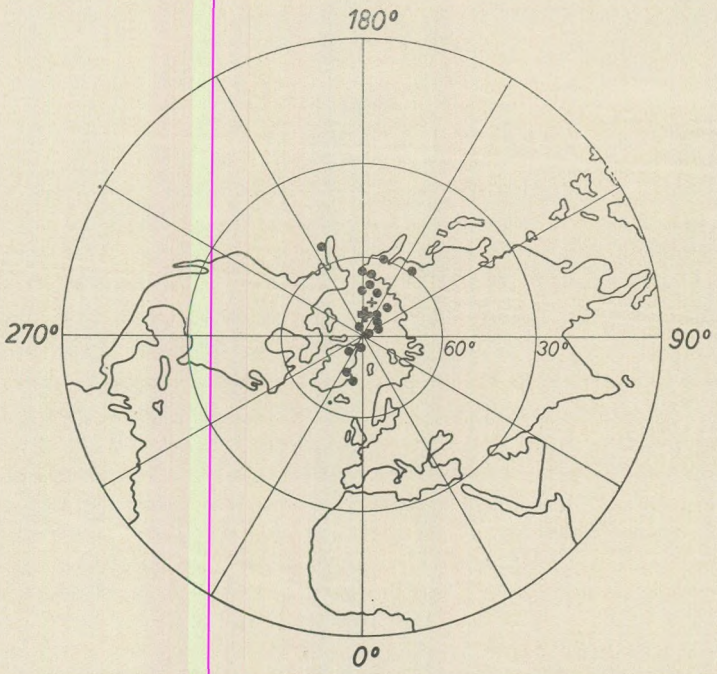

Fig. 12. Cretaceous Eurasian VGP's with the mean direction (cf. Table I)
Legend:
● : VGP
+ : mean Cretaceous Eurasian VGP
✚ : Lower Cretaceous VGP computed from Mecsek Mountains data (cf. Table V)

REFERENCES

Bucha, V. et al. (1963): Paleomagnitnie issledovanija gornych porod devonskovo-chetvertichnovo vozrastov na territorii Chekhoslovakii. Geofysikální Sbornik 187, p. 293.

Khramov, A. N. – Sholpo, L. E. (1967): Paleomagnetizm. Nedra, Leningrad.

Cox, A., Doell, R. R. (1961): Paleomagnetism. Advances in Geophysics 8, p. 221.

Costa-Foru, A. L. et al. (1964): Recherches paléomagnétiques sur des roches d'âge mésozoïque en Roumanie. Géophysique. (Rev. Roum. Geol. Geophysi. et Geogr. 8, p. 111.

Fischer, R. A. (1953): Dispersion on a sphere. Proc. Roy. Soc. Ser. A 217, p. 295.

Irving, E. (1964): Paleomagnetism. John Wiley, New York/London/Sydney.

Kienzle, J. et al. (1966): Paleomagnetic comparison of Cretaceous rocks from South Korea and Late Paleozoic and Mesozoic rocks of Japan. Jour. Geomagnetism and Geoelectricity 18, No. 3, p. 413.

Nairn, A. E. M. (1960): Paleomagnetic results from Europe. Journ. of Geol. 68, No. 3, p. 285.

Vadász, E. (1935): A Mecsekhegység (The Mecsek Mountains), Budapest.

Vadász, E. (1960): Magyarország Földtana (Geology of Hungary), Akademiai Kiadó, Budapest.

Vlasov, A. Ya., Nikolaichik, M. V. (1964): Paleomagnitnye issledovaniya mezozoia Taimyra i tsentral'noy chasti Krasnoyarskogo kraya (Paleomagnetic investigations of the Mesozoic of the Taimyr and the central part of the Krasnoyar Territory). Akad. Nauk. SSR Izv. Ser-Geofiz. 11, p. 1700.

NOTES ON THE DETECTION AND ELIMINATION OF GHOST REFLECTIONS BY MEANS OF SINGLE CHANNEL FILTERS

by

A. MESKÓ

Department of Geophysics, L. Eötvös University, Budapest, VIII Kun B. tér 2.

(Received: 10 December 1968)

SUMMARY

The possible errors of the ghost parameters determined from the autocorrelation function of the ghosted trace have been investigated. The range of errors in T (delay between primary and ghost reflections) is ± 4 ms (if $k \cong 0.2$) and the relative errors in k (reflection coefficient) vary between -30% and $+50\%$ (if $T \cong 40$ ms).

The errors in these parameteres significantly influence the ghost rejection capability of the deghosting filter (Table III). Better methods for the determination of ghost parameters should be developed to improve the effectiveness of deghosting filters.

Introduction

The detection and elimination of ghost arrivals have been widely discussed in literature. Less attention has been paid to the limitations of the techniques proposed. These limitations play, however, an important role in interpretation. One is obviously interested in the consequences of having filters with incorrect parameters if it turns out that estimations may yield incorrect values.

The methods used to attenuate ghost energy may be grouped as single-channel and multi-channel (mostly two-channel) techniques. The advantages of the multi-channel technique are obvious. But this technique requires special shooting patterns (Schneider et al.). Once the recorded data to be processed have been made on a single shooting geometry and field work is completed, one is compelled to use single-channel filtering, no other choice being left. A single-channel filter for rejection of ghost reflections has been devised by Lindsey (1960) The Laplace transform of the weighting function of the filter reads

$$F(s) = \frac{1}{1 - k\,H(s)e^{-sT}}, \tag{1}$$

where k = near-surface reflection coefficient,
$H(s)$ = near-surface filter accounting for differences in the shapes of primary and ghost wavelets,
T = delay between primary and ghost reflections.

In many cases, primary and ghost are of approximately the same shape and it is not necessary to involve the near-surface filter $H(s)$; the deghosting filter then simplifies to

$$F(s) = \frac{1}{1 - k e^{-sT}}. \tag{2}$$

This filter may be realised as a simple feed-back system (L i n d s e y, 1960). The digital realization using the z-transform method is also well-known (e.g. R o b i n s o n, 1966).

The filter in the simplified version contains two parameters the values of which may be determined from the autocorrelation function for the ghosted trace (L i n d s e y, 1960). The errors of these parameters obviously influence the effectiveness of the deghosting filter.

A series of statistical investigations has been carried out in the years 1967 and 1968 to obtain quantitative information about possible errors in estimates concerning the parameters T and k, and about their influence on the ghost attenuation capability of the corresponding filter. Part of these investigations is reported in this paper

Determination of T and k using autocorrelation functions

The connexion between the autocorrelation function of the original trace and that of the ghosted trace has been discussed by L i n d s e y (1960). His analysis is reviewed and somewhat extended below. Possible sources of error will be pointed out. The problem treated is that of a single ghost.

The original trace free of ghosts and representing the primary reflection sequence will be denoted by $f(t)$. Its truncated autocorrelation function determined for a time gate of the length $t_1 - t_0$ is by definition

$$\varphi_{ff}(\tau) = \frac{1}{t_1 - t_0} \int_{t_0}^{t_1} g(t)\, g(t+\tau)\, dt,$$

$$|\tau| \leqq \tau_{\max}. \tag{3}$$

(Let us suppose that the length of the original trace is at least $t_1 - t_0 + \tau_{\max}$, where $\tau_{\max}$ represents the maximum delay between the original trace and its shifted version.)

Leaving out of consideration the shaping effect of the near-surface earth filter, the ghosted trace may be described by the function

$$g(t) = f(t) - kf(t-T), \ (0 < k < 1), \tag{4}$$

where k denotes the reflection coefficient of the near-surface reflection complex and T denotes the delay between primary and ghost reflections.

The autocorrelation function of the ghosted trace is

$$\varphi_{gg}(\tau) = \frac{1}{t_1 - t_0} \int_{t_0}^{t_1} g(t)\, g(t+\tau)\, dt =$$

$$= \frac{1}{t_1 - t_0} \int_{t_0}^{t_1} [f(t) - k f(t-T)][f(t+\tau) \quad k f(t-T+\tau)]\, dt =$$

$$= \frac{1}{t_1 - t_0} \int_{t_0}^{t_1} f(t) f(t+\tau)\, dt - \frac{k}{t_1 - t_0} \int_{t_1}^{t_1} f(t) f(t-T+\tau)\, dt -$$

$$- \frac{k}{t_1 - t_0} \int_{t_0}^{t_1} f(t-T) f(t+\tau)\, dt + \frac{k^2}{t_1 - t_0} \int_{t_0}^{t_1} f(t-T) f(t-T+\tau)\, dt.$$

Comparing the terms with the autocorrelation function of the original trace we obtain

$$\varphi_{gg}(\tau) = (1+k^2)\varphi_{ff}(\tau) - k[\varphi_{ff}(\tau - T) + \varphi_{ff}(\tau + T)]. \tag{5}$$

The autocorrelation function for the ghosted trace consists of three components each of which has the shape of the autocorrelation function for the primary reflection sequence. The first component remains in its original place and is multiplied by $(1+k^2)$, whereas the delayed and anticipated components change sign and are scaled down by the factor k.

This structure provides a possibility for the determination (or, properly speaking, for the estimation) of the parameters T and k.

The negative peak (or trough) at positive time is due to the delayed component. Its argument indicates the origin of the delayed component and so gives the value of T. It is supposed that the unshifted and anticipated components do not shift the trough. This is obviously an approximation the accuracy of which is to be investigated.

The ratio of the amplitude of the trough to the amplitude of the peak at the origin is, by Eq. (5),

$$\frac{\varphi_{gg}(T)}{\varphi_{gg}(0)} = \frac{(1+k^2)\,\varphi_{ff}(T) - k[\varphi_{ff}(0) + \varphi_{ff}(2T)]}{(1+k^2)\varphi_{ff}(0) - k[\varphi_{ff}(-T) + \varphi_{ff}(T)]}. \tag{6}$$

Let us suppose that the values at the arguments T and $2T$ of the autocorrelation function for the original trace are negligibly small compared with the value at the origin, i.e.

$$\varphi_{ff}(T) \equiv \varphi_{ff}(-T) \ll \varphi_{ff}(0)$$

and

$$\varphi_{ff}(2T) \ll \varphi_{ff}(0). \tag{7}$$

Neglecting the small terms, Eq. (6) yields

$$\frac{\varphi_{gg}(T)}{\varphi_{gg}(0)} \approx \frac{-k\,\varphi_{ff}(0)}{(1+k^2)\,\varphi_{ff}(0)} = -\frac{k}{1+k^2}.$$

The left-hand-side of this equation gives the value of the normalized autocorrelation function for the ghosted trace at $\tau = T$. Let the normalized autocorrelation function be denoted by $\varphi_{gg}^{(n)}(\tau)$. Then the latter equation simplifies to

$$|\varphi_{gg}^{(n)}(T)| = \frac{k}{1+k^2}, \tag{8}$$

The connection between $|\varphi_{gg}^{(n)}(T)|$ and the parameter k is shown in Fig. 2. By Eq. (8), k may be determined from the amplitude of the trough.

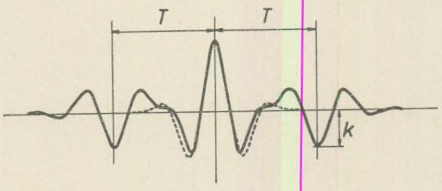

Fig. 1. Autocorrelation function for a ghosted trace

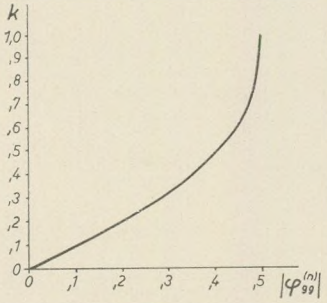

Fig. 2. Connection between the amplitude of the negative peak and the reflection coefficient k

Eq. (8) is, however, itself only an approximation. The neglection of the terms $\varphi_{ff}(\mathrm{T})$ and $\varphi_{ff}(2T)$ may cause some error. It must be emphasized that these neglections are imposed by the limitations of our knowledge about the ghost mechanism. The degree to which the estimate may be correct depends upon the "resolving power" of the first autocorrelation function, $\varphi_{ff}(\tau)$. If it decays rapidly enough away from its origin, both assumptions made above remain valid to a fairly good approximation. If, on the other hand, $\varphi_{ff}(\tau)$ is a slowly decaying function, the picture is severally distorted and our ability to detect the trough as well as the validity of approximations (7) are greatly impaired.

A number of numerical experiments have been made with digital computers to estimate the errors in T and k.

Synthetic traces have been constructed by summarizing Ricker wavelets having random amplitudes and random consecutive delays. A typical example of a synthetic trace is presented in Fig. 3. The trace shown is considered to be the primary reflection sequence.

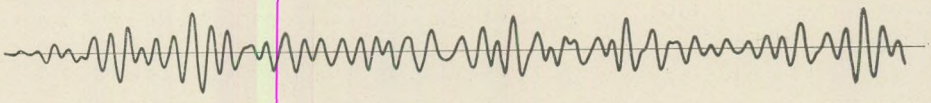

Fig. 3. Synthetic seismic trace

Ghosted traces have subsequently been computed for several values of parameters T and k. Some examples of ghosted traces are shown in Fig. 4. The values of k equals 0.5 in each case, whereas T varies from 40 ms to 58 ms. It is remarkable that the ghost reflections are not seen separately on the traces

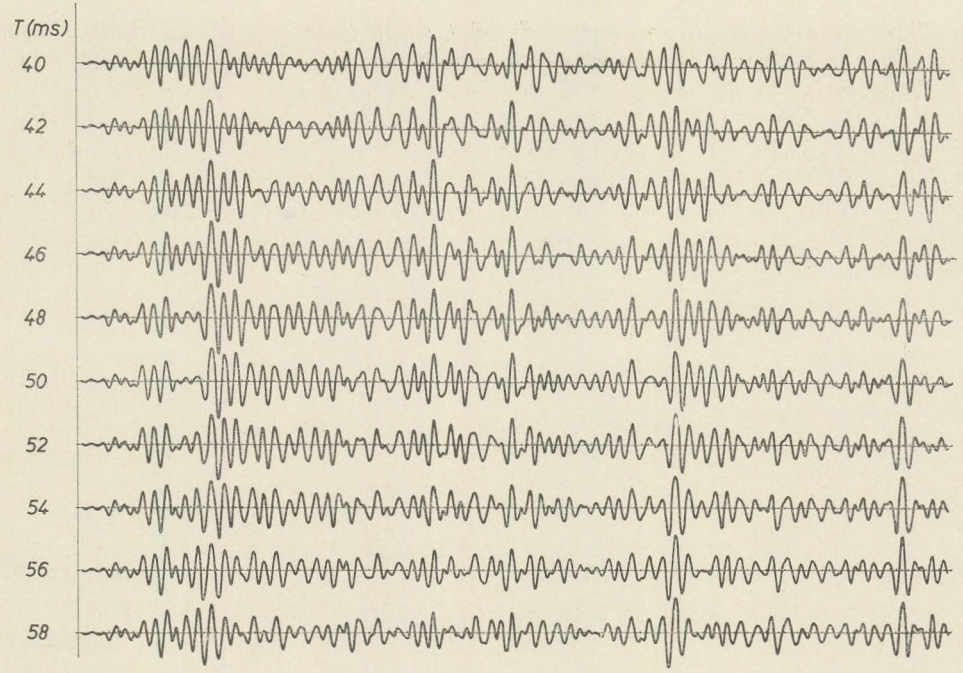

Fig. 4. Ghosted traces computed from the synthetic trace
Parameters: $k = 0.5$; $T = 40$ ms, 42 ms, ... 58 ms

despite the fairly high value of the reflection coefficient. The appearance of the ghost reflections results in a complicated interference which destroys the original pattern of the primaries. It would be most difficult to determine the numerical values of the parameters from the original traces.

The autocorrelation functions of the ghosted traces have been computed and the values of T and k have been determined using the method outlined above. Two representative examples of these attempts are presented as Figs. 5. and 6. In the first case T is fixed at 40 ms and k varies from 0.2 to 0.6. The numerical results are summarized in Table I. The parameters determined from the autocorrelation function are denoted by T^m and k^m. The relative errors of the k (in percent) are given in the last column.

Table I

$T = 40$ ms					
k	T^m	ΔT^m	k^m	Δk	$\frac{\Delta k}{k}$ (in %)
0.2	40	0	0.13	−0.07	−35
0.3	40	0	0.23	−0.07	−23
0.4	40	0	0.32	−0.08	−20
0.5	40	0	0.40	−0.10	−20
0.6	40	0	0.48	−0.12	−20

The second example refers to a fixed k and varying T ($k = 0.5$, T varies from 40 ms to 80 ms in 2-ms steps). The numerical results are given in Table II.

The relative error of k may be considered a function of the delay T. The connection is shown in Fig. 7., where the values of the original autocorrelation function as well as the relative errors have been plotted against T. The tendency is a fairly clear-cut one. Positive values of the autocorrelation function cause negative errors. This follows from the structure of the autocorrelation function for the ghosted trace, and from the interpretation of the negative peak, the whole amplitude of which is considered to be due to the delay term: see Fig. 1.

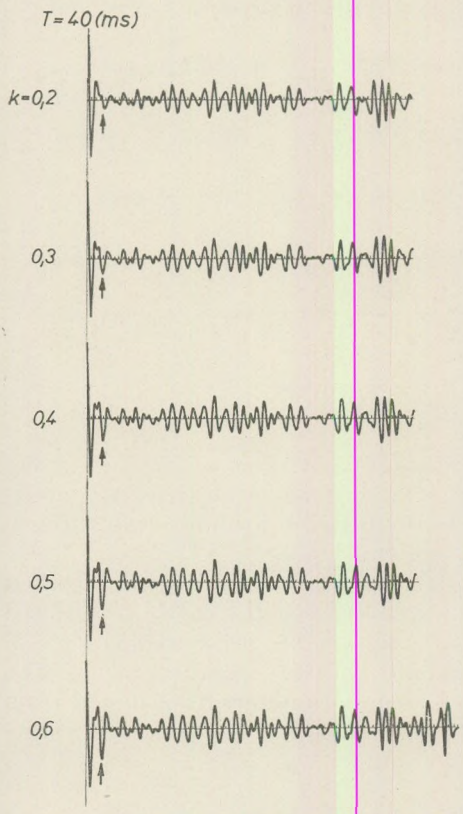

Fig. 5. Autocorrelation functions for some ghosted traces
Parameters: $T = 40$ ms, $k = 0.2, 0.3, \ldots 0.6$

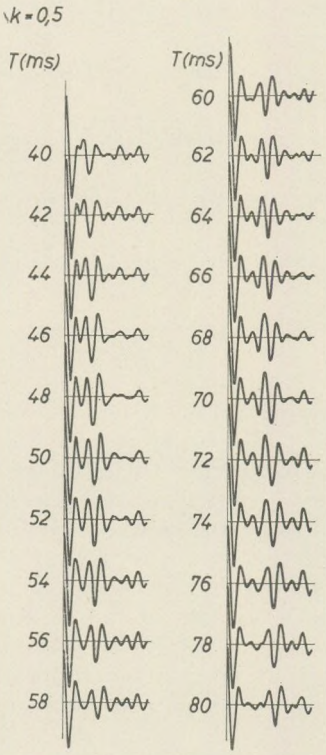

Fig. 6. Autocorrelation functions for some ghosted traces
Parameters: $k = 0.5$, $T = 40$ ms, 42, ... 80 ms

These and other investigations have shown that the errors in T may be ± 4 ms (if $k \geqq 0.2$) and the relative error of k varies within the limits -30 percent and $+50$ percent (if $T \geqq 40$ ms). These limits are rather extreme and the real errors may be somewhat less. The errors usually decrease with increasing T and (or) increasing k.

Table II

$k=0,5$					
T	T^m	ΔT^m	k^m	Δk	$\frac{\Delta k}{k}$ (in %)
40	40	0	0.39	−0.11	−22
42	42	0	0.46	−0.04	− 8
44	45	+1	0.57	+0.07	+14
46	46	0	0.70	+0.20	+40
48	48	0	0.75	+0.25	+50
50	50	0	0.70	+0.20	+40
52	50	−2	0.66	+0.16	+32
54	53	−1	0.57	+0.07	+14
56	55	−1	0.42	−0.08	−16
58	58	0	0.35	−0.15	−30
60	61	+1	0.43	−0.07	−14
62	63	+1	0.50	0	0
64	64	0	0.46	−0.04	− 8
66	67	+1	0.44	−0.06	−12
68	68	0	0.52	+0.02	+ 4
70	70	0	0.63	+0.13	+26
72	72	0	0.60	+0.10	+20
74	74	0	0.60	+0.10	+20
76	76	0	0.60	+0.10	+20
78	78	0	0.52	+0.02	+ 4
80	80	0	0.48	−0.02	− 4

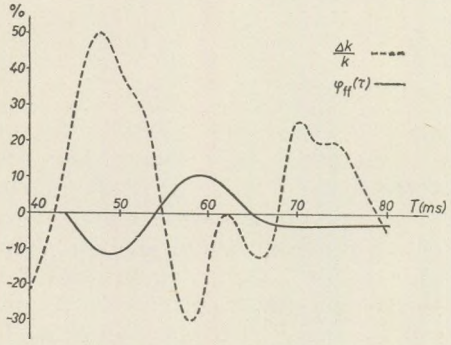

Fig. 7. The relative error of the reflection coefficient k vs. T (dotted line) and the original autocorrelation function (continuous line)

Effectiveness of the single deghosting filter

The effectiveness of the filter designed for the attenuation of ghost reflections (the so called deghosting filter) is significantly influenced by errors of the ghost parameters. A series of investigations has been carried out to obtain a quantitative picture of the effectiveness of deghosting filters with slightly deficient parameters.

A single-channel deghosting operator may be derived very simply by using the z-transform method (R o b i n s o n, 1966). At first we transform the time functions describing the original and ghosted traces into digital data systems (i.e. into time series) by sampling. Let the sampling interval be τ, and the delay T an integer multiple of the sampling interval, i.e.

$$T = l\tau.$$

The z-transform of the original and of the ghosted trace will be denoted by $F(z)$ and $G(z)$, respectively.

The time-domain connection between original and ghosted traces is given by Eq. (4). The corresponding relation in the z-domain is obtained by applying the z-transform to both sides:

$$G(z) = F(z) - kF(z)z^l = (1 - kz^l)F(z). \tag{9}$$

The z-transform of the original trace yields by a simple modification

$$F(z) = \frac{G(z)}{1 - kz^l} = G(z)\frac{1}{1 - kz^l}. \tag{10}$$

The latter factor may be considered as the sum of an infinite geometrical series. Eq. (10) thus expands into

$$F(z) = G(z)\,(1 + kz^l + k^2z^{2l} + \ \ldots) \tag{11}$$

and thus the deghosting operator is

$$\underset{\widehat{0}}{1},\ \underset{\widehat{1}}{0},\ \underset{\widehat{2}}{0},\ \ldots\ ,\ \underset{\widehat{l}}{0},\ k,\ 0,\ \ \ldots,\ \underset{\widehat{2l}}{0},\ k^2,\ 0,\ \ldots \tag{12}$$

The deghosted trace may be obtained as the convolution of the ghosted trace and the deghosting operator. It is clearly seen that the operator contains the ghost parameters T and k ($T = l\tau$). As a matter of fact, in practice we must apply deghosting operators with slightly deficient parameters T^m and k^m in lack of an exact knowledge about the real values T and k. The operator containing the parameters T^m and k^m (instead of T and k) may be applied in the same manner as the correct one. Some ghost attenuation may be expected if the differences between T^m and T and between k^m and k are small. But it is obvious that the attenuation of ghost energy becomes less and less effective as the differences increase.

A subsequent series of investigations was aimed at getting a quantitative picture of the influences of these errors. In these experiments single primary and ghost wavelets were used (instead of whole traces) in order to facilitate computation and interpretation.

Some examples for the sums of primary and ghost wavelets are shown in Fig. 8.

A large number of deghosting operators containing various parameters k^m and T^m were convolved with the primary and ghost complex. The length of the operators was always $4T$. The parameters and the numerical results

are summarized in Table III. The last column, q, gives the attenuation of ghost energy in dB, i.e.

$$q = 10 \overset{10}{\smile} \log \frac{E_a}{E_b},$$

where E_a and E_b denote the ghost energies after and before the application of the deghosting filter.

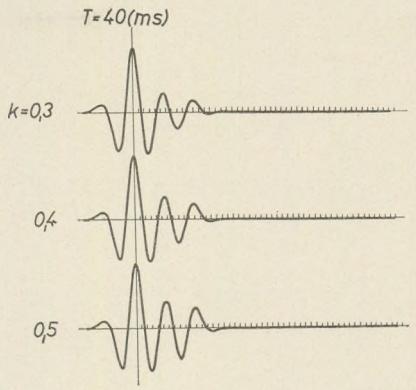

Fig. 8. Primary + ghost wavelets for parameters T = 40 ms; k = 0.3, 0.4 and 0.5

Ghost energy is not fully eliminated even in the cases $T = T^m$, $k = k^m$; this is due to the finite length of the operator.

Some examples for deghosted traces are shown in Fig. 9. Some results given in Table III. are shown in Fig. 10. in order to facilitate interpretation. The q values have been plotted against T^m for various k^m values (T = 40 ms, k = 0.5). It is clearly seen that errors in k influence the results more significantly than the errors in T.

Computations using other wavelets or other synthetic traces gave similar results. Limits of errors and limitations of an approximate deghosting filter were practically the same for the other synthetic examples.

We may conclude that for more effective ghost attenuation either a better method for determining parameters must be developed or other filtering techniques should be used which require no exact knowledge of the ghost mechanism.

Table III

Attenuation of ghost energy vs. the parameters T^m and k^m

T = 40 ms k = 0,3

k^m	T^m (ms)	$-q$ (dB)
0.1	38	2.9
	39	3.3
	40	3.5
	41	3.4
	42	3.0
0.2	38	6.3
	39	8.3
	40	9.4
	41	8.4
	42	6.4
0.3	38	7.4
	39	13.4
	40	41.8
	41	13.4
	42	7.3
0.4	38	4.0
	39	7.0
	40	8.8
	41	7.1
	42	4.2
0.5	38	0.1
	39	1.6
	40	2.3
	41	1.8
	42	0.4

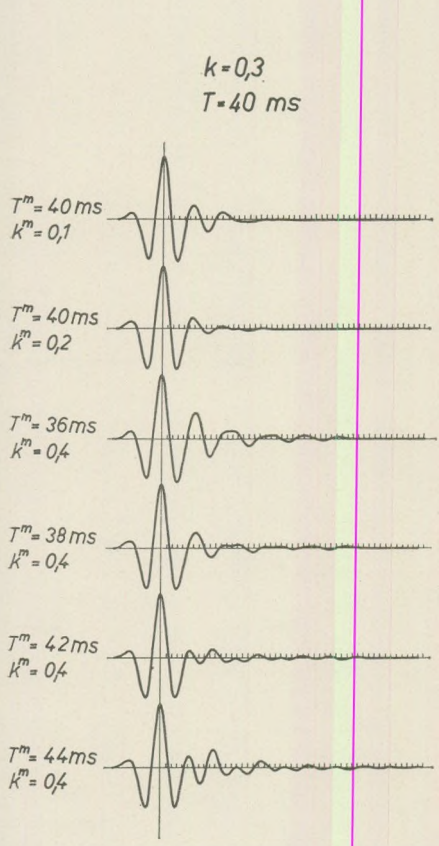

Fig. 9. Primary plus ghost wavelets filtered by some deghosting filters

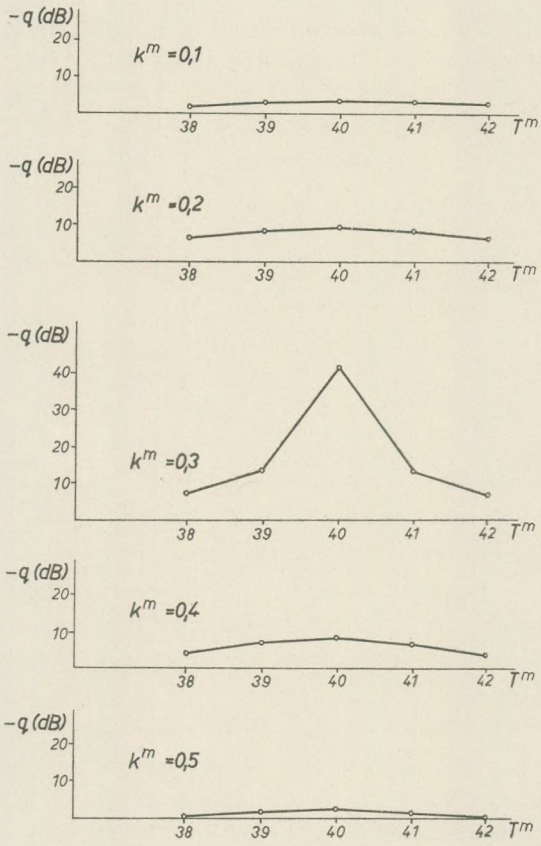

Fig. 10. The attenuation of ghost energy vs. of the parameters T^m and k^m (T = 40 ms, k = 0.3)

REFERENCES

Lindsey, J. P. (1960): Elimination of seismic ghost reflections by means of a linear filter. Geophysics, Vol. XXV. No. 1. pp. 130–140.

Meskó, A. – Rádler, B. (1968): Utilization of model computations in the digital processing of seismic data (in Hungarian). Magyar Geofizika, Vol. IX. No. 4–5. pp. 152–164.

Robinson, E. A. (1966): Multichannel z-transform and minimum delay. Geophysics, Vol. XXXI. No. 3. pp. 482–500.

GRAVITY INTERPRETATION AND INFORMATION THEORY IV. THE METHOD OF DOWNWARD CONTINUATION

by
A. MESKÓ
(Geophysical Institute of L. Eötvös University
Budapest, VIII. Kun B. tér 2)
(Received: 10 December 1968)

SUMMARY

The method of downward continuation and its formulas of approximation are studied by applying the filter theory. It is proved that the transfer functions of the Constantinescu – Botezatu formulas are far from that of the theoretical operation. These formulas show strong directivity which may give rise to serious misunderstandings in the interpretation of geological structural trends.

The sets of coefficients proposed by Oldham, Waithman and Tsuboi give a good approximation of the theoretical operation even in their truncated version. Their dependence on orientation remains negligibly small. It is these formulas rather than others that should be used for downward continuation.

Introduction

This is the fourth paper of a series on systematic investigations into the concepts and formulas used in modern gravity interpretation. Our studies are based on filter theory, which permits a self-consistent and fairly general treatment of the topic. The essence of filter theory has already been discussed in previous papers (M e s k ó, 1965, 1966, 1967). A concise summary has been given in the second paper of the series. The way of application was illustrated in the second and third papers dealing with smoothing, computation of regionals and the second derivative method. Thus we may proceed directly to discuss the method of analytical continuation without reviewing the filter theory involved.

The present paper gives an account of investigations on downward continuation. After deriving the transfer function of the theoretical operation we shall describe the transfer properties of some practical formulas proposed by Constantinescu – Botezatu and Oldham – Waithman – Tsuboi. The first group (the Constantinescu – Botezatu formulas) is of particular interest, being often used by Hungarian geophysicists (F a c s i n a y, 1966, 1967). Thus we considered it necessary to direct attention to the disadvantages of these formulas.

The second group (the Oldham – Waithman – Tsuboi formulas) proved to give the best approximation to the theoretical operation. The latter formulas have been qualified impractical in their original form because of their cumbersomeness (the authors gave 31×31 coefficients). But even their truncated versions (7×7 coefficients) assure an excellent approximation.

The transfer functions of some other formulas are available at the Geophysics Dept. of L. Eötvös University, Budapest, but will not be presented in this paper.

Here, the problem of gravity interpretation is dealt with. It has to be mentioned, however, for the sake of completeness, that the method of continuation may be applied to all cases where the field to be continued satisfies the Laplace equation. Thus it applies to certain magnetic fields and some electromagnetic fields as well (Roy, 1966).

The theoretical operation and its transfer function

Suppose the strength of the gravity field to be known on a plane denoted by S_1. Take the x and y coordinates in this plane. The gravity field may be described by the function

$$g_0(x, y) = g(x, y, z = 0)$$

(The subscript "o" refers to "original".) The aim of the continuation upward is to determine the gravity field in another plane, S_2, located at a higher level i.e. at a larger distance from the sources of the field, and parallel to the plane S_1. (Fig. 1.) If there are no sources between the planes S_1 and S_2, the function $g(x, y, z)$ satisfies the Laplace equation in this part of the space:

$$\Delta g(x, y, z) = 0. \tag{1}$$

The problem of continuing $g_0(x, y)$ into the space above the plane S_1 is a matter of solving equation (1) subject to certain boundary conditions. The solution $g(x, y, z)$ reduces to the known values on S_1 and vanishes at great distance above it:

$$g(x, y, z = 0) = g_0(x, y)$$

and

$$g(x, y, z \to \infty) \to 0.$$

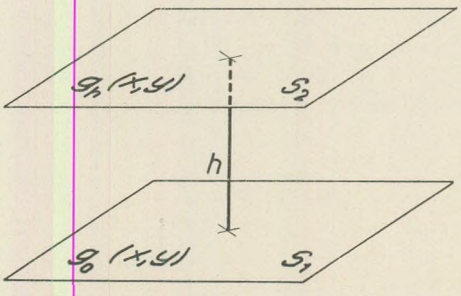

Fig. 1. The problem of upward continuation

This is a classic problem of mathematical physics known as the first boundary value problem (or Dirichlet problem) for the plane. The solution may be obtained by Green's theorem, using a Green's function of the first kind; it has the form

$$g_h(x, y) = g(x, y, z = h) = \frac{1}{2\pi} \int_{-\infty}^{+\infty} \int_{-\infty}^{+\infty} \frac{h g_0(\xi, \eta) d\xi \, d\eta}{\sqrt{[h^2 + (x-\xi)^2 + (y-\eta)^2]^3}} \tag{2}$$

where h is the distance between the planes S_1 and S_2.

The operation (2) may be considered a convolution

$$g_h(x, y) = \left\{ \frac{1}{2\pi} \frac{h}{(h^2 + x^2 + y)^{3/2}} \right\} * g_0(x, y).$$

This latter equation makes it obvious that the operation in question corresponds to a linear filtering The input and output of the filter are $g_0(x, y)$ and $g_h(x, y)$, and the weighting function is

$$s(x, y, h) = \frac{h}{2\pi(h^2 + x^2 + y^2)^{3/2}}. \tag{4}$$

The transfer function of the upward continuation, $S_{up}(\omega, \psi; h)$, presents itself as the Fourier transform of the weighting function

$$S_{up}(\omega, \psi; h) = \int_{-\infty}^{+\infty} \int_{-\infty}^{+\infty} \frac{h e^{-j(\omega x + \psi y)}}{2\pi(h^2 + x^2 + y^2)^{3/2}} dx dy = e^{-h\sqrt{\omega^2 + \psi^2}} \tag{5}$$

The connection between the spectra of the original and continued fields is described by the equation

$$G_h(\omega, \psi) = S_{up}(\omega, \psi; h) G_0(\omega, \psi). \tag{6}$$

Practical applications more often need the inverse operation known as downward continuation which consists in deriving the strength of the gravity field in a horizontal plane S_1 *below* S_2 from the field strength in the plane S_2. That is, now we have in hand the function $g_h(x, y)$, and $g_0(x, y)$ is to be found. Equation (6) yields

$$G_0(\omega, \psi) = \frac{1}{S_{up}(\omega, \psi; h)} G_h(\omega, \psi), \tag{7}$$

i.e. the transfer function of the downward continuation is the reciprocal of the upward continuation:

$$S_{down}(\omega, \psi; h) = \frac{1}{e^{-h\sqrt{\omega^2 + \psi^2}}} = e^{h\sqrt{\omega^2 + \psi^2}}. \tag{8}$$

It is to be mentioned that the gravity field satisfies the Laplace equation between the two planes if and only if there are no sources (i.e. no masses)

between the planes. Consequently the depth of continuation must not exceed the shallowest depth of the bodies causing the gravity field to be investigated. Computations may be carried out formally even in the presence of disturbing bodies, but they result in a divergent (oscillating) field. It is the appearance of oscillations that may be used to detect the depth of the top of the body (R o y, 1967). We do not intend to discuss divergence in detail but some points merit to be mentioned.

If the gravity field to be continued downward contains components of high frequency, it is because there are near-surface masses that contribute to the field. Such effects should be absent by our basic hypothesis. Before embarking on the continuation operation, it is therefore usually necessary to apply a high-cut (or low-pass) filter, which suppresses any near-surface contributions to the gravity field. The use of low-pass filters before downward continuation is justified by practice. Only the smooth part of the field can be continued to any considerable depth. The smooth part does not necessarily originate at greater depth, but it may. On the other hand, the rapidly changing part of the field is certainly due to near-surface masses, and has to be removed. (Low-pass filters have been treated in detail in a previous publication: M e s k ó, 1966).

A last remark seems to be necessary. The operation is applied to the anomaly field instead of the total field. But the normal field satisfies the Laplace equation as well as the total field. It follows from the linearity of the equation that the anomaly field (the difference between total and normal fields) satisfies it as well.

The weighting function of the downward continuation may be obtained from the corresponding transfer function [Eq. (8)] by the inverse Fourier transform:

$$s(x, y; h) = \frac{1}{4\pi^2} \int_{-\infty}^{+\infty} \int_{+\infty}^{+\infty} e^{h\sqrt{\omega^2+\psi^2}} e^{-j(\omega x+\psi y)} \, d\omega d\psi. \tag{9}$$

The function $s(x, y; h)$ may then be converted into a digital data system of coefficients attached to grid points. Let us consider a regular square grid with spacing d:

$$\begin{aligned} x &= k \cdot d \quad (k = 0, \pm 1, \pm 2, \ldots) \\ y &= l \cdot d \quad (l = 0, \pm 1, \pm 2, \ldots) \end{aligned} \tag{10}$$

The coefficients are

$$c_{kl} = s(kd, ld; h). \tag{11}$$

The derivation of digital weighting functions (i.e. sets of coefficients) outlined above seems fairly straightforward. Using a computer the set may be determined to any accuracy required. It suffices to put the values (10) and the depth of the continuation into the integral (9) which may then be evaluated numerically using routine computer programs. The formulas will supply coefficients for arbitrary values of the parameters h and d. Nevertheless, many authors have published sets of coefficients (i.e. formulas) derived by various assumptions and approximate methods.

An objective appreciation of the formulas proposed can be carried out by means of filter theory. For the purpose, the transfer functions of the formulas are compared with that of the theoretical operation (8). This comparison yields a measure of the goodness of approximation. However, before making comparisons, let us establish some features of the transfer function belonging to the theoretical operation.

After introducing dimensionless variables for frequencies and depth of continuation by the definitions

$$\omega' = \omega d,$$
$$\psi' = \psi d,$$
$$\chi = \frac{h}{d},$$

Eq. (8) can be rewritten to read

$$S(\omega', \psi'; \chi) = e^{\chi\sqrt{\omega'^2+\psi'^2}}. \tag{12}$$

The radial dimensionless frequency ϱ' has been defined by

$$\varrho' = +\sqrt{\omega'^2+\psi'^2}$$

(see e.g. paper II, M e s k ó, 1967). With the new, ϱ' variable Eq. (12) gives

$$S(\varrho'; \chi) = e^{\chi\varrho'}. \tag{13}$$

Clearly, the transfer performed by the theoretical operation is direction-independent.

We expect the results of consecutive continuations referring to depths χ_1 and χ_2, respectively, to equal a single continuation referring to the depth

$$\chi = \chi_1 + \chi_2$$

i.e.

$$S(\chi_1)S(\chi_2) = S(\chi_1+\chi_2). \tag{14}$$

Let us check whether this equation holds. We have

$$S(\chi_1) = e^{\chi_1\varrho'},$$
$$S(\chi_2) = e^{\chi_2\varrho'},$$
$$S(\chi_1+\chi_2) = e^{(\chi_1+\chi_2)\varrho'}.$$

Hence

$$S(\chi_1)S(\chi_2) = e^{\chi_1\varrho'}e^{\chi_2\varrho'} = e^{(\chi_1+\chi_2)\varrho'} = S(\chi_1+\chi_2)$$

and Eq. (14) is indeed valid.

For small values of the parameter χ ($\chi \leqq 0.5$) the difference between the original and continued field is relatively small. Amplification equals unity for the regional component (i.e. for $\varrho' \approx 0$) and does not exceed 6 even in the high-frequency range. For $0.5 < \chi < 1.0$, the continued maps are similar to

second derivative maps of the original field. In this case, the transfer functions of the two operations in the middle- and high-frequency range are close to each other. They differ, however, even in this case in the low-frequency range. The second derivative method completely removes the regional component from the original field, whereas downward continuation preserves it irrespective of the depth of continuation.

If $\chi > 1$, downward continuation more strongly emphasizes the high-frequency range than any other residual or higher derivative method.

The above-mentioned features are apparent in Fig. 2. which shows the transfer function of the exact second-derivative method and that of the downward continuation for the depths $\chi = 0.5$ and $\chi = 1$.

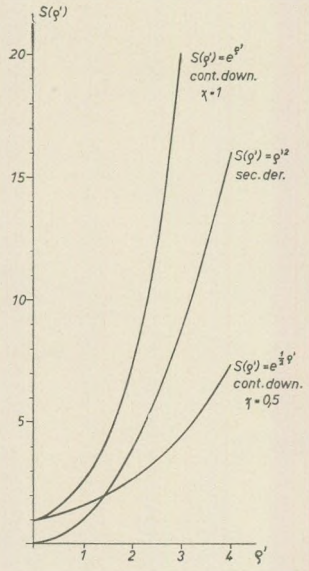

Fig. 2. Transfer functions of the second derivative method and downward continuation referring to depths $h = d/2$ and $h = d$

Investigation of practical formulas

The practical formulas have the form

$$g_h(x, y) = \sum_k \sum_l c_{kl}\, g_0(x + kd, y + ld), \qquad (14)$$

where the c_{kl} are numerical coefficients which in the cases to be studied here constitute a symmetrical pattern. The transfer function of the right-hand side of Eq. (14) has already been computed (M e s k ó, 1968). It reads

$$S_{appr}(\omega', \psi'; \chi) = c_{00} + 2\sum_{k=1}^{n} c_{k0} \cos k\omega' + 2\sum_{l=1}^{n} c_{0l} \cos l\psi' +$$

$$+ 4\sum_{k=1}^{n}\sum_{l=1}^{n} c_{kl} \cos k\omega' \cos l\psi'. \qquad (15)$$

Figs. 3. to 9. are two-dimensional representation of the transfer functions of the following formulas:

Constantinescu – Botezatu:
$\chi = 1.0,$
$\chi = 1.5,$
$\chi = 2.0,$
$\chi = 2.5,$
$\chi = 3.0,$

Tsuboi – Oldham – Waithman: $\chi = 0.5,$
(truncated formulas) $\chi = 1.0.$

In the two latter cases, the transfer functions of the central parts ($k = 5$, $l = 5$) of the original sets of coefficients are shown. The part remaining after truncation yields a set of coefficient of moderate size, suitable for practical application. The original pattern ($k = 15$, $l = 15$) is too large to be useful for most practical purposes. Figs. 8. and 9. clearly show that even the transfer functions corresponding to the central parts approach the theoretical operation to a fairly high degree.

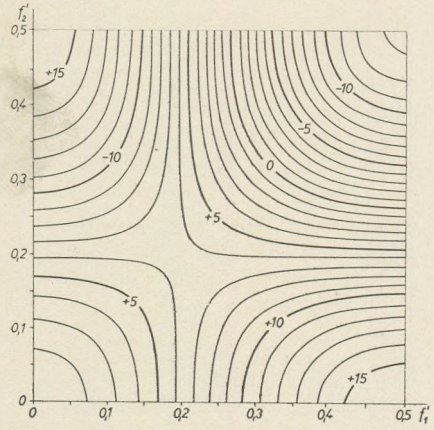

Fig. 3. Two-dimensional transfer function of Constantinescu – Botezatu's formula $\chi = 1$

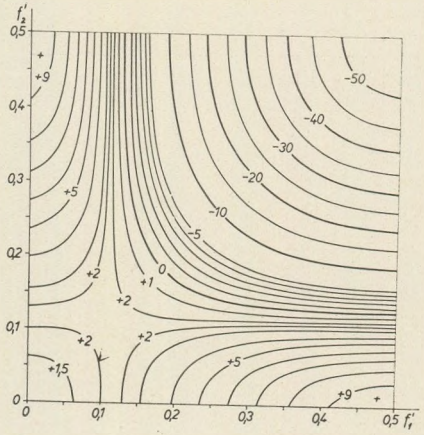

Fig. 4. Two-dimensional transfer function of Constantinescu – Botezatu's formula $\chi = 1.5$

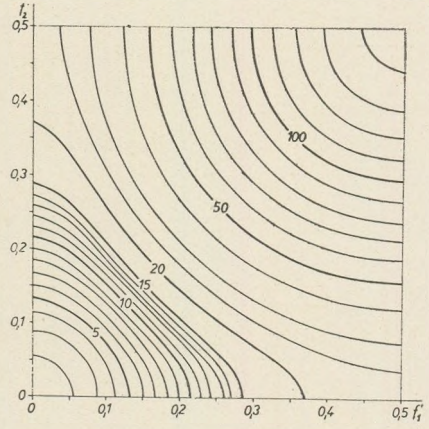

Fig. 5. Two-dimensional transfer function of Constantinescu – Botezatu's formula $\chi = 2.0$

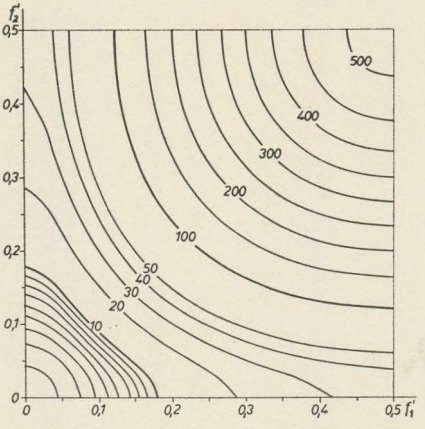

Fig. 6. Two-dimensional transfer function of Constantinescu – Botezatu's formula $\chi = 2.5$

The transfer properties of the formulas proposed by Constantinescu and Botezatu are rather far from the desirable. Moreover, they show strong dependence on orientation and their application may consequently give rise to misinterpretations. We might discover "structural lines" on the continued map which do not exist in reality and merely result from the direction-dependent properties of the sets of coefficients applied. (See also the corresponding part of Meskó, 1967.)

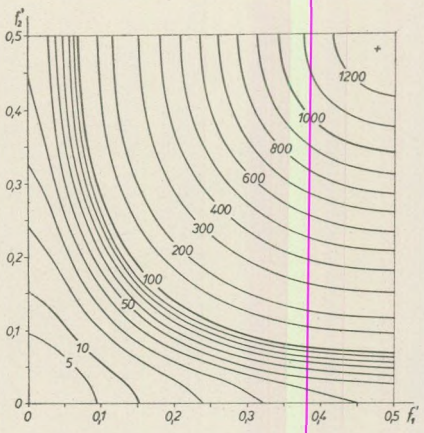

Fig. 7. Two-dimensional transfer function of Constantinescu – Botezatu's formula $\chi = 3.0$

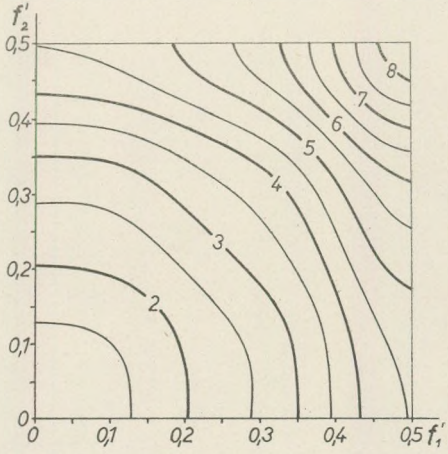

Fig. 8. Two-dimensional transfer function of the Tsuboi – Oldham – Waithman formula $\chi = 0.5$

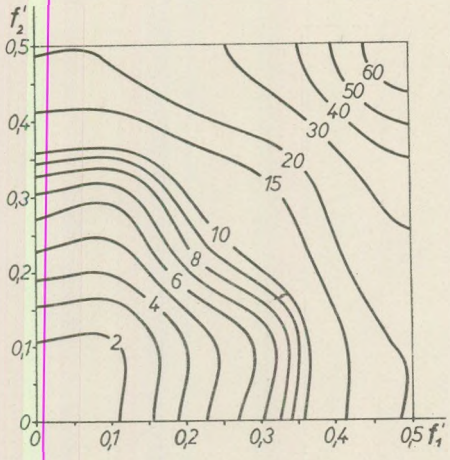

Fig. 9. Two-dimensional transfer function of the Tsuboi – Oldham – Waithman formula $\chi = 1.0$

The sets of curves

$$S(\varrho' = k \cdot 30°, \alpha) \quad (k = 1, 2, \ldots, 6)$$

are shown as Figs. 10. and 11. to emphasize the dependence on orientation of the formulas given by Constantinescu and Botezatu. Dependence on orientation is strikingly strong.

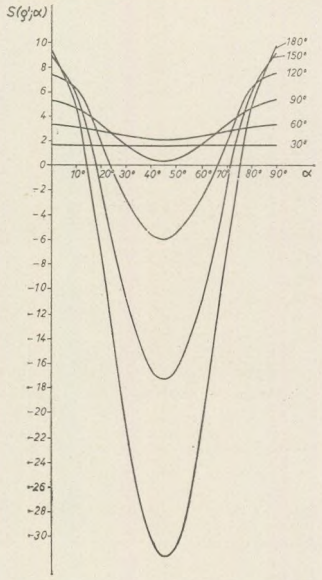

Fig. 10. Curves representing the transfer properties of Constantinescu – Botezatu's formula, $\chi = 1.5$

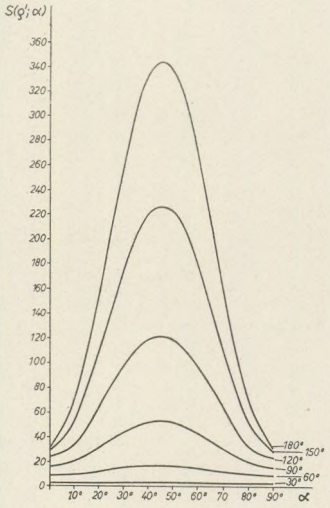

Fig. 11. Curves representing the transfer properties of Constantinescu – Botezatu's formula, $\chi = 2.5$

It is sometimes mentioned as an advantage of the Constantinescu – Botezatu formulas that they contain few coefficients ($k = 1$, $l = 1$) and thus their use is very simple. (F a c s i n a y, 1966). Although in the "computer age" this "advantage" plays no significant role, it is worthwhile to investigate the behaviour of other formulas truncated to the same size. Other sets of coefficients are found to have more favourable transfer properties than those of Constantinescu – Botezatu. The dependence on direction of the truncated Oldham – Waithman – Tsuboi formulas ($k = 1$, $l = 1$) may be estimated from Figs. 12 and 13. The transfer no more approximates the ideal one but remains closer to optimal than that of the Constantinescu – Botezatu formulas. Using moderately truncated versions (e.g $k = 5$, $l = 5$), dependence on orientation becomes negligibly small.

We may conclude that in all instances the Tsuboi – Oldham – Waithman formulas should be applied rather than any others. The sets of coefficients are given in Table I. If the desired depth of continaution exceeds $\chi = 1$, the opera-

tion may be performed by a number of successive continuations for depths $\chi = 0.5$ or $\chi = 1$.

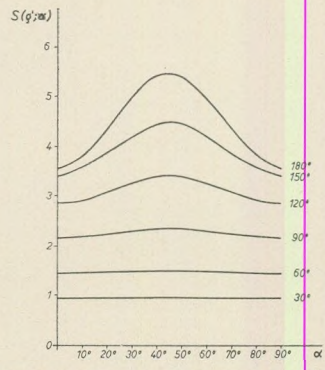

Fig. 12. Curves representing the truncated Tsuboi – Oldham – Waithman formula $\chi = 0.5$ (k=1, l=1)

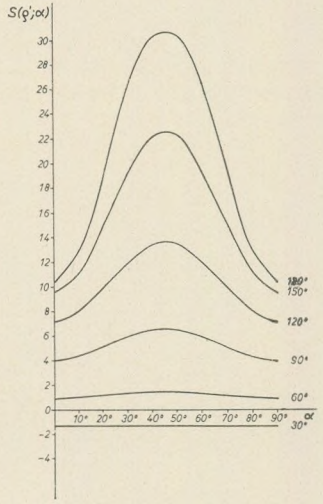

Fig. 13. Curves representing the transfer properties of the truncated Tsuboi – Oldham – Waithman formula $\chi = 1.0$ (k=1, l=1)

Table I.

Coefficients for downward continuation

(Truncated Tsuboi – Oldham – Waithman formulas)

$\chi = 0.5$

l \ k	0	1	2	3	4	5
0	+3.657	−0.742	+0.192	−0.095	+0.051	−0.034
1	−0.742	+0.022	−0.020	+0.003	−0.004	+0.002
2	+0.192	−0.020	±0	−0.003	±0	−0.001
3	−0.095	+0.003	−0.003	±0	−0.001	±0
4	+0.051	−0.004	±0	−0.001	±0	±0
5	−0.034	+0.002	−0.001	±0	±0	±0

$\chi = 1.0$

l \ k	0	1	2	3	4	5
0	+15.785	−5.847	+2.185	−1.090	+0.632	−0.414
1	− 5.847	+1.353	−0.487	+0.224	−0.135	+0.085
2	+ 2.185	−0.487	+0.153	−0.078	+0.041	−0.029
3	− 1.090	+0.224	−0.078	+0.036	−0.023	+0.014
4	+ 0.632	−0.135	+0.041	−0.023	+0.010	−0.008
5	− 0.414	+0.085	−0.029	+0.014	−0.008	+0.005

REFERENCES

Constantinescu, L. – Botezatu, R. (1961): Contributii la interpretarea ... Probleme de Geofisica, Acad. Rep. Populare Romine.

Facsinay, L. (1966): Experiments in the application of the downward continuation (in Hungarian). Geofizikai Közlemények, XVII, 1 – 2. pp. 3 – 15.

Meskó, A. (1965): Gravity interpretation and information theory. Annales Univ. Sci. Budapestinensis IX. pp. 15 – 29.

– (1966): Gravity interpretation and information theory II. Smoothing and computation of regionals Annales ... X, pp. 15 – 27.

– (1967): Gravity interpretation and information theory III. The method of second derivative. Annales ... XI, pp. 37 – 60.

Roy, A. (1966): Downward continuation and its application to electromagnetic data interpretation. Geophysics, XXXI, No 1, pp. 167 – 185.

– (1967): Convergence in downward continuation for some simple geometries. Geophysics, XXXII, No 5, pp. 853 – 867.

Tsuboi, Ch. – Oldham, C. H. G. – Waithman, V. B. (1958): Numerical tables facilitating three-dimensional gravity interpretation. Journ. of Phys. of the Earth VI, pp. 7 – 13.

THEORY OF AN IN SITU THERMAL CONDUCTIVITY SONDE

by
P. SALÁT
(Geophysical Institute of Loránd Eötvös University)
(Received: 6 January 1969.)

SUMMARY

The author discusses the possibilities of an *in situ* heat conductivity sonde containing no heat source. The sonde is a copper rod placed in the terrestrial heat field. The temperature difference between the two ends of the rod is measured. From the result the heat flow may be calculated in the knowledge of the geothermal gradient.

The main difficulties of realizing the idea are the necessity of measuring very accurately a small temperature difference, the handling of the heavy sonde, and the relatively long duration of the measurement.

At the price of surmounting these difficulties, however, *in situ* values of thermal conductivity encompassing a rock domain of a vertical extent equalling sonde length may be obtained.

1. Introduction

An important problem of terrestrial heat flow measurement is the transfer to field conditions of the thermal conductivity values measured in the laboratory. This is a particularly difficult task if the deposit in question is poorly consolidated and highly porous. The uncertainties inherent in any such adaptation constitute the reason why measurements *in situ*, in the field, are to be preferred. In the following the author will outline the theoretical basis for the realization of an *in situ* sonde suited to determine terrestrial heat flow exclusively out of temperature differences.

Consider the terrestrial temperature field and suppose that it is stationary and homogeneous in a certain domain of space (e.g. in a homogeneous layer of rock). Insert in that same domain a probe whose thermal conductivity differs considerably from that of the domain. The temperature distribution within the domain is rendered inhomogeneous by the presence of the probe. If both the undisturbed and the inhomogeneous temperature distribution are determined, a comparison of the two yields, in the knowledge of the conductivity of the probe, the conductivity of the domain on the one hand and the heat flow on the other.

2. Potential-theory fundamentals

It is expedient to deal with elongated sondes, as the probes to be placed in the terrestrial heat field are most likely to be inserted in boreholes or holes drilled in mines or in the bottom of the sea.

Let us consider a theoretical model of the thermal conductivity sonde placed into the borehole, as follows:

Consider an elongated ellipsoid of thermal conductivity λ' placed in a substance of thermal conductivity λ (Fig. 1). The equation of the ellipsoid in the xyz coordinate space is

$$\frac{x^2}{a^2}+\frac{y^2+z^2}{b^2}=1. \tag{1}$$

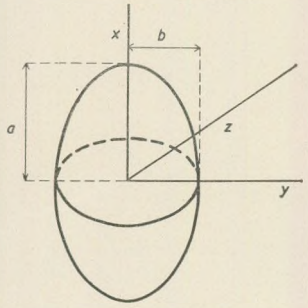

Fig. 1. The model of an ellipsoid shape sonde

Let the temperature tend towards

$$T = gx, \tag{2}$$

at a great distance from the origin. g is a constant; in the present case it is the geothermal gradient.

The temperature distribution within the ellipsoid is then given by

$$T=\frac{gx}{1+A_0\left(\frac{\lambda'}{\lambda}-1\right)}=g'x, \tag{3}$$

g' being the temperature gradient within the sonde.

The external temperature is

$$T_k = gx-\frac{\left(\frac{\lambda'}{\lambda}-1\right)gA_l x}{1+A_0\left(\frac{\lambda'}{\lambda}-1\right)} \tag{4}$$

The A_l function satisfies the Laplace equation.

$$A_l = \frac{1-e_0^2}{e_0^3}\left[\frac{1}{2}\ln\frac{1+e_l}{1-e_l}-e_l\right] \tag{5}$$

In this equation, l is a positive root of the equation

$$\frac{x^2}{a^2+l}+\frac{y^2+z^2}{b^2+l}=1 \tag{6}$$

at any point (xyz). For any l = const. the corresponding points (xyz) are situated on an ellipsoid confocal with the surface of the sonde and having the eccentricity

$$e_l=\left[\frac{a^2+b^2}{a^2+l}\right]^{\frac{1}{2}}. \tag{7}$$

Furthermore,

$$e_0 = e_l\Big|_{l=0} = \left[\frac{a^2-b^2}{a^2}\right]^{\frac{1}{2}} \tag{8}$$

and

$$A_0 = A_l\Big|_{l=0}. \tag{9}$$

The above considerations have been adapted from the book by Carslaw and Jaeger [1], with some slight changes of notation.

3. Dimensions of the sonde

The ratio of the geothermal gradient g, prevailing far off the sonde, to the gradient g' measured in the sonde is obtained by rearranging (3):

$$K = \frac{g}{g'} = 1 + A_0\left(\frac{\lambda'}{\lambda} - 1\right). \tag{10}$$

An approximate value of A_0 is obtained making use of the series expansion of e_0:

$$A_0 = \frac{b^2}{a^2}\left(\ln\frac{2a}{b} - 1\right). \tag{11}$$

Substituting into (10) we have

$$K = \frac{g}{g'} = 1 + \left[\frac{b^2}{a^2}\ln\left(\frac{2a}{b} - 1\right)\right]\left(\frac{\lambda'}{\lambda} - 1\right). \tag{12}$$

Employing this formula, the author has calculated the gradient ratio K for some possible values of thermal conductivity, for copper sondes ($\lambda' = 0.930$ cgs) of various shapes (Table I).

Table I.

$K = \frac{g}{g'}$ values

λ ↓ $\quad \frac{a}{b}\rightarrow$	10	15	20	25	30	40
$2 \cdot 10^{-3}$ cgs	10.28	5.96	4.12	3.16	2.59	1.979
3	7.18	4.31	3.08	2.44	2.06	1.652
4	5.64	3.48	2.56	2.08	1.796	1.490
5	4.70	2.98	2.25	1.862	1.634	1.390
6	4.08	5.65	2.04	1.718	1.528	1.325
7	3.64	2.41	1.888	1.615	1.433	1.279
8	3.30	2.23	1.774	1.536	1.394	1.243
9	3.04	2.09	1.686	1.475	1.350	1.215
10	2.84	1.984	1.619	1.429	0.315	1.194

In the possession of the values of Table I we can determine the most advantageous a/b ratio, that is, the best sonde shape.

In order to find out the best sonde shape let us estimate the error of the measurement.

For a copper sonde, λ'/λ varies from 100 to 400, and it is justified to drop the unity in the parenthesis on the right hand side of (10) Hence,

$$\frac{g}{g'} = 1 + \frac{\lambda'}{\lambda} A_0; \tag{13}$$

and solving for λ,

$$\lambda = \frac{\lambda' A_0}{\frac{g}{g'} - 1} = \frac{\lambda' A_0}{K - 1}. \tag{14}$$

The term actually measured is $K = g/g'$. The value of g' is best determined out of the temperature difference between the two ends of the sonde, the length of which is $2a$:

$$g' = \frac{T'}{2a}. \tag{15}$$

Let us calculate the error of the thermal conductivity λ if the error of T' is dT'. Let us consider g as accurate for the time being. From the equation

$$\lambda = \frac{\lambda' A_0}{\frac{2ga}{T'} - 1} \tag{16}$$

we obtain the differential

$$d\lambda = \frac{-\lambda' A_0}{\frac{2ga}{T'} - 1} \cdot \frac{-2ga}{T'^2} dT', \tag{17}$$

whence the relative error of λ (17 by 16) is

$$\frac{d\lambda}{\lambda} = \frac{2ga}{\left(\frac{2ga}{T'} - 1\right) T'^2} dT' = \frac{2ga}{2ga - T'} \cdot \frac{dT'}{T'}. \tag{18}$$

For a constant dT' the relative error of λ is a minimum if the denominator is a maximum. Now the maximum of the expression

$$2gaT' - T'^3 \tag{19}$$

is at

$$T'_m = ga. \tag{20}$$

That is, the K value belonging to the minimum relative error of λ is given by

$$K = \frac{g}{g'} = \frac{g}{T'_m/2a} = \frac{g}{ga/2a} = 2. \tag{21}$$

Hence, the most favourable sonde shape is that for which $K = 2$. If the mean heat conductivity of the rocks involved is set at $6 \cdot 10^{-3}$ cgs, this is realized at $a/b = 20$.

4. Problems of realization

4.1 Temperature measurement

Consider a sonde for which $a/b = 20$. This is the most favourable shape if the thermal conductivity to be measured is around $6 \cdot 10^{-3}$ cgs. As the maximum possible diameter of a sonde which is to fit the average borehole is 20 cm, the length of the sonde as prescribed by the above ratio is 4 metres ($a = 200$ cm, $b = 10$ cm). Let us estimate the temperature difference prevailing between the two ends of this sonde.

For an ambient thermal conductivity of $6 \cdot 10^{-3}$ cgs in the hole, the gradient that builds up in the sonde is, according to Table I,

$$g' = \frac{g}{2.04}. \tag{22}$$

Let us set the undisturbed gradient at $g = 2.5$ degrees centigrade per 100 metres. The temperature difference is then

$$T' = g' 2a \approx 0.050 \text{ degree centigrade} \tag{23}$$

If the sonde is thinner ($a = 100$ cm, $b = 5$ cm), and the thermal conductivity poorer ($\lambda = 4 \cdot 10^{-3}$ cgs), we have, for the same gradient as above,

$$T' = 0.020 \text{ °C} \tag{24}$$

These estimates show up the main difficulty of the measurement envisaged, namely, the need for very accurate temperature measurement. From (18) we obtain for $K = 2$

$$\frac{d\lambda}{\lambda} \approx 2 \frac{dT'}{T}, \tag{25}$$

whence the relative error of the thermal conductivity thus measured is about twice that of the temperature measurement. Thus in the above two examples an accuracy of 10^{-3} degree centigrade in temperature measurement entails an accuracy to within 4 and 10 percent, respectively, of the thermal conductivity derived therefrom, disregarding every other theoretical and practical source of error.

A temperature measurement to an accuracy of 10^{-3} degree centigrade is relatively simple in the laboratory, but the gradientmeters employed in the field do not yet attain this sensitivity.

The possible ways of solution are:

a) thermocolumns,
b) increasing the sensitivity of thermistor amplifies [2],
c) differential connections of thermosensitive oscillators [3].

4.2. Displacing the sonde

A further technical difficulty is the safe handling of the sonde within the borehole. The weight of the above-mentioned sonde of 4-metre length is in the range of 1.1 metric ton. Such a heavy weight will have to be lowered by a very strong cable. Another possible solution is to make the sonde body out of aluminium.

4.3. Measuring the undisturbed gradient

Conventional gradientmeters are well suited to the measurement of the original gradient g, and g' may be determined also simultaneously, as follows:

By the aid of formulae (4, 5, 6, 7) we have calculated the temperature distribution in the surroundings of the sonde for the parameters $a/b = 20$ and $\lambda'/\lambda = 250$. The isotherm pattern is shown as Fig. 2.

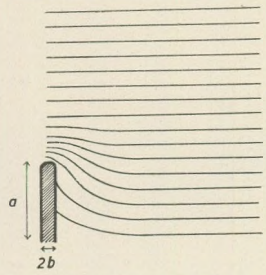

Fig. 2. Isotherms around the sonde

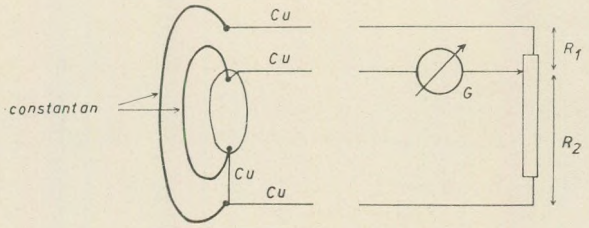

Fig. 3. Theoretical schema of measurement of gradient ratio

It is easy to see from the above calculation and is likewise apparent in Fig. 2 that at a distance $3a$ from the origin the temperature distribution is already undisturbed. If the gradient is measured along this distance, it will deviate less than 0.5 percent from true g. Hence, the sondes for measuring g and g' may be coupled and the ratio of their lengths may be set at 3/1.

If the temperature difference is to be measured e.g. by means of an appropriate number of thermocouples connected in series, the schematic circuit pattern of the measurement may be of the type shown as Fig. 3.

The galvanometer is reset to zero by the appropriate setting of the resistors R_1 and R_2. In the knowledge of the resistance readings and of the sensitivity of the thermocolumns it is possible to obtain directly the gradient ratio $K = g/g'$.

4.4. The influence of convection currents in the drilling mud

The isotherm pattern of Fig. 2. shows clearly that the change of the field against the undisturbed pattern is greatest at the two ends of the sonde. In this vicinity the heat flow in the sonde may be 80 to 100 times greater than the original flow value. [$\lambda' g' \approx (80-100)\lambda g$]. This circumstance makes the formation of convection currents in the drilling mud filling the borehole around the sonde highly likely, since the liquid column in the hole becomes unstable if the heat flow is that strong (Diement and Robertson, [4]). Thus the assump-

tion that the probe is imbedded in a medium of heat conductivity λ might not even approximately hold.

In order to eliminate any disturbances due to convection it is expedient to prolong the sonde by an attachment whose conductivity closely approximates that of the surrounding rock. It seems useful to have several exchangeable attachments of this kind. To stop convection currents it is best to give the attachment the shape of a "bottle washer" as proposed by Jaeger, Beck and Newstead [5].

4.5. Duration of the measurement

Let us estimate the time needed for the inhomogeneous field around the sonde to grow stationary.

At the instant the sonde stops at some point of the borehole, its temperature will differ by some degrees from the ambient temperature. Its cooling (or warming up) may be approximately described by considering an infinite cylinder. Fig. 4. showing these conditions has been adapted from the book by Carslaw and Jaeger. The notations are:

$\varkappa$ is thermal diffusivity of the medium surrounding the cylinder,
t is time,
α is the parameter of the curves with $\alpha = \dfrac{2(\varrho c) \text{ ambient}}{(\varrho c) \text{ cylinder}}$
ϱ is density and
c is specific heat.

In the case considered, $\alpha \approx \dfrac{2 \cdot 0.4}{0.8} = 1.$

T is the instantaneous temperature of the cylinder,
T_0 is the measure of temperature disturbance.

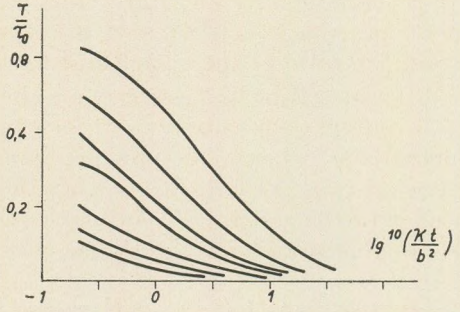

Fig. 4. The cooling curves of an infinite cylinder after Carslaw and Jaeger

It is apparent from the figure that for $\alpha = 1$ there belongs to a state, approximating the steady state to within a few percent, the value

$$\overset{10}{\log} \frac{Kt}{b^2} \approx 1 \text{ to } 2, \tag{26}$$

that is, this state sets in in 1 to 10 days. ($K = 0.01$ cm^2 sec^{-1}, $b = 10$ cm.) For a sonde of finite length less time is needed.

Waiting time can be further reduced by decreasing the disturbance, that is, by displacing the sonde in small steps down the borehole.

The deformation of the homogeneous field into an inhomogeneous one takes place simultaneously with the setting in of thermal equilibrium in the sonde. The final isotherm pattern corresponds approximately to the fields of two point sources of opposite sign superposed onto a homogeneous field. Let us consider as a rough approximation of the sonde a point source of intensity q whose discharge begins at $t = 0$. According to [1], the temperature field of such a source is

$$T = \frac{q}{4\pi K r} \operatorname{erfc} \frac{r}{\sqrt{4Kt}}. \tag{27}$$

By the calculation presented in *4.3.*, the temperature deviation along the sonde axis, at a distance of $2a$ from the origin, is about 2 percent of that arising at a, that is, at the end of the sonde. Let us now ask at what time after "switching on" does the temperature deviation attain 1 percent, that is, half the full value? Let $r = 2a - a = a = 200$ cm, $K = 0.01$; since

$$\operatorname{erfc} 0.5 = 0.48, \tag{28}$$

and

$$\operatorname{erfc} 0 = 1, \tag{29}$$

if

$$\frac{T(r, t_0)}{T(r, \infty)} = 0.48, \tag{30}$$

then

$$0{,}50 = \frac{200}{\sqrt{4 \cdot 0.01 t_0}}. \tag{31}$$

Solving for t_0, we have

$$t_0 = 4 \cdot 10^6 \text{ sec} \approx 40 \text{ days}. \tag{32}$$

Hence, a point situated at a distance of $2a$ from the origin will attain 48 percent of the full disturbance in 40 days. Of course, nearer to the end of the sonde the temperature attains the steady state much more rapidly.

This calculation is but a very rough approximation. The real situation is very complicated. In any case it is apparent that a heat conductivity value representative of a larger domain of space must be paid for by a prolongation of the measurement.

The accurate determination of optimum duration necessitates further theoretical and practical research. A possible solution is to avoid the steady state and, after having determined theoretically or empirically the rate at which the temperatures tend towards equilibrium, to register the front ends of the curves only and to infer therefrom the temperature distribution of the steady state.

5. Ways of refining the theoretical model

The above calculation has been carried out under the assumption of a highly conductive ($\lambda' \gg \lambda$) ellipsoid placed in a medium of conductivity λ. This is essentially the model of a sonde introduced into a borehole. In the following we shall investigate the influence of the mud surrounding the sides and the ends of the sonde and of the casing. As a second approximation let us set up the following model:

The sonde is an ellipsoid of conductivity λ'. ($l = 0$ at its outer surface.) Let the mud and the casing be approximated by an ellipsoid confocal with the sonde and having a conductivity of λ_i, with $l = l_i$ at its outer surface. Outside this ellipsoid there is rock of conductivity λ. At a great enough distance from the sonde, the direction of the heat flow passing trough the rock is parallel to the long axis of the sonde.

The author has established that solution of the Laplace equation which satisfies the appropriate boundary conditions. The gradient ratio derived from the solution is

$$K = \frac{g}{g'} = \frac{(1-\mu)(\varepsilon-\mu)E_{l_i} \cdot A_{l_i} + (E_{l_i} - \mu A_{l_i})(\mu E_0 - \varepsilon A_0)}{\mu(E_{l_i} - A_{l_i})}. \tag{33}$$

Most notations signify the same as above; the newly introduced symbols are

$$\varepsilon = \frac{\lambda'}{\lambda}, \tag{34}$$

$$\mu = \frac{\lambda_i}{\lambda}, \tag{35}$$

$$E_l = A_l - \frac{1-e_0^2}{e_0^3} \cdot \frac{e_l^3}{1-e_l^2}. \tag{36}$$

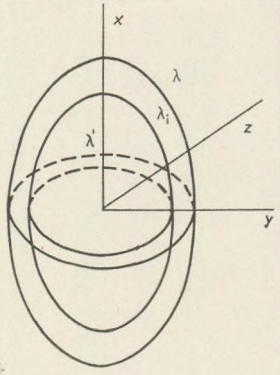

Fig. 5. The model of a sonde taking into consideration the influence of the mud

By the aid of the above formulas one can calculate the heat conductivity of the rock, provided the thickness d of the mud and its heat conductivity are known , even if the sonde does not snugly fit the hole. For a sonde of unit radius ($b = 1$),

$$d = \sqrt{1+l_i} - 1 \tag{37}$$

Detailed calculation proves that a thin layer of mud causes very little distortion, that is, it is expedient to employ a sonde fitting the casing as closely as possible.

If the heat conductivity of the mud is unknown, it is possible to employ two sondes of different a/b ratios. From the values measured with these two sondes, λ_i can be determined.

The influence of mud and casing can of course be better approximated with more complicated models more closely resembling the real conditions.

REFERENCES

[1] H. S. Carslaw, J. C. Jaeger: Conduction of Heat in Solids. Oxford, Clarendon Press. 1959, p. 427, p. 343, p. 261.
[2] E. C. Bullard, A. E. Maxwell, R. Revelle: Heat flow trough the Deep Sea Floor. Advances in Geophysics Vol. 3. p. 155.
[3] W. L. Smith and W. J. Spencer: Quartz Crystal Thermometer for Measuring Temperature Deviations in the 10^{-3} to 10^{-6} C° Range. The Review of Scientific Instruments. Vol. 34, No. 3. p. 268.
[4] W. H. Diement, E. C. Robertson: Temperature, Thermal conductivity, and Heat Flow in a Drilled Hole near Oak Ridge, Tennessee. Journal of Geophys. Res. Vol. 68. No. 17, p. 5040.
[5] A. E. Beck, J. C. Jaeger, G. N. Newstead: The Measurement of the Thermal Conductivity of Rocks by Observations in Boreholes. Instr. Jour. Phys. Vol. 9. 1956.

О ТОЧНОСТИ ИЗМЕРЕНИЯ ПРОТОНО-ПРЕЦЕССИОННЫМ МАГНИТОМЕТРОМ

П. СЕМЕРЕДИ
Геофизическая кафедра Будапештского университета им. Л. Этвеша
(Подписано к печати: 21 июля 1968 г.)

SUMMARY

For a unification of the basis values of the magnetic observatories to apply the proton-precession magnetometers is proposed. This suggestion is based on the supposition that the a.c. current flowing in the probe coil cannot affect the precession frequency to a considerable degree. The paper presents the verification of this supposition.

В основе измерения напряженности геомагнитного поля протонно-прецессионным магнитометром лежит соотношение

$$\omega = \gamma_p F \tag{1}$$

где ω — прецессионная частота магнитного момента протона; γ_p — коэффициент гиромагнитной пропорциональности и F — абсолютная величина геомагнитного поля.

Величина коэффициента пропорциональности γ_p известна с весьма малой погрешностью ($\gamma_p = 2{,}67513 \cdot 10^4 \pm 0{,}2$ рад. гаусс$^{-1}$сек$^{-1}$).

Получив величину ω по измерениям, по вышеуказанному соотношению можно вычислить значение F. Не учитывая ошибку γ_p, погрешность величины F будет пропорциональна погрешности ω.

Измерение прецессионной частоты ω может осуществляться при помощи катушки, включающей в себя протонный образец. Данная катушка имеет двойное предназначение.

С одной стороны, на этапе подготовки к измерению частоты, через нее пропускается ток, магнитное поле которого вызывает ядерную поляризацию в протонном образце. С другой стороны эта же катушка служит, после прекращения поляризующего тока, для наблюдения над протонной прецессией. При этом парамагнитная ядерная поляризация, вращающаяся вокруг геомагнитного поля, возбуждает переменное напряжение. Частота этого переменного напряжения аналогична прецессионной частоте. Усиливая переменное напряжение можно измерить частоту. Погрешность изме-

рения частоты тем меньше, чем больше отношение сигнал/шум у сигнала, применяемого для измерения частоты. Поскольку переменное напряжение, возбуждаемое протонной прецессией в катушке, имеет очень низкую величину (порядка 1 мкв), оно близко по значению к уровню термических помех. Фон помех сигнала увеличивается за счет усиления, в связи с чем измерение частоты выполняется, при таких условиях, при весьма неблагоприятном отношении сигнал/шум.

Преобразуя катушку зонда в колебательный контур, резонансная частота которого аналогична прецессионной частоте, можно в значительной мере улучшить отношение сигнал/шум. Отношение сигнал/шум, существующее при измерении частоты, увеличивается с улучшением качества колебательного контура, а также с увеличением мощности, подаваемой на вход усилителя. Если эти условия выполняются, то увеличивается противодействие колебательного контура зонда на протонную систему. Ток, протекающий через колебательный контур зонда, возбуждает магнитное поле, изменяющее свободную прецессию протонов.

Возникает вопрос, в какой мере данное противодействие колебательного контура зонда изменяет прецессионную частоту, связанную с магнитным полем интенсивностью F.

В типичных случаях интенсивность переменного тока зонда, настроенного на частоту $\omega = \gamma_p F$, имеет величину порядка 10^{-7} А. При существующих конструкциях зондов в катушке, в поляризационном участке возбуждается магнитное поле порядка 100 Э/А. В связи с этим ток колебательного контура вызывает в протонном образце переменное магнитное поле интенсивностью порядка 1 гаммы.

В дальнейшем будет показано, что сравнительно интенсивное магнитное поле — порядка 1 гаммы — влияет на прецессию лишь в пренебрегаемой мере.

Поведение вектора парамагнитной ядерной поляризации выражается системой дифференциальных уравнений Блоха.

Пусть вектор напряженности геомагнитного поля $\overline{F}$ будет параллелен оси z, а ось катушки зонда — оси x системы координат. При этом система дифференциальных уравнений Блоха может быть записана в виде

$$\dot{M}_x - \omega M_y + \frac{M_x}{T_2} = 0$$

$$\dot{M}_y + \Omega M_z + \omega M_x + \frac{M_y}{T_2} = 0 \qquad /2/$$

$$\dot{M}_z + \Omega M_y + \frac{M_z}{T_2} = \frac{M_F}{T_1}$$

где M_x, M_y, M_z — составляющие вектора ядерной поляризации, выполняющего прецессионное движение; M_F — статическая ядерная поляризация, возникающая на воздействие геомагнитного поля; ω — прецессионная частота, создающаяся в геомагнитном поле F; $\Omega = \Omega(t) = \gamma_p H_x(t)$ — „прецессионная частота", являющаяся следствием переменного тока $I(t)$, протекающего в катушке зонда, коаксиальной оси x координатной системы.

Переменный ток, протекающий в колебательном контуре зонда выполняет условие дифференциального уравнения

$$L\dot{I}-RI+\frac{1}{C}\int_0^t Id = -\frac{4\pi}{10^8} nA\dot{M}_x \qquad /3/$$

где L, R и C — соответственно самоиндукция, сопротивление потери и емкость настройки колебательного контура зонда; n — число витков катушки зонда и A — поперечное сечение протонного образца.

На воздействие переменного тока $I(t)$, протекающего в соленоидообразной катушке длиной l, в протонном образце возбуждается напряженность магнитного поля

$$H_x(t) = \frac{0{,}4\pi n}{l} I(t).$$

В данном магнитном поле создается прецессионная частота

$$\Omega(t) = \gamma_p H_x(t) = \frac{0{,}4\,\pi\, n}{l} I(t)\gamma_p.$$

Подставляя $I(t)$ в /3/, после упорядочения получаем:

$$\dot{\Omega} + \frac{R}{L}\Omega + \frac{1}{LC}\int_0^t \Omega(s)\,ds = -\frac{1{,}6\,\pi^2 A\,\gamma_p n^2}{10^8 lL}\dot{M}_x \qquad /4/$$

Для M_x из /2/ получается интегрально-дифференциальное уравнение

$$M_x'' + \frac{2}{T_2\omega}M_x' + \left(1+\frac{1}{T_2^2\omega^2}\right)M_x + \frac{\Omega}{\omega^2}\int_0^\tau \Omega\left(\frac{M}{T_2\omega}+M_x\right)ds +$$

$$+\frac{\Omega}{T_1\omega}\int_0^\tau \frac{1}{\Omega}\left[M_x'' + \frac{2}{T_2\omega}M_x' + \left(1+\frac{1}{T_2^2\omega^2}\right)M_x\right]ds = \frac{M_F\Omega\tau}{T_1\omega^2} \qquad /5/$$

Нами были введены параметр собственного времени $\omega t = \tau$ и обозначение $\frac{d}{d\tau} = (\ )'$.

Посмотрим порядок получаемых величин:

Порядок величины γ_p составляет 10^4, в связи с чем порядок $|\Omega_{\text{макс}}| - 10^{-1}$, порядок ω — 10^4. $M_F \approx 10^{-2}M_\tau$, где M_τ — начальная ядерная поляризация, возникающая на воздействие вспомогательного магнитного поля.

По соотношениям вышеуказанных порядков величин, четвертым членом и правой стороной уравнения /5/ можно пренебречь и записать последнее уравнение в виде

$$M_x'' + \frac{2}{T_2\omega}M_x' + \left(1+\frac{1}{T_2^2\omega^2}\right)M_x + \frac{\Omega}{T_1\omega}\int_0^\tau \frac{1}{\Omega}\left[M_x'' + \frac{2}{T_2\omega}\left(1+\frac{1}{T_2^2\omega^2}\right)M_x\right]ds = 0$$

Коэффициент интеграла (после выполнения замены $\Omega(\tau) = \Omega_0 \varepsilon(\tau)$) будет иметь величину порядка 10^{-4}, следовательно вопрос о пренебрежении им остается спорным.

Применяя обозначение

$$\lambda(\tau) = \int_0^\tau \frac{1}{\Omega}\left[M_x'' + \frac{2}{T_2\omega}M_x' + \left(1 + \frac{1}{T_2^2\omega^2}\right)M_x\right]ds \qquad /7/$$

наше уравнение принимает вид

$$\lambda' + \frac{1}{T_1\omega}\lambda = 0.$$

Решение данного уравнения:

$$\lambda(\tau) = \lambda_0 e^{-\frac{\tau}{T_1\omega}}. \qquad /8/$$

Следовательно, полное решение уравнения /6/ сводится к общему решению однородного уравнения

$$M_x'' + \frac{2}{T_2\omega}M_x' + \left(1 + \frac{1}{T_2^2\omega^2}\right)M_x = 0$$

и к партикулярному решению неоднородного уравнения

$$M_x'' + \frac{2}{T_2\omega}M_x' + \left(1 + \frac{1}{T_2^2\omega^2}\right)M_x = \lambda'(\tau)\,\Omega(\tau)$$

Однако правая сторона последнего уравнения также равна нулю, так как по равенству /7/

$$\lambda(0) = 0,$$

а с другой стороны, по /8/ $\lambda(0) = \lambda_0$.

Оба условия могут быть выполнены только при $\lambda_0 = 0$.

Так член уравнения /6/, содержащий интеграл, не оказывает никакого влияния на решение данного уравнения. Его воздействие может сказываться только через члены уравнения /5/, имеющие величины порядка $10^{-10} - 10^{-12}$. При рассмотрении системы дифференциальных уравнений, в отношении $\Omega(\tau)$ — кроме порядковых ограничений — не применялись никакие допущения. Таким образом, учитывая практические требования к погрешностям измерения, можно высказать, что точность измерения не ограничивается за счет переменного тока, проходящего через колебательный контур зонда.

ЛИТЕРАТУРА

Szemerédy, P. (1968): A protonprecesszión alapuló mérések alapjai. Magyar Geofizika, 3.

BELEMNITE FAUNA OF THE AMMONITE-RICH CALLOVIAN BED AT VILLÁNY, SOUTH HUNGARY

by

A. GALÁCZ – A. VÖRÖS

(Chair of Palaeontology, Eötvös University)

(Received: 2 Dec. 1968.)

РЕЗЮМЕ

Описывается 10 видов белемнитов из аммонитового слоя келловея Вилланьских гор. По ранее опубликованным данным К. Гофманном было определено 5 видов в образцах, полученных из этого же слоя. Из них 3 могли быть выявлены и при переобработке материалов.. Обшая картина белемнитовой фауны позволяет делать палеоэкологические и палеогеографические выводы. Что касается вопросов хронологии, белемнитовая фауна также свидетельствует о келловейском возрасте.

The belemnites studied derive from the classical Callovian deposit of the Villány Hills, largely from the Templom Hill locality at Villány and partly from Somsich Hill. (Fig. 1.) In the area, belemnites were collected earlier by Hofmann, Szontágh, Lóczy jun., Rakusz, and lately by Kopek. In 1959 a large-scale layer-by-layer collection of fossils was carried

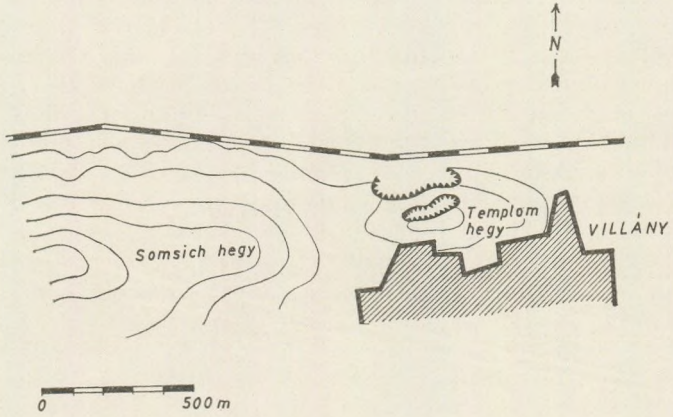

Fig. 1.
Map showing the localities of occurrence of the Villány Hills belemnites

out under the direction of I. F ü l ö p. The material to be described here was put at our disposal by the Hungarian Geological Institute. It was complemented by the results of our own collection in the summer of 1967. A majority of the several hundred specimens making up the material in hand consists of unidentifiable fragments. The hundred or so identifiable ones belong to 10 species.

Outline history of the knowledge of Villány belemnites

The first to mention belemnites from the Dogger beds of the Villány Hills was L e n z (1872). H o f m a n n in 1874 collected a rather copious material in which he identified five belemnite species:

Belemnites Württembergicus, Opp.
Belemnites Gillieroni, May
Belemnites Argovianus, May
Belemnites hastatus, Blainv.
Belemnites Calloviensis, Opp.

This list was published by P á l f y (1901). It was reproduced without change in L ó c z y jun. (1912). L ó c z y jun. in his monograph on the Callovian ammonites of the Villány Hills (1915) did not, owing to the nature of his treatise, study the accessory fauna in detail and only gave the earlier authors' data concerning the belemnites.

Since then, several papers on the geology of the Villány Hills have been published (N o s z k y jun. 1959, K a s z a p 1959, 1961), but no further mention of belemnites has been made.

Some remarks on paleoecology and biostratinomy

In the Villány Hills, the Bathonian and Callovian stages of the Middle Jurassic are represented by a complex of layers whose maximum thickness is 10 m. On the Templom Hill at Villány, most of this complex consists of conglomerate, calcareous sandstone and sandy limestone placed in the Bathonian; only the uppermost 40 cm is taken up by the Callovian ammonite-rich bed. At the other belemnitiferous locality, on Somsich Hill, only the ammonite-rich Callovian bed crops out: its thickness is about 40 cm there also.

Belemnites occur in the sandy limestone of the Bathonian and in the ammonite-rich bed of the Callovian. The belemnite assemblages of the two beds are, however, strikingly different. The former contains stocky forms of the subfamily *Passaloteuthinae;* the latter abounds in species and specimens of slender, fusiform rostra. The absence of *Passaloteuthinae* from the Callovian might be due to the differentiation of their line of evolution in that stage. However, the absence from the Bathonian sandy limestone of the subfamily *Belemnopsinae* indicates beyond doubt a sharp change in ecology. This is proved also by other features of the fauna (Vörös 1968) and by the change in lithology. The belemnites too tend to underscore the hypothesis that the slightly bituminous sandy Bathonian limestone came to exist in a relatively isolated, tranquil part of the sea, whereas the Callovian ammonite-rich bed was deposited in a shallow open sea whose waters were intensely agitated.

Biostratinomic observations on the belemnites embedded in the ammonite-rich bed also indicate an intensely agitated water. The belemnites were often embedded as fragments and this relatively abundant assemblage is quite poor in rostra fossilized together with the phragmocone. Despite their fair state of preservation, no proostracum could be demonstrated on any of the fossils. Rostra of scrubbed-down or otherwise damaged surface are frequent (Pl. 4, Figs. 4–5). This is the case particularly with specimens liberated from separate stromatolith nodes.

In the big quarry, on the Templom Hill at Villány, several sq. metres of the bedding plane of the ammonite-rich bed are exposed. The numerous belemnites visible on this plane exhibit no appreciable preferred orientation.

Paleogeographical aspects of the belemnite fauna

The paleogeographical spread of the Jurassic and Cretaceous belemnite genera is known in broad outline. Stevens (1963, 1965) stated the separation of the three great faunal provinces of belemnites (Boreal, Mediterranean, Indo-Pacific) to have commenced in the Callovian. The most striking manifestation of this process is that the genera of the subfamilies *Passaloteuthinae* and *Cylindroteuthinae*, which in the Bajocian and Bathonian still occur together with the genera *Hibolites* and *Belemnopsis*, are restricted from the Callovian onwards to the Boreal region. In the Bathonian part of the Villány sequence, belemnites of the subfamily *Passaloteuthinae* are rather abundant. On the other hand, in the ammonite-rich bed of the Villány Callovian the genera *Belemnopsis* and *Hibolites* constitute the bulk of the assemblage, besides some species of *Hastites* and *Rhopaloteuthis*. This agrees quite well with the hypothesis of separating faunal provinces.

A review of the distribution of the individual species has been given by Pugaczewska (1961). It is apparent even from the earlier literature (Gemmellaro 1872, Lissajous 1925) that the most abundant species of the Villány Callovian, *H. hastatus*, is ubiquitous throughout the Mediterranean Province.

The distribution of *B. subhastatus* and *R. sauvanausus* is similar. *H. privatensis*, *B. fusiformis*, *B. latesulcatus*, *H. semihastatus* and *R. gillieroni* are known from the European part of the Mediterranean region. The extent of *H. girardoti* seems more restricted, but even this species is known from Switzerland, Poland and Hungary, which suggests that it must occur also in a number of other areas, without having been identified thus far. The case with *B. semiarcuatus* Pugaczewska (1961) is a similar one.

The task of outlining areas of distribution for species and even for genera of belemnites is rather difficult, because up-to-date literature on belemnites is somewhat scanty.

Chronostratigraphic evaluation

The chronostratigraphic value of belemnites is not very high. Still, a fauna rich in species permits some tentative inferences as to the age of the embedding deposit.

The Villány belemnite fauna of ten species is dominated by Callovian forms (Table I).

Table I.

Name	Age distribution of the Villány belemnite fauna				
	Bathonian	Callovian			Oxfordian
		L.	M.	U.	
H. privatensis	+	+	+	+	+
B. fusiformis	+				
B. latesulcatus	+	+	+	+	+
B. subhastatus	+	+	+	+	
B. semiarcuatus			?	+	?
H. hastatus	+	+	+	+	+
H. semihastatus	+	+	+	+	+
H. girardoti	+	+	+	+	+
R. sauvanausus				+	+
R. gillieroni	+	+	+	+	

The only form restricted so far to the Bajocian and Bathonian is *B. fusiformis*.

B. sauvanausus is frequent in the Oxfordian, but has been described also from the Upper Callovian (Waagen 1873–75, Pugaczewska, 1961). *B. semiarcuatus* was described by Pugaczewska (1961) from the Upper Callovian: its stratigraphic spread is known only for Poland.

All in all, also the belemnite fauna of the ammonite-rich bed indicates a Callovian age. The presence of *B. fusiformis* beside nine Callovian species merely suggests a longer life span for this species.

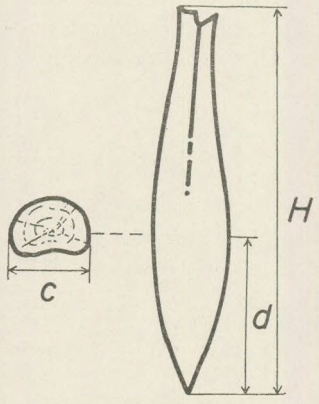

Fig. 2.

Dimensions serving as a basis for the description of belemnites

H = length of rostrum, *d* = length of apical portion (between apex and maximum diameter), *c* = maximum diameter

Systematic description

In the use of higher-order systematic units we have followed the classical system, similarly to several other authors (Müller 1965, Pugaczewska 1961, Stevens 1965). Some new trends in the systematization of belemnites have lately appeared (Jeletzky 1966), but we considered the classical system to be satisfactory until the publication of the fundamental systematic work (Treatise on Invertebrate Paleontology. M.)

In identification we have taken as a basis the traditional morphological features (Krimholz 1960). The growth index introduced by Pugaczewska (1961), which is the ratio of the length of the apical part of the rostrum (d) to its maximum diameter (c) (Fig. 2) was found to be useful.

Suborder Belemnoidea Naef 1912.
Family BELEMNITIDAE d'Orbigny 1845.
Subfamily Hastitinae Naef 1922.
Genus Hastites Mayer 1882.

HASTITES PRIVATENSIS (MAYER) 1866

Plate 1., Figure 1.

1866. *Belemnites privatensis* Mayer	Mayer, Ch. p. 366.
1871. *Belemnites Privasensis* Mayer	Dumortier, E. p. 20. Pl. III. 1–8.
1961. *Hastites privatensis* (Mayer, 1866).	Pugaczewska, H. 126. Pl. 3. 1–5.

Number of specimens: 1 (No. 88)

Dimensions:	H	c	d	d/c
	51 mm	8 mm	15 mm	1,9

Description: Small specimen of fair preservation. Slender, fusiform, elongate, with a thin alveolar region. Median portion swollen, gradually thickening, apical part difficult to examine, relatively short, gradually tapering. Cross section initially circular in the alveolar region, then growing square. In the median portion the four edges grow gradually rounded, and the cross section of the apical part is circular again. No dorsal or ventral furrow is visible. On the lateral walls there is a marked shallow double line from the alveolar region to about the beginning of the apical part. Here the furrows gradually flatten out and then disappear. There is no apical groove.

Remarks: The author of the species, Mayer, gave but a description; the first to figure it was Dumortier (1871). Figs. 1 to 6 of his Plate III represent specimens from Mayer's collection, of which Figs. 1. to 4 show the probable holotype. The Villány specimen agrees with Dumortier's figures in size, in its double lateral line and in its square cross section. According to its label it was formerly identified as *B. württembergicus*.

Distribution: The species is known from the Callovian and Oxfordian of Europe. According to Roman (1924), it is frequent also in the Upper Bathonian of Southern France. The type was described from the French Callovian.

Subfamily Belemnopsinae Naef 1922.

Genus Belemnopsis Bayle 1878.

BELEMNOPSIS FUSIFORMIS (PARKINSON) 1811

Plate 1., Figure 2.

1811. *Belemnites fusiformis* Park.	Parkinson, J. p. 128. Pl. VIII. 13.
1842. *Belemnites Fleuriausus*, d'Orb.	d'Orbigny, A. p. 111. Pl. 13. 14–18.
1851–55. *Belemnites fusiformis* Park. sp.	Morris, J.–Lycett, J. p. 8 Pl. I. 6, 8.
1851–55. *Belemnites Bessinus* d'Orb. sp.	Morris, J.–Lycett, J. p. 8 Pl. II. 5–7.
1865–70. *Belemnites aripistillum*, Lwoyd	Phillips, J. p. 107. (partim) Pl. XXVI. 64 v'''
1904. *Belemnites fusiformis*, Park.	Clerc, M. p. 5. Pl. 2. 5.
1961. *Belemnopsis fusiformis* (Parkinson, 1811)	Pugaczewska, H. p. 147. Pl. 10. 1–7.
non 1829. *Belemnites fusiformis*	Phillips, J. Pl. III. 1.
non 1858. *Belemnites fusiformis*	Quenstedt, F.A. p. 411. Pl. 56. 7–12.

Number of specimens: 4 (Nos. 81, 83, 85, 89).

Dimensions:	H	c	d	d/c
81.	61 mm	7.2 mm	36 mm	5.0
83.	40 mm	7.0 mm	21.4 mm	3.0
85.	62 mm	7.6 mm	35.5 mm	4.7
89.	75 mm	8.0 mm	31.0 mm	3.9

Description: (No. 85.) Fragmentary specimen of medium size. Elongate, slightly fusiform, lateral walls subparallel throughout, convergent only near the apex: the apical part is elongate and pointed in consequence. Ventral furrow of medium width, with rather sharp edges on the alveolar region and more or less flattened ones in the apical part. The furrow reaches up to the apex. Cross section circular in the alveolar region, ventrally flattening towards and oval at the apical part. No lateral lines or apical grooves visible.

Remarks: B. fleuriausus introduced by d'Orbigny (1842) is identical with *B. fusiformis* on the basis of the shape of its rostrum and of its medium-width ventral furrow reaching up to the apex. Fig. 17. of d'Orbigny is an erroneous cross section, as his Figs. 14. and 15. show the cross section to be ventrally flattened at the maximum diameter. A rostrum figured by Phillips (1865–70) by the name *B. aripistillum* Lwoyd (Pl. XXVI, 64 v''') belongs on the basis of its parallel sides and narrow ventral furrow to *B. fusiformis*. On the other hand, Phillips (1829) figured a rostrum by the name *B. fusiformis*, which owing to its squatness and pronouncedly fusiform outline cannot

be identified with this species. Quenstedt (1858, Pl. 56, Figs. 7 to 12) figured some *Hibolites* by the name *B. fusiformis* (cf. Pugaczewska 1961, p. 177).

Distribution: This species described from England is known also from France, Switzerland and Poland, from Bathonian beds in every case. The Villány specimens have come from the Callovian ammonite-rich bed.

BELEMNOPSIS LATESULCATUS (D'ORBIGNY) 1845

Plate 1., Figure 3.

1845. *Belemnites latesulcatus* d'Orb.	d'Orbigny, A. p. 301. Pl. 50. 3–8.
1910. *Belemnites latesulcatus* d'Orb.	Benecke, E.W. p. 129. Figure 1, 2.
1932. *Hastites latesulcatus* d'Orbigny sp.	Corroy, G. p. 167. Pl. 18. Figure 3.
1951. *Hibolites latesulcatus* d'Orb. sp.	Jeannet, A. p. 24. Pl. 3. 12., Pl. 4. 3–6.
1961. *Belemnopsis latesulcatus* (d'Orbigny, 1845)	Pugaczewska, H. p. 150. Pl. 11. 1–12, Pl. 12. 1.

Number of specimens. 7 (Nos. 21, 41, 45, 55, 57, 67, 70).

Dimensions:	H	c	d	d/c
41.	80 mm	19.0 mm	38.5 mm	2.0
67.	117 mm	13.7 mm	44.5 mm	3.24
70.	73 mm	14.5 mm	38.5 mm	2.7

Description: (No. 67.) Large specimen of fair preservation. Hastate, with a relatively broad alveolar region gradually widening towards the median part, it tapers into a relatively short apical portion. Alveolar cross section circular, median and apical cross section pronouncedly elliptic, flattened dorso-ventrally Each lateral wall bears a well visible blunt edge beginning in the alveolar region. The ventral furrow is relatively narrow and sharp-edged on the alveolar portion, growing broader and shallower with smoothed edges towards the apical part. The furrow reaches up to the apex. Specimen No. 55 exhibits well visible narrow and shallow furrows which continue also in the apical portion.

Remarks: Specimen No. 45. was according to its label earlier identified as *B. hastatus* On the basis of its subparallel sides it belongs to the genus *Belemnopsis* and on the basis of its ventral furrow reaching to the apex and of the furrow running along its side it belongs to the species *B. latesulcatus.*

Distribution: Known from both the Mediterranean and Central European area, the species has been identified in Bathonian, Callovian and Oxfordian deposits. The Villány specimens derive from the ammonite-rich Callovian bed.

BELEMNOPSIS SUBHASTATUS (ZIETEN) 1830

Plate 2., Figure 1.

1830. *Belemnites subhastatus* Zieten	Zieten, C.H.v. p. 27. Pl. 21. 2a–e.
?1875. *Belemnites subhastatus* Zieten	Waagen, W. p. 14. Pl. II. 1a–e.
1961. *Belemnopsis subhastatus* (Zieten, 1827)	Pugaczewska, H. p. 154. Pl. 12. 2. Pl. 13. 1–7.

Number of specimens: 2 (Nos. 45, 80).

Dimensions:	H	c	d	d/c
45.	59 mm	15.0 mm	45.7 mm	3.41
80.	50 mm	9.0 mm	40.0 mm	4.44

Description: (No. 80). Poorly preserved, fragmentary specimen. Long cylindrical form. Only part of the median portion is preserved. Apical part very long and gently, elongately tapering. Cross section ventrally flattened in the median portion, apical part more squashed, of reniform cross section. Ventral furrow fairly deep, narrow, with somewhat rounded ledges. Proceeding towards the apex the furrow grows narrower, but the ledges do not flatten out. About 1 cm from the apex, the furrow tapers out. No lateral line visible.

Remarks: Specimen No. 45 had been identified according to the Hungarian Geological Institute label as *Belemnites hastatus*. Both the shape of the rostrum and the features of the furrow agree well with Zieten's (1830) type. The species differs from *B. latesulcatus* in its long apical part and narrow ventral furrow.

Distribution: In Bathonian and Callovian beds, Germany, France, England and Poland. At Villány it occurs in the Callovian.

BELEMNOPSIS CF. SEMIARCUATUS PUGACZEWSKA 1961.

Plate 2., Figure 2.

1961. *Belemnopsis semiarcuatus* n. sp.	Pugaczewska, H. p. 161. Pl. 15. Figure 1–19.

Number of specimens: 2 (Nos. 28, 64).

Dimensions:	H	c	d	d/c
28.	87 mm	18.2 mm	36.0 mm	1.97
64.	74 mm	19.7 mm	36.6 mm	1.85

Description: (No. 28). Medium size specimen of poor preservation. Hastate. Alveolar region missing, median portion relatively broad, slightly thickening towards the apex, apical part short. In side view, the rostrum is slightly bent, the point of strongest curvature is nearer to the apex on the dorsal side than on

the ventral side. Cross section ventrally flattened throughout; flattening more pronounced in the apical part. Ventral furrow deep, flattened on the apical part and broadened. No lateral lines visible.

Remarks: The characteristic curvature and low value growth index identify this form with the type described by Pugaczewska (1961). There is, however, a difference in size, as the type has a length of but 40 mm, whereas the Villány specimens exceed this size even in their fragmentary state.

Distribution: The type has been described from the Polish Upper Callovian; the Villány specimens are likewise Callovian.

Genus Hibolites Mayer, 1883.

HIBOLITES HASTATUS (BLAINVILLE) 1827

Plate 2., Figure 3., Plate 3., Figure 1.

1827. *Belemnites hastatus* Blainville	Blainville, D. p. 71. Pl. 2. 4–4a. 5c–i. Pl. 5. 3–3a.
1858. *Belemnites semihastatus rotundus* Quenstedt	Quenstedt, F.A. p. 548. Pl. 72. 13–15, Pl. 74., Figure 11.
1865–70. *Belemnites hastatus*, Blainville	Phillips, J. p. 111. (partim) XXVIII. 67, 69, 70
1872. *Belemnites hastatus* Blain	Gemmellaro, G.G. p. 165. Pl. V. 1–2.
1922. *Hibolites hastatus* Blainv. 1827.	Naef, A. p. 249. 71. k.p. 89. f.
1925. *Hibolites hastatus* Blainville	Lissajous, M. p. 36. Figure 20.
1951. *Hibolites hastatus* Blainville sp.	Jeannet, A. p. 23. Pl. 3. 6–11.
1961. *Hibolites hastatus* (Blainville, 1827)	Pugaczewska, H. p. 165. Pl. 16–18.

Number of specimens: 14.

Dimensions.	H	c	d	d/c
1.	148 mm	11.5 mm	33.0 mm	2.87
3.	119 mm	20.0 mm	53.5 mm	2.67
4.	141 mm	20.2 mm	47.4 mm	2.33
5.	122 mm	14.2 mm	46.7 mm	3.28

Description: (No. 1). Large, well-preserved, complete specimen. The rostrum has the shape of a slender mace, with a relatively thin alveolar, broadening median and relatively short, tapering apical part. Alveolus deep (36 mm). Cross section on the alveolar region circular, slightly flattened laterally. In the median portion, the cross section becomes ventrally flattened and this flatten-

ing is even more pronounced in the apical part. Ventral furrow deep and strongly incised in the alveolar region, with fairly sharp ledges. Towards the apical part the furrow grows shallower with gradually more rounded edges and tapers out on the apical part. No lateral line visible.

Remarks No. 37 had been described earlier as *B. hastatus* Size, cross section and features of the ventral furrow concur in identifying our specimens with the type published by Blainville.

Distribution. This frequent species of the Central European and Mediterranean regions has been identified at a number of Middle and Upper Jurassic localities. It is the most frequent form of the Villány Hills belemnite fauna. Over and above the specimens, described here the Callovian ammonite-rich bed has yielded several hundred fragmentary ones as well.

HIBOLITES SEMIHASTATUS (BLAINVILLE) 1827

Plate 3., Figure 2.

1827. *Belemnites semihastatus*, Blainville	Blainville, D. p. 72. (partim) Pl. 2. 5—5a,b.
1865—70. *Belemnites hastatus*, Blainville	Phillips, J. p. 111. Pl. XXVIII. Figure 68.
1951. *Hibolites semihastatus* de Blainville sp.	Jeannet, A. p. 23. Pl. 4. 1—2.
1961. *Hibolites semihastatus* (Blainville, 1827)	Pugaczewska, H. p. 170. Pl. 19. Figure 1—8.

Number of specimens: 2 (Nos. 44, 76).

Dimensions:	H	c	d	d/c
44.	60 mm	13.4 mm	32.4 mm	2.41
76.	66 mm	12.7 mm	31.0 mm	2.44

Description: (No. 76). Small fragmentary specimen. Rostrum slender, mace-shaped, with a slightly thickened median and very pointed apical part. Cross section circular in median portion, slightly flattened ventrally near the maximum diameter. Ventral furrow narrow in median portion, medium-deep with rounded edges. In the apical part the furrow gradually grows wider and shallower. The edges are gradually smoothed out in the apical part and the furrow disappears shortly before the apex. No lateral line visible; on the lateral walls of specimen No. 44 there is a vague flat longitudinal band.

Remarks: The Villány specimens agree well as to shape and size with the holotype figured by Blainville. According to Pugaczewska, the growth index is typical of the species. In her material she observed values ranging from 2.0 to 2.8; those of our specimens are also within this range.

Distribution: This species, frequent in Europe, has been mentioned from the Bathonian, Callovian and Oxfordian stages. The Villány specimens are Callovian.

HIBOLITES GIRARDOTI (LORIOL) 1902

Plate 3., Figure 3.

1902. *Belemnites (Hibolites) Girardoti* Loriol	Loriol, P. p. 6. Pl. 1. Figure 2–7.
1961 *Hibolites girardoti* (Loriol, 1902)	Pugaczewska, H. p. 181. Pl. 23. Figure 1–7.

Number of specimens: 5 (Nos. 90, 91, 92, 93, 94).

Dimensions.	H	c	d	d/c
90.	94.0 mm	14.5 mm	43.0 mm	2.9
93.	76.0 mm	14.0 mm	46.8 mm	3.3
94.	121.7 mm	18.0 mm	55.5 mm	3.1

Description: (No. 90). Large specimen of good preservation. Shape elongate fusiform, alveolar region missing, medium portion somewhat thickened, apical portion rather long. Cross section circular at middle, ventrally slightly flattened near the maximum diameter, circular again in the apical part. Ventral furrow short, not attaining the point of maximum diameter. Its median part is deeper: in its progress towards the apex it grows shallower without widening and is then smoothed out. The lateral walls bear a marked longitudinal prominence. Specimen No. 92 exhibits a thin double lateral line.

Remarks: By their circular cross section flattened only in the middle portion and by the features of their ventral furrow, the Villány specimens agree well with the type published by L o r i o l (1902).

Distribution: The species had been described from the Lower Oxfordian of Switzerland. In Poland it occurs also in the Upper Callovian. The Villány specimens derive from the upper part of the Callovian ammonite-rich bed.

Subfamily Duvaliinae Pavlov 1914.
Genus Rhopaloteuthis Lissajous 1915.

RHOPALOTEUTHIS SAUVANAUSUS (D'ORBIGNY) 1842

Plate 4., Figure 1.

1842. *Belemnites Sauvanausus* d'Orb.	d'Orbigny, A. p. 128. Pl. 21. Figure 1–10.
1875. *Belemnites Sauvanausus*, Orb.	Waagen, W. p. 8. Pl. II. Figure 6a–f.
1886. *Belemnites Sauvanausus* d'Orb.	Zakrzewski, A.J.A. p. 51. Pl. I. Figure 15.
1900. *Belemnites (Hibolites) Sauvanaui*, d'Orbigny	Loriol, P. p. 6. Pl. II. Figure 2.

1925. *Rhopaloteuthis Sauvanaui* d'Orb.	Lissajous, M. p. 42. Figure 23.
1961. *Rhopaloteuthis sauvanausus* (d'Orbigny, 1842)	Pugaczewska, H. p. 194. Pl. 6. Figure 7 – 8.

Number of specimens: 1 (No. 95).

Dimensions:	H	c	d	d/c
	59 mm	12 mm	18 mm	1.5

Description. Complete specimen of excellent preservation. Club-shaped; alveolar region relatively slender, thin; medium portion strongly thickened, apical part short. Cross section slightly squarish in the alveolar region, the lateral walls and the ventral side forming a blunt edge. In the median portion, the rostrum is flattened dorso-ventrally: the cross section is elliptical here. In the apical part, the cross section is somewhat less elliptic. Dorsal furrow very short, deeply incised in the alveolar region, narrow with sharp edges. Narrowing and thinning at the beginning of the median portion, it suddenly disappears shortly thereafter. The edges are still sharp near the point of disappearance. Lateral lines are vague shallow broad depressions reaching down to the maximum diameter.

Remarks: D' O r b i g n y on his Plate 21 figures at least 4 specimens. His Figs. 4 – 5. show a rostrum deformed in the lifetime of the animal. Figs. 1. to 3. represent a big specimen which was considered the type by subsequent authors (L i s s a j o u s 1925, W a a g e n 1875). The Villány specimen is more intensely thinning near the end of the alveolus, wherefore it stands closer to Figs. 9 and 10 (paratype) of d' O r b i g n y. According to the label, the specimen described above had earlier been identified as *B. gillieroni.*

Distribution: This species occurring both in the Central European and Mediterranean regions had been described from the Lower Oxfordian. In Poland it occurs also in the Upper Callovian. The Villány specimen was collected from the ammonite-rich Callovian bed.

RHOPALOTEUTHIS GILLIERONI (MAYER) 1866.

Plate 4., Figure 2, 3.

1866. *Belemnites Gillieroni* May.	Mayer, Ch.M. p. 365.
1881. *Belemnites Gillieroni* Mayer	Böckh J. p. 10. Pl. III. 4a – b.
1923. *Rhopaloteuthis Gillieroni* Mayer	Lissajous, M. p. 47. Pl. I. 9 – 9a.
1924. *Rhopaloteuthis Gillieroni* Mayer	Roman, F. p. 41 Pl. I. Figure 2.
1961. *Rhopaloteuthis gillieroni* (Mayer, 1866)	Pugaczewska, H. p. 196. Pl. 26. 1 – 7

Number of specimens: 3 (Nos. 97, 89, 99).

Dimensions:	H	c	d	d/c
98.	54 mm	11 mm	18 mm	1.65
99.	60 mm	16 mm	27 mm	1.07

Description: (No. 98). Small, of fair preservation. Curved club shape, with a long, relatively broad alveolar region. Median portion broadening, apical part very short and ending in a curved point, with a small thin apical spine. Cross section a rounded square in the alveolar region, with flat lateral walls. Cross section of apical part circular. Dorsal furrow medium narrow, strongly incised, with somewhat rounded edges. It reaches little beyond the alveolar region, shallowing out and suddenly disappearing far before the cross section of maximum diameter. The lateral walls bear a marked broad flat sideline disappearing before the apical part.

Remarks: Specimens Nos. 97. and 98. agree well with the description by Mayer (1886) and with the subsequently published figures of other authors. Specimen No. 99 (Pl. 4., Fig. 2.) deviates from these in its greater thickness. According to its label it had earlier been identified as *B. argovianus*. Despite the greater growth index, however, it certainly belongs to the species *R. gillieroni* by its markedly club-like shape and short dorsal furrow.

Distribution: Species fairly frequent in Europe. It has been indentified in Bathonian and Callovian deposits. The Villány species derives from the Callovian.

REFERENCES

Arkell, W. J. (1956): Jurassic Geology of the World. Oliver and Boyd, Edinburgh, London

Benecke, E. W. (1910): Über Belemnites latesulcatus und Pronoelia lotharingica. Zentralbl. f. Min.

Blainville, D. (1827): Mémoire sur les Belemnites considérées zoologiquement et géologiquement. Paris.

Böckh J. (1881): Adatok a Mecsek hegység és dombvidéke jurakorabeli lerakodásainak ismeretéhez. (Contributions to the knowledge of the Jurassic deposits of the Mecsek Mountains and the hummocks around it.) Parts I–II. Értekezések a Természettudományok Köréből. X–XI. Budapest.

Bülow Trummer, E. v. (1920): Fossilium Catalogus. I. Animalia, II. Cephalopoda, Dibranchiata. Neubrandenburg.

Clerc, M. (1904): Etude monographique des fossiles du Dogger de quelques gisements classiques du Jura neuchâtelois et vaudois. Mém. Soc. pal. Suisse. XXXI.

Corroy, G. (1932): Le callovien de la Bordure orientale du Bassin de Paris. Mém. carte géol. dét. France.

Dumortier, E. (1871): Sur quelques gisements de l'Oxfordien inférieur du département de l'Ardèche. Savy ed. Paris.

Fülöp J. (1964): A Villányi hegység krétaidőszaki képződményei. (Cretaceous of the Villány Hills.) Geol. Hung., Ser. Geol. 15.

Galácz A. – Vörös A. (1967): Belemnoideák vizsgálata. (Belemnite studies.) Tan. Term. Tud. Köréből. Budapest.

Gemmellaro, G. G. (1872): Sopra I Cephalopodi della Zona con Stephanoceras macrocephalum Schloth. Atti. Acad. Gienia Ser. 3, t. VIII.

Hofmann K. (1876): Aufnahmsbericht. Verh. der K. K. Geol. Reichsanst.

Jeannet, A. (1951): Stratigraphie und Palaeontologie des oolitischen Eisenerzlagers von Herznacht und seiner Umgebung. Bern.

Kaszap A. (1959): Dogger rétegek a Villányi hegységben. (Dogger deposits in the Villány Hills.) Földt. Közl. 89.

Kaszap A. (1961): Bath-kallovi rétegek a Villányi hegységben. (Bathonian-Callovian deposits in the Villány Hills.) M. Áll. Földt. Int. Évkönyve, XLIX. 2.

Krimholz, G. Ya. (1958): Podklass Endocochlia. In: Osnovy Paleontologii, ed. Orlov, Moscow.

Krimholz, G. Ya. (1960): Metodika opredelenia mezozoyskikh Golovonogikh. Izd. Leningr. Univ., Leningrade.

Lenz, O. (1872): Aus dem Baranyaer Komitate. Verh. der K. K. Geol. Reichsanst.

Jeletzky, J. A. (1966): Comparative Morphology, Phylogeny, and Classification of fossil Coleoidea. Univ. Kansas Publications, Mollusca, Article 7.

Lissajous, M. (1923): Étude sur la faune du Bathonien des environs de Mâcon. Trav. Lab. geol. Fac. Sci. Lyon, III. 3.

Lissajous, M. (1925): Répertoire alphabétique des Bélemnites Jurrassiques. Trav. Lab. Geol., Fac. Sci. Lyon VIII. 7.

Lóczy L., jun. (1912): A Villányi és Báni hegység geológiai viszonyai. (Geology of Villány and Bán Hills.) Földt. Közl. 42.

Lóczy L. jun. (1915): A villányi callovien ammonitesek monográfiája. (Monograph of the Callovian ammonites of the Villány Hills.) Geol. Hung. 1., 3—4.

Loriol, P. (1900): Étude sur les Mollusques et Brachiopodes de l'Oxfordien inférieur ou zone à Ammonites Renggeri du Jura lédonien. Mém. Soc. pal. Suisse. XXVII.

Loriol, P. (1902): Étude sur les Mollusques et Brachiopodes de l'Oxfordien supérieur et moyen du Jura lédonien. Mém. Soc. pal. Suisse. XXIX—XXXI.

Mayer, Ch. (1866): Diagnoses de deux Belemnites nouvelles. Journ. Conchyliologie. Sér. 3, IV. vol. XIV.

Morris, J. — Lycett, J. (1851—55): A monograph of the Mollusca from the Great Oolite, chiefly from Minchinhampton and the coast of Yorkshire. Palaeont. Soc. London.

Müller, A. H. (1965): Lehrbuch der Paläozoologie. Band II. Invertebraten, Teil 2., 2. Aufname. Jena.

Naef, A. (1922): Die fossilen Tintenfische. Jena.

Noszky J. jun. (1959): A Villányi hegység mezozóos képződményei. (Mesozoic of the Villány Hills.) In: Excursion guide for the participants on the Symposium on the Hungarian Mesozoic.

Noszky J. jun. (1961): Magyarország jura képződményei. (Jurassic of Hungary.) M. Áll. Földt. Int. Évkönyve, XLIX. 2.

d'Orbigny, A. (1842): Paléontologie Française. Description des Mollusques et Rayonnés fossiles. Terrains jurassiques. I. Céphalopodes. Paris.

d'Orbigny, A. (1845): Paléontologie universelle des Coquilles et des Mollusques. Paris.

Pálfy M. (1901): Geológiai jegyzetek néhány dunamenti kőbányáról. (Geological notes on some quarries along the Danube.) Földt. Közl. 31.

Parkinson, J. (1811): Organic remains of a former World. III. London.

Phillips, J. (1865—69): A monograph of British Belemnitidae. Pal. Soc. XXIII. London.

Phillips, J. (1829): Illustrations to the Geology of Yorkshire. 3. ed. London.

Pugaczewska, H. (1961): Belemnoids from the Jurassic of Poland. Acta Pal. Polonica. Vol. VI. no 2.

Quenstedt, F. A. (1862): Handbuch der Petrefactenkunde. Tübingen.

Quenstedt, F. A. (1858): Der Jura. Tübingen.

Radwanski, A. — Szulczewski, M. (1965): Stromatolitok a Villányi hegység jura rétegeiben. (Stomatoliths in the Villány Jurassic). Földt. Közlöny, 95.

Rakusz Gy. — Strausz L. (1953): A Villányi hegység földtana. (Geology of the Villány Hills.) M. Áll. Földt. Int. Évkönyve, XLI. 2.

Riche, A. – Roman, F. (1921): La Montagne de Crussol. Trav. Lab. géol. Fac. Sci., Lyon. 1.

Roemer, J. (1911): Die Fauna der Aspidoides-Schichten von Lechstedt bei Hildesheim. Hannover.

Roman, F. (1924): Études sur le Callovien de la Vallée du Rhone. Trav. Lab. géol. Fac. Sci. Lyon. VI. Mém 5.

Stevens, G. R. (1963): Faunal Realms in Jurassic and Cretaceaus Belemnites. Geol. Mag. vol. 100 No. 6. London.

Stevens, G. R. (1965): The Jurassic and Cretaceous Belemnites of New Zealand and a Review of the Jurassic and Cretaceous Belemnites of the Indo-Pacific Region. Paleont. Bull. 36. N. Z. Geol. Soc.

Szabó P. (1957): A klasszikus villányi szelvény üledékföldtani újravizsgálata. (Lithologic reexamination of the classical profile of Villány.) Manuscript.

Till, A. (1906): Der fossilführende Dogger am Villány. Verh. der K. K. Geol. Reichsanst.

Vörös A. (1968): Földtani és őslénytani vizsgálatok a Villányi hegység K-i részén, különös tekintettel a bath-kallóvi kagyló- és csiga-faunára. (Geological and palaeontological studies in the western Villány Hills, with particular regard to the Bathonian-Callovian gastropod and bivalve fauna.) Manuscript.

Waagen, W. (1873–75): The Jurassic Fauna of Kutch. The Cephalopoda. Palaeont. Indica Ser. 9. 1.

Zakrzewski, A. J. (1886): Die Grenzschichten des Braunen zum Weissen Jura in Schwaben. Stuttgart.

Zieten, C. H. v. (1830): Die Versteinerungen Württembergs. Stuttgart.

Plate 1.

Fig. 1. Hastites privatensis (Mayer)
a = ventral view, b = lateral view (No. 88.)

Fig. 2. Belemnopsis fusiformis (Parkinson)
a = ventral view, b = lateral view (No. 85), c = cross section (No. 81)

Fig. 3. Belemnopsis latesulcatus (d'Orbigny)
a = ventral view, b = lateral view (No. 67), c = cross section (No. 21)
v = ventral side
All natural size

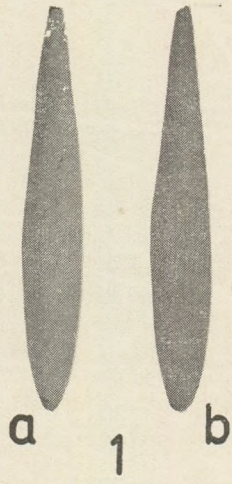
a
b
1

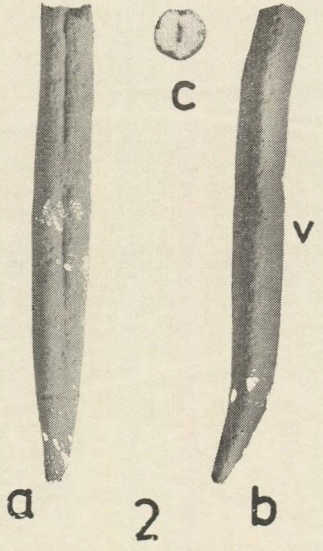
c
v
a
2
b

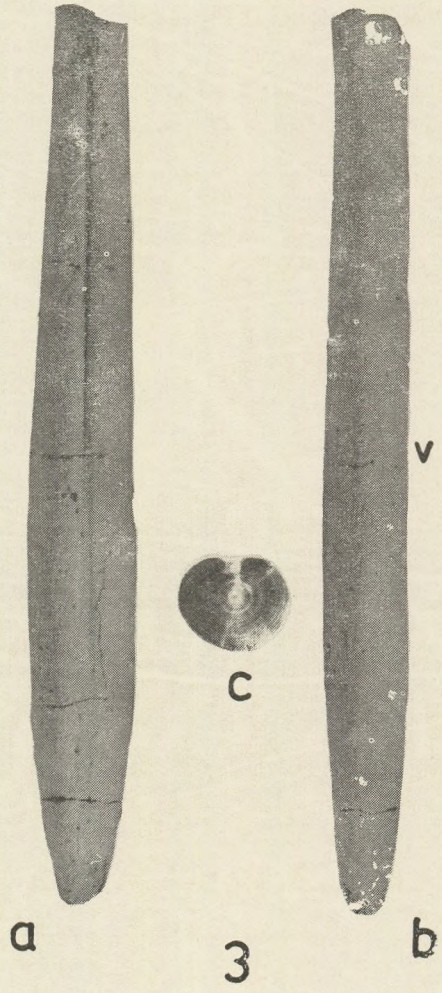
v
c
a
3
b

Plate 2.

Fig. 1. Belemnopsis subhastatus (Zieten)
a = ventral view, b = lateral view (No. 80), c = cross section (No. 45)

Fig. 2. Belemnopsis cf. semiarcuatus Pugaczewska
a = ventral view, b = lateral view (No. 28)

Fig. 3. Hibolites hastatus (Blainville)
a = ventral view, b = lateral view (No. 1)
v = ventral side
All natural size

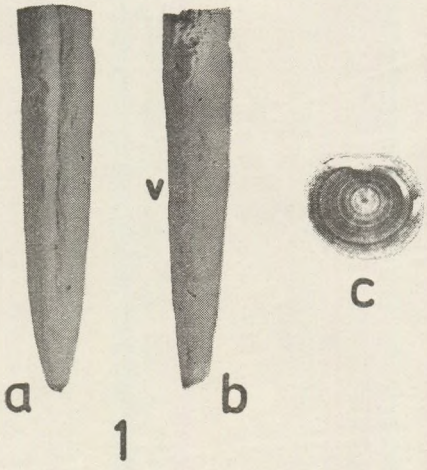
v
c
a
b
1

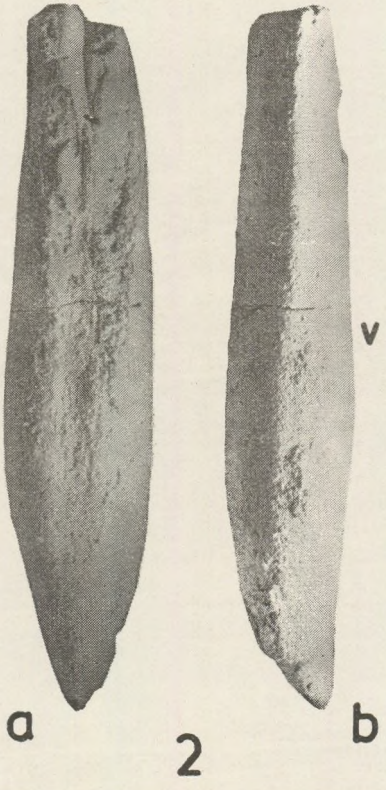
v
a
b
2

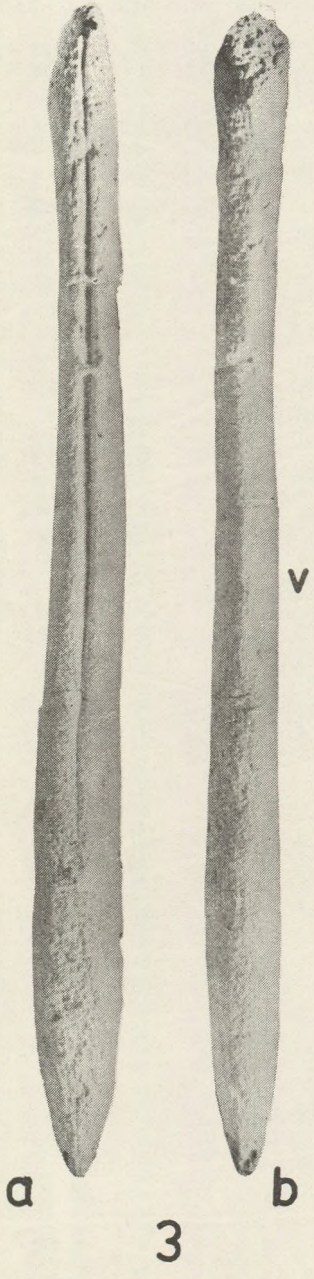
v
a
b
3

Plate 3.

Fig. 1. Hibolites hastatus (Blainville)
a = ventral view (No. 3), b = cross section (No. 101)

Fig. 2. Hibolites semihastatus (Blainville)
a = ventral view, b = lateral view (No. 76), c = cross section (No. 44)

Fig. 3. Hibolites girardoti (Loriol)
a = ventral view, b = lateral view (No. 90), c = cross section (No. 92)
v = ventral side
All natural size

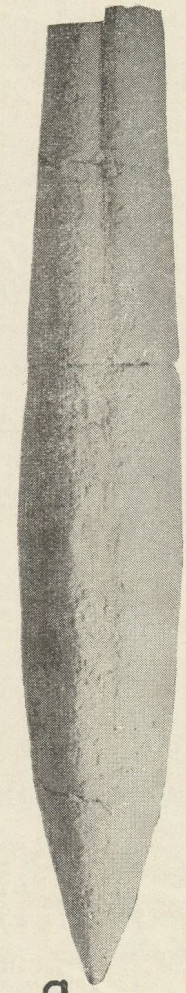

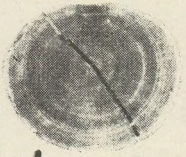

1

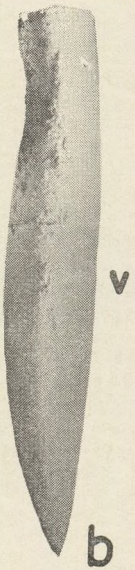

2

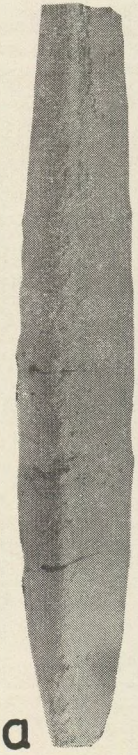

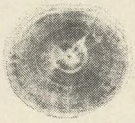

3

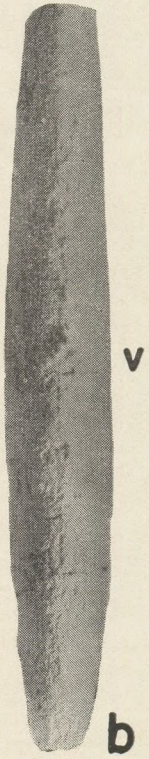

Plate 4.

Fig. 1. Rhopaloteuthis sauvanausus (d'Orbigny)
a = dorsal view, b = lateral view (No. 95)

Fig. 2. Rhopaloteuthis gillieroni (Mayer)
a = dorsal view, b = lateral view (No. 99)

Fig. 3. Rhopaloteuthis gillieroni (Mayer)
a = dorsal view, b = lateral view (No. 98)

Fig. 4. Cross section of a scrubbed-down rostrum with stromatolith incrustation

Fig. 5. Scrubbed-down rostrum (side view)
v = ventral side
All natural size

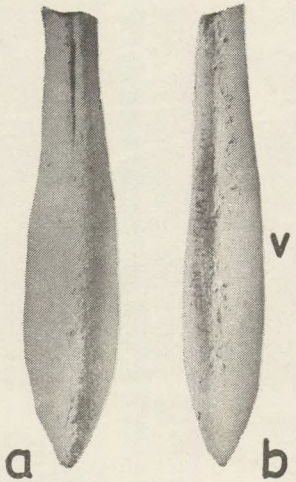

1

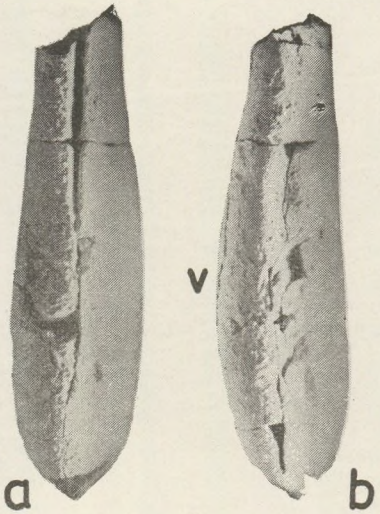

2

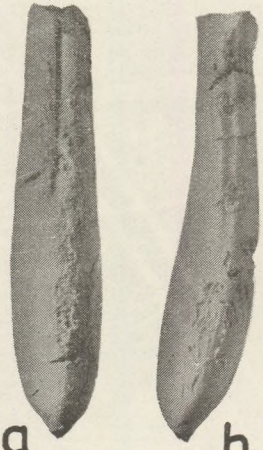

3

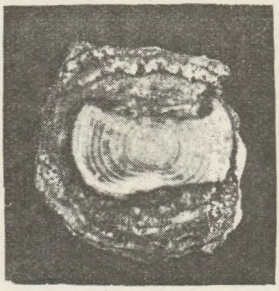

4

5

INDEX

A kiadásért felelős: az Eötvös Loránd Tudományegyetem rektora
A kézirat nyomdába érkezett: 1969. február — Megjelent: 1969. december
Terjedelem: 12.5 (A/5) ív + 4 mell. — Példányszám: 530
Készült monó szedéssel, íves magasnyomással, az MSZ 5061—59 és az 5602—55
szabvány szerint
69.463. Állami Nyomda, Budapest